

AERODYNAMICS AND ITS APPLICATIONS

Edited by

WaqarAsrar

Ashraf A Omer

Department of Mechanical Engineering

International Islamic University Malaysia

Preface

This book contains topics of interest to Aerospace engineering students in their undergraduate program. Some aspects of Aerodynamics have been included in this volume. These are compressible flows, brief introduction to computational fluid dynamics, a step by step guide to using the commercial CFD code FLUENT, introductory methods in building and testing aerodynamic models in a wind tunnel, topics in estimation of drag, and an introduction to rotary wing aerodynamics.

The guide to FLUENT is greatly influenced by the tutorials of Prof. Bhaskaran of Cornell University, which are available online. The topics on drag have been contributed by Prof. Ashraf Omer, rotary wing aerodynamics by Dr. MoumenIdres both of the Dept. of Mechanical Engineering, IIUM, the chapters on FLUENT were written by Mr. Anwar M Sood,(former student in the Dept. of Mech. Engg., IIUM, now at PROTON Bhd) and WA, and the chapters on model building and wind tunnel testing were written by Mr. Mohammad Zaimi (former student in the Dept. of Mechanical Engg., IIUM) and WA. The chapters on FLUENT and model building and wind tunnel testing are introductory in nature and meant for undergraduate students.

The publication cost of the book has been borne entirely by the International Islamic University Malaysia, to which the authors are indebted.

The errors and omissions are entirely of the authors and they would be grateful to readers for their help in locating them. It is hoped that these would be corrected in future editions of the book. Correspondence concerning this book should be addressed to WaqarAsrar, Department of Mechanical Engineering, IIUM, P. O. Box 50728, Kuala Lumpur, Malaysia. Email: waqar (at iium.edu.my), Phone: 03-6196-4590, Fax: 03-6196-4455.

The editors and authors would like to thank Ms. Alaman Altaf, graduate student in the Dept. of Mechanical Engg., IIUM for her painstaking efforts in formatting the manuscript.

WaqarAsrar
Ashraf A Omer

AERODYNAMICS AND ITS APPLICATIONS

Table of Contents

ABSTRACT.....	5
CHAPTER 1 <i>Waqar Asrar</i>	6
INTRODUCTION TO GAS DYNAMICS.....	6
CHAPTER 2 <i>Waqar Asrar</i>	12
CONSERVATION LAWS	12
CHAPTER 3 <i>Waqar Asrar</i>	18
FUNDAMENTALS OF COMPRESSIBLE FLUID FLOW	18
CHAPTER 4 <i>Waqar Asrar</i>	26
NORMAL SHOCKS	26
CHAPTER 5 <i>Waqar Asrar</i>	32
OBLIQUE SHOCKS	32
CHAPTER 6 <i>Waqar Asrar</i>	37
FLOW THROUGH VARIABLE AREA DUCTS	37
CHAPTER 7 <i>Waqar Asrar</i>	42
INTRODUCTION TO AERODYNAMIC DRAG.....	42
CHAPTER 8 <i>Ashraf A Omer</i>	53
TRANSONIC FLOW AND CRITICAL MACH NUMBER	53
CHAPTER 9 <i>Ashraf A Omer</i>	62
ESTIMATION OF SUPERSONIC AERODYNAMICS FORCES USING LINEARIZED THEORY	62
CHAPTER 10 <i>Ashraf A Omer</i>	70
FRICTION FORCE AND BOUNDARY LAYER DEVELOPMENT	70
CHAPTER 11 <i>Ashraf A Omer</i>	77
FLAT PLATE BOUNDARY LAYER SKIN FRICTION DRAG	77
CHAPTER 12 <i>Ashraf A Omer</i>	85
SOLVED PROBLEMS IN BOUNDARY LAYER THEORY	85
CHAPTER 13 <i>Ashraf A Omer</i>	96
INTRODUCTION TO HELICOPTERS	96
CHAPTER 14 <i>Moumen M Idres</i>	102

AERODYNAMICS AND ITS APPLICATIONS

VERTICAL FLIGHT: MOMENTUM THEORY	102
CHAPTER 15 <i>Moumen M Idres</i>	108
VERTICAL FLIGHT: BLADE ELEMENT THEORY	108
CHAPTER 16 <i>Moumen M Idres</i>	114
FORWARD FLIGHT: ROTOR MECHANISMS	114
CHAPTER 17 <i>Moumen M Idres</i>	123
FORWARD FLIGHT: ROTOR AERODYNAMICS	123
CHAPTER 18 <i>Moumen M Idres</i>	130
HELICOPTER PERFORMANCE: HOVER, VERTICAL FLIGHT, FORWARD FLIGHT AND CLIMB IN FORWARD FLIGHT	130
CHAPTER 19 <i>Moumen M Idres</i>	136
HELICOPTER PERFORMANCE: OPTIMUM SPEEDS, MAXIMUM LEVEL SPEED, ROTOR LIMITS ENVELOPE	136
CHAPTER 20 <i>Moumen M Idres</i>	141
INTRODUCTION TO AIRCRAFT CONCEPTUAL DESIGN PROCESS	141
CHAPTER 21 <i>Ashraf A Omer</i>	150
LIGHTER THAN AIR VEHICLES	150
CHAPTER 22 <i>Mohammad Zaimi and Waqar Asrar</i>	158
INTRODUCTION TO COMPUTATIONAL FLUID DYNAMICS	158
CHAPTER 23 <i>Anwar M Sood and Waqar Asrar</i>	166
FLOW PAST AN AIRFOIL	166
CHAPTER 24 <i>Anwar M Sood and Waqar Asrar</i>	175
CREATING FAR FIELD BOUNDARY IN GAMBIT	175
CHAPTER 25 <i>Anwar M Sood and Waqar Asrar</i>	181
MESH GENERATION IN GAMBIT	181
CHAPTER 26 <i>Anwar M Sood and Waqar Asrar</i>	190
CREATING BOUNDARIES IN GAMBIT	190
CHAPTER 27 <i>Anwar M Sood and Waqar Asrar</i>	195
SETTING UP A PROBLEM IN FLUENT	195
CHAPTER 28 <i>Anwar M Sood and Waqar Asrar</i>	204
SOLVING PROBLEM IN FLUENT	204

AERODYNAMICS AND ITS APPLICATIONS

CHAPTER 29	<i>Anwar M Sood and Waqar Asrar</i>	209
COMPUTING FORCES AND CONVERGENCE IN FLUENT		209
CHAPTER 30	<i>Anwar M Sood and Waqar Asrar</i>	215
ANALYSING RESULTS IN FLUENT		215
CHAPTER 31	<i>Anwar M Sood and Waqar Asrar</i>	222
FLUENT RESULTS FOR NACA 0012		222
CHAPTER 32	<i>Anwar M Sood and Waqar Asrar</i>	232
FLUENT RESULTS FOR NACA 4412		232
CHAPTER 33	<i>Anwar M Sood and Waqar Asrar</i>	238
DESIGNING A MODEL FOR WIND TUNNEL TESTING		238
CHAPTER 34	<i>Mohammad Zaimi and Waqar Asrar</i>	245
SELECTING MATERIAL AND CONSTRUCTING MODEL FOR WIND TUNNEL TESTING		245
CHAPTER 35	<i>Mohammad Zaimi and Waqar Asrar</i>	256
FINAL MODEL ASSEMBLY TECHNIQUES		256
CHAPTER 36	<i>Mohammad Zaimi and Waqar Asrar</i>	267
SETTING UP MODEL FOR WIND TUNNEL TESTING		267
CHAPTER 37	<i>Mohammad Zaimi and Waqar Asrar</i>	275
WIND TUNNEL TEST RESULTS		275
APPENDIX		284

ABSTRACT

This book is an introduction to the subject of Aerodynamics and talks about some of its fundamentals and applications. These are one dimensional compressible flow, a brief introduction to computational fluid dynamics, a step by step guide to using the commercial CFD code FLUENT, introductory simple methods in building and testing aerodynamic models in a wind tunnel for undergraduates, topics in estimation of drag, and an introduction to rotary wing aerodynamics. References are made to texts required for further study.

Keywords: aerodynamics, inviscid flow, viscous flow, incompressible flow, compressible flow.

CHAPTER 1

INTRODUCTION TO GAS DYNAMICS

Aerodynamics as a subject relates to predicting the forces and moments acting on an object moving in air. The relative speed between the object and the surrounding air creates normal and shear stresses on the object, whose net effect are the forces and moments on the body. These forces and moments are termed: lift, drag, side force and the pitching, yawing, and rolling moments.

The subject of aerodynamics is further classified into low speed and high speed aerodynamics. High speed aerodynamics is also known as compressible aerodynamics or gas dynamics. This happens when the relative speed between the body or object is nearly 30% of the local speed of sound or higher.

Why do we study compressible aerodynamics or gas dynamics? The answer lies in the following: Knowledge of compressible aerodynamics/gas dynamics will equip the aerospace engineer to compute:

- (a) Lift,
- (b) Drag,
- (c) Moments; on any vehicle moving at high speed.

Recall that lift is the force which keeps the aircraft at the flying altitude, drag is the force due to the resistance of the air moving past the aircraft, and moments or aerodynamic moments are produced by the pressure and shear stress distribution on the aircraft body. The coefficients of

AERODYNAMICS AND ITS APPLICATIONS

each of the above are more commonly computed for applications. These forces and moments or their coefficients are used in stability, control, propulsion, structures, and aircraft design.

Definitions:

Compressibility: Is a measure of the change in density of a fluid due to a specified change in pressure.

Compressible Flow: Changes in density and temperatures in the flow field are significant (if ignored, will result in large (>10%) errors.)

Incompressible Flow: Density and temperature are assumed to remain constant in the flow field. (Error introduced may be <10%).

It should be pointed out that all fluids are compressible. However the relative motion between a body and the surrounding air which produces the flows past a body are incompressible or compressible.

1. In general, liquids have low compressibility while gases are highly compressible.

Compressibility is a measure of the rate of change of density with respect to pressure while the entropy remains constant.

AERODYNAMICS AND ITS APPLICATIONS

We study aerodynamics (high speed or low speed) to estimate

- (a) Normal stresses (pressure)
- (b) Shear stresses
- (c) Surface temperature

which leads to the estimation of all forces and moments acting on the aircraft and hence its lift, drag, and moments or their coefficients.

The study of high speed aerodynamics or gas dynamics has the following applications:

- (a) Design and analysis of high speed aircraft.
- (b) Gas turbines.
- (c) Steam turbines.
- (d) Reciprocating engines
- (e) Gas transmission lines
- (f) Combustion chambers and many others.

Fundamental Assumptions in Inviscid Gas dynamics

Assumptions for 1D, Inviscid, Compressible flows

- (i) Gas/Fluid is continuous
- (ii) No chemical changes occur ($T < 2000\text{K}$)
- (iii) Perfect gas with constant specific heat
- (iv) Gravitational effects are negligible
- (v) Magnetic and electrical field effects are negligible
- (vi) Flow is inviscid

AERODYNAMICS AND ITS APPLICATIONS

To determine normal and shear stresses we must know the details of the flow field around the body. The flow field is described by:

Velocity

Pressure, and

Temperature

When the above quantities are known at all points in the flow field, including the body surface we say that the flow around a body is determined.

Velocity, pressure, temperature, and all flow properties are *related to each other*. These relationships are through rules/laws. These laws are:

Conservation of mass

Conservation of momentum

Conservation of energy

Equation of state

To determine the flow around a particular shape the boundary condition must be specified too. When applied to fluid flow problems conservation of mass is known as the continuity equation, the momentum equation is known as the Navier-Stokes equation in viscous flows and Euler's equation in inviscid flows, the conservation of energy results in the steady flow energy equation. The equation of state depends on the fluid through which the body moves. In the case of air, most often the assumption of a perfect gas is made and the standard equation of state is used.

AERODYNAMICS AND ITS APPLICATIONS

Perfect Gas

A perfect gas obeys the law:

$$p = \rho RT = \frac{\mathfrak{R}}{m} T \quad (1.1)$$

Where p is pressure, ρ is density, T is the absolute temperature, \mathfrak{R} is the universal gas constant, which has a value of 8314.3 J/kg mole K, and m is the molar mass. The molar mass for air is 28.966, R is the gas constant for a particular gas, and for air it is equal to $8314.3/28.966 = 287.04$

The specific heats for gases are: specific heat at constant volume and specific heat at constant pressure, which are given the symbols c_v and c_p respectively. The ratio of specific heats is known as $\gamma = \frac{c_p}{c_v}$.

The gas constant is also related to the specific heats of a gas through the well-known relationship

$$R = c_p - c_v \quad (1.2)$$

Throughout this introductory book, it will be assumed that the gas is calorically perfect, which implies that the temperature changes are not large and the gas temperature is below 2000K. This assumption helps us in assigning constant values to the specific heats of a perfect gas. It is also assumed here that no chemical reactions or magnetic or electrical effects are present.

Example 1.1

The pressure and temperature of a gas in a large chamber are found to be 600 kPa and 50°C respectively. Determine the gas density if the gas is (a) air (b) hydrogen.

AERODYNAMICS AND ITS APPLICATIONS

Solution:

It is assumed that air behaves as a perfect gas (although it is mixture of Oxygen a perfect gas and Nitrogen – also a perfect gas, as well as other gases and water vapour, dust particles etc.). From the law for perfect gases: $\rho = \frac{pm}{RT}$ and m equal to 28.97 for air and 2 for hydrogen, one obtains

$$\rho_{air} = \frac{600 \times 1000 \times 28.97}{8314.4 \times 323} = 6.47 \text{ kg/m}^3$$

and

$$\rho_{hydrogen} = \frac{600 \times 1000 \times 2}{8314.4 \times 323} = 0.4468 \text{ kg/m}^3$$

Suggestions for further reading

1. Shapiro, A. H. (1953). *The Dynamics and Thermodynamics of Compressible Fluid Flow*, Vols. 1 and 2. New York: Ronald Press.
2. Oosthuizen, P. H. & Carscallen, W. E. (1997). *Compressible Fluid Flow*, Singapore: McGraw-Hill.
3. Anderson, J. D. Jr. (2002). *Modern Compressible Flows with Historical Perspectives*, 3rd edition. New York: McGraw-Hill.

CHAPTER 2
CONSERVATION LAWS

Basic Equations for Steady, Inviscid, One Dimensional Compressible Flow

The behavior of a flow field about a body is governed by fundamental laws of physics. These are conservation of mass, conservation of momentum, conservation of energy and the equation of state. The flow field is computed by applying these rules together with the boundary conditions to obtain the pressure, velocity, and temperature on and around the body.

Conservation of mass:

The statement for the conservation of mass is:

$$\text{Rate of increase of mass in CV} = \text{rate of mass entering CV} - \text{rate of mass leaving CV}$$

Where, the first term on the LHS is zero for steady flow.

Conservation of momentum (newton's 2nd law):

The statement for conservation of momentum is:

$$\text{Net force on fluid In CV} = \text{rate of increase of momentum in CV} + \text{rate of momentum leaving CV} - \text{rate of momentum entering CV}$$

Where the first term on the rhs is zero for steady flow.

Conservation of energy:

The conservation of energy may be stated as:

AERODYNAMICS AND ITS APPLICATIONS

Rate of increase in internal + rate of enthalpy - rate of enthalpy = rate of heat - rate of work done
 & KE in CV & KE leaving CV & KE entering CV transfer into CV by fluid in CV

Where the first term on the LHS is zero for steady flow

The conservation laws when applied to a control volume may be written as:

1D, steady, compressible flow equations:

Conservation of mass (Continuity equation)

$$\rho_1 V_1 A_1 = \rho_2 V_2 A_2$$

Where, V is the velocity, and A is the area through which the fluid flows. The continuity equation for a differentially small element may be obtained by applying simple differentiation rules to the continuity equation given above:

$$\frac{d\rho}{\rho} + \frac{dV}{V} + \frac{dA}{A} = 0$$

The momentum equation under the assumptions of steady, inviscid flow, for 1 D application leads to Euler's equation:

$$-\frac{dp}{\rho} = VdV$$

Integrating along the x-direction yields:

AERODYNAMICS AND ITS APPLICATIONS

$$\frac{V^2}{2} + \int \frac{dp}{\rho} = \text{const.}$$

The Steady Flow Energy Equation obtained by applying the second law of thermodynamics to a fluid control volume leads to

$$h_2 + \frac{V_2^2}{2} = h_1 + \frac{V_1^2}{2} + q - w$$

where h is enthalpy, q is heat added, and w is the work done.

for zero work and calorically perfect gas $w = 0$

$h = c_p T$, and we get

$$c_p T_2 + \frac{V_2^2}{2} = c_p T_1 + \frac{V_1^2}{2} + q$$

for adiabatic flows $q = 0$, hence

$$c_p T + \frac{V^2}{2} = \text{const}$$

Where T_2 is the temperature at the second point and T_1 is the temperature at the first point in the flow.

The Equation of State for a perfect gas is given by

$$pv = RT$$

which can be reduced to

$$\frac{dp}{p} - \frac{d\rho}{\rho} - \frac{dT}{T} = 0$$

which is valid for a differentially short control volume.

AERODYNAMICS AND ITS APPLICATIONS

The above four fundamental equations; continuity, momentum, energy, and the equation of state are applied to one-dimensional inviscid compressible flows together with boundary conditions which describe The flow condition/flow environment and the shape of the body about which flow is to be computed.

Example

Measurements in a variable area duct indicate the temperature and velocity at a point to be 10°C and 100 m/s respectively. At another location downstream a temperature of -25°C is measured in the flow. Estimate the velocity at this location while assuming the flow to be adiabatic, inviscid and one-dimensional.

Solution

Since the only variables involved are velocity and temperature, and the flow is assumed to be adiabatic, a quick look at the fundamental equations of compressible fluid flow reveals that application of the steady flow energy equation is sufficient to determine the unknown flow variable- velocity in this case.

The steady flow adiabatic energy equation with zero work yields:

$$\frac{V_2^2}{2} = c_p T_1 + \frac{V_1^2}{2} - c_p T_2$$

Where $c_p=1006$ J/KgK, the temperatures and velocity on the RHS of the equation are known.

Their substitution yields $V_2 = 283.6$ m/s.

AERODYNAMICS AND ITS APPLICATIONS

Exercises

1. A gas with a molecular weight of 4 and specific heat ratio of 1.67 flows through a variable area duct. At a section of the duct the velocity is 150 m/s and temperature is 15°C. At another point in the duct the velocity is 75 m/s. Find the temperature at this location. Make suitable assumptions and state them.
2. Air being released from an automobile tire through a valve is found to have a temperature of 12°C. Assuming that the air temperature inside the tire is 30°C, compute the velocity of air as it leaves the tire valve. State your assumptions and justify them.
3. Using the standard equation of state, derive the equation of state for a differentially small element.
4. Using the continuity equation, derive the following equation:

$$\rho V \frac{dA}{dx} + \rho A \frac{dV}{dx} + VA \frac{d\rho}{dx} = 0$$

Suggestions for further reading

1. Shapiro, A. H. (1953). *The Dynamics and Thermodynamics of Compressible Fluid Flow*, Vols. 1 and 2. New York: Ronald Press.
2. Oosthuizen, P. H. & Carscallen, W. E. (1997). *Compressible Fluid Flow*, Singapore: McGraw-Hill.

AERODYNAMICS AND ITS APPLICATIONS

3. Anderson, J. D. Jr. (2002). *Modern Compressible Flows with Historical Perspectives*, 3rd edition. New York: McGraw-Hill.

CHAPTER 3

FUNDAMENTALS OF COMPRESSIBLE FLUID FLOW

ENTROPY

The entropy of a flow is related to its temperature and pressure through the specific heat and gas constant. The concept of entropy is useful to exclude flow processes which are physically impossible to exist.

The change in entropy between any two points in the flow is given by:

$$s_2 - s_1 = c_p \ln \left[\frac{T_2}{T_1} \right] - R \ln \left[\frac{p_2}{p_1} \right]$$

Recall the second law of Thermodynamics which states that for physically possible flow processes, the change in entropy between two states may be zero or positive. If the state conditions imply that the change in entropy is negative, such a flow situation or process cannot exist in reality. s refers to entropy, T is the temperature, and p is the pressure.

Using the relationship between the gas constant R and the specific heats, the following relationships between flow variables may be obtained for isentropic flows (no change in entropy):

$$\frac{T_2}{T_1} = \left(\frac{p_2}{p_1} \right)^{\frac{\gamma-1}{\gamma}}$$

AERODYNAMICS AND ITS APPLICATIONS

Using the perfect gas law in the above equation we can write for isentropic flows:

$$\frac{p_2}{p_1} = \left(\frac{\rho_2}{\rho_1}\right)^\gamma$$

Where ρ is the density.

The Mach number is defined as: Mach no. $M = \frac{V}{a}$

while the speed of sound : $a = \sqrt{\frac{\gamma p}{\rho}} = \sqrt{\gamma RT}$

Isentropic flow \Rightarrow Inviscid flow with no heat transfer

Basic Equations of Isentropic Flow

From Euler's equation and defn of speed of sound

$$\frac{dp}{\rho} = -\gamma M^2 \frac{dV}{V}$$

AERODYNAMICS AND ITS APPLICATIONS

From the Energy equation for adiabatic flows

$$\frac{dT}{T} = -(\gamma - 1)M^2 \frac{dV}{V}$$

and from the Equation of state

$$\frac{d\rho}{\rho} = -M^2 \frac{dV}{V}$$

for $M \approx 0.1$, $\frac{d\rho}{\rho}$ will be 1% of $\frac{dV}{V}$

for $M \approx 0.33$, $\frac{d\rho}{\rho}$ will be 10% of $\frac{dV}{V}$

for $M \approx 0.4$, $\frac{d\rho}{\rho}$ will be 16% of $\frac{dV}{V}$

Hence for $M < 0.3$, flows are modelled as incompressible flows.

AERODYNAMICS AND ITS APPLICATIONS

Speed of Sound :

Sound is generated by very weak pressure waves. Effects of viscosity and heat can be ignored. Generation of sound is an isentropic process.

The speed of sound a is defined as (following isentropic relationships) as :

$$a = \sqrt{\left(\frac{\partial p}{\partial \rho}\right)_s}$$

Mach Waves : Small disturbances in a flow result in the generation of Mach waves, which travel at the speed of sound.

Mach Cone : The enveloping cone which contains all the disturbances generated by a body moving at supersonic speeds is called a Mach cone, its vertex angle is called the Mach angle, defined below.

$$\text{Mach angle : } \sin \alpha = \frac{1}{M}$$

AERODYNAMICS AND ITS APPLICATIONS

One - dimensional Isentropic Flow

Isentropic Flow : Flow is adiabatic and inviscid

Governing Equations :

Using the equation of state, definition of speed of sound and energy or the momentum equation we get :

$$\frac{T_2}{T_1} = \frac{1 + \frac{1}{2}(\gamma - 1)M_1^2}{1 + \frac{1}{2}(\gamma - 1)M_2^2}$$

$$\frac{p_2}{p_1} = \left[\frac{1 + \frac{1}{2}(\gamma - 1)M_1^2}{1 + \frac{1}{2}(\gamma - 1)M_2^2} \right]^{\frac{\gamma}{\gamma - 1}}$$

$$\frac{\rho_2}{\rho_1} = \left[\frac{1 + \frac{1}{2}(\gamma - 1)M_1^2}{1 + \frac{1}{2}(\gamma - 1)M_2^2} \right]^{\frac{1}{\gamma - 1}}$$

Stagnation Conditions

Stagnation conditions are imaginary flow conditions that would exist, if the flow at any point in a fluid stream was brought to rest isentropically. For isentropic flows, stagnation conditions are those properties of the flow field where $V=0$. Stagnation quantities are denoted by a subscript of '0'

Stagnation quantities are the largest values of the quantity in the flow field.

AERODYNAMICS AND ITS APPLICATIONS

From previous equations for isentropic flow :

$$\frac{p_0}{p} = \left[1 + \frac{\gamma-1}{2} M^2 \right]^{\frac{\gamma}{\gamma-1}}$$

$$\frac{\rho_0}{\rho} = \left[1 + \frac{\gamma-1}{2} M^2 \right]^{\frac{1}{\gamma-1}}$$

$$\frac{T_0}{T} = \left[1 + \frac{\gamma-1}{2} M^2 \right]$$

Since Bernoulli's equation is no longer valid, the compressible flow equations can be used to relate the stagnation and static pressures measured by the Pitot-static tube to determine the free stream Mach number. As usual the nose measures the stagnation pressure. The isentropic flow equations can be used if the flow is subsonic. If the flow is supersonic, a shock will develop in front of the nose and the flow is no longer isentropic in the shock. The shock equations must also be used in this case to relate the stagnation pressure to the free stream Mach number.

Critical Conditions

Critical conditions of a flow field are those which would exist at a point if the flow were brought to a speed of $M=1$ at that point isentropically. Again, this could be an imaginary situation. Symbols for critical quantities have an asterisk '*' as a superscript. These quantities may be

AERODYNAMICS AND ITS APPLICATIONS

computed by using the following equations which are derived from the isentropic flow equations

$$\frac{T^*}{T} = \left[\frac{2}{\gamma+1} + \frac{\gamma-1}{\gamma+1} M^2 \right]$$

$$\frac{a^*}{a} = \left[\frac{2}{\gamma+1} + \frac{\gamma-1}{\gamma+1} M^2 \right]^{\frac{1}{2}}$$

easily:

$$\frac{p^*}{p} = \left[\frac{2}{\gamma+1} + \frac{\gamma-1}{\gamma+1} M^2 \right]^{\frac{\gamma}{\gamma-1}}$$

$$\frac{\rho^*}{\rho} = \left[\frac{2}{\gamma+1} + \frac{\gamma-1}{\gamma+1} M^2 \right]^{\frac{1}{\gamma-1}}$$

Setting $M = 0$ in the previous equations we can easily get the equations which provide a relationship between critical and stagnation conditions:

$$\frac{T^*}{T_0} = \frac{2}{\gamma+1}$$

$$\frac{p^*}{p_0} = \left[\frac{2}{\gamma+1} \right]^{\frac{\gamma}{\gamma-1}}$$

$$\frac{\rho^*}{\rho_0} = \left[\frac{2}{\gamma+1} \right]^{\frac{1}{\gamma-1}}$$

AERODYNAMICS AND ITS APPLICATIONS

Suggestions for further reading

1. Shapiro, A. H. (1953). *The Dynamics and Thermodynamics of Compressible Fluid Flow*, Vols. 1 and 2. New York: Ronald Press.
2. Oosthuizen, P. H. & Carscallen, W. E. (1997). *Compressible Fluid Flow*, Singapore: McGraw-Hill.
3. Anderson, J. D. Jr. (2002). *Modern Compressible Flows with Historical Perspectives*, 3rd edition. New York: McGraw-Hill.

CHAPTER 4
NORMAL SHOCKS

A sudden change in flow properties (velocity, temperature, pressure, density, speed of sound etc.) which occurs over a very thin region (a very short distance in the flow direction) is called a shock wave. The flow is perpendicular to the shock, before and after a normal shock.

TYPES OF SHOCK WAVES:

1. Normal
2. Oblique
3. Bow/curved
4. Shock waves can be stationary or moving w.r.t. the flow field.

STATIONARY NORMAL SHOCKS

Normal shocks usually occur in internal flows. Part of bow shocks may be considered as normal shocks. Application of conservation of mass yields:

AERODYNAMICS AND ITS APPLICATIONS

$$\rho_1 V_1 A_1 = \rho_2 V_2 A_2$$

Conservation of momentum yields:

$$V_2^2 - V_1^2 = (p_1 - p_2) \left(\frac{1}{\rho_1} + \frac{1}{\rho_2} \right)$$

Conservation of energy yields:

$$\frac{-V_1^2}{2} + C_p T_1 = \frac{V_2^2}{2} + C_p T_2$$

Using the equation of state, defns of the gas constant, and ratio of specific heat we obtain the Rankine - Hugoniot relationships for flow properties before and after the shock.

$$\frac{p_2}{p_1} = \frac{\left[\left(\frac{\gamma+1}{\gamma-1} \right) \frac{\rho_2}{\rho_1} - 1 \right]}{\left[\left(\frac{\gamma+1}{\gamma-1} \right) - \frac{\rho_2}{\rho_1} \right]}$$

AERODYNAMICS AND ITS APPLICATIONS

$$\frac{\rho_2}{\rho_1} = \frac{\left[\left(\frac{\gamma+1}{\gamma-1} \right) \frac{p_2}{p_1} + 1 \right]}{\left[\left(\frac{\gamma+1}{\gamma-1} \right) + \frac{p_2}{p_1} \right]}$$

$$\frac{V_1}{V_2} = \frac{\rho_2}{\rho_1}$$

$$\frac{T_2}{T_1} = \frac{\left[\left(\frac{\gamma+1}{\gamma-1} \right) + \frac{p_2}{p_1} \right]}{\left[\left(\frac{\gamma+1}{\gamma-1} \right) + \frac{p_1}{p_2} \right]}$$

The quantity $\frac{p_2}{p_1}$ is known as the "strength of the shock".

The second law of thermodynamics $ds \geq 0$, requires that p_2/p_1 be greater than 1 across a shock wave, where p_2 is the pressure downstream of a shock wave. From the expression for change in entropy across a shock it can be deduced that the upstream Mach number must be greater than or equal to 1. Since $\gamma > 1$, the flow downstream of the shock is subsonic as implied by the expression for the Mach number after the shockwave.

NORMAL SHOCK SLOWS DOWN THE FLOW!!

If a flow is isentropic and a shock occurs, the flow is non-isentropic only within the thin region of the shock. The flow upstream and the flow downstream of a shock will be isentropic.

AERODYNAMICS AND ITS APPLICATIONS

The stagnation temperature across a shock does not change, however the stagnation pressure always decreases across a shock.

$$\frac{P_{02}}{P_{01}} = \exp[-(s_2 - s_1)/R]$$

It is much more convenient to express the shock wave relations in terms of the Mach number.

The pressure ratio, the temperature ratio, density ratio and downstream Mach number in terms of the upstream Mach number are shown below:

$$\frac{p_2}{p_1} = \frac{2\gamma M_1^2 - (\gamma - 1)}{(\gamma + 1)}$$
$$\frac{\rho_2}{\rho_1} = \frac{(\gamma + 1)M_1^2}{2 + (\gamma - 1)M_1^2}$$
$$\frac{T_2}{T_1} = \left\{ \frac{[2\gamma M_1^2 - (\gamma - 1)][2 + (\gamma - 1)M_1^2]}{(\gamma + 1)^2 M_1^2} \right\}$$

and

$$M_2^2 = \frac{(\gamma - 1)M_1^2 + 2}{2\gamma M_1^2 - (\gamma - 1)}$$

These equations are presented in a tabular form for air ($\gamma = 1.4$) in the Appendix. Here the subscripts 1 and 2 refer to flow properties before and after the shock respectively.

Pitot tube in Supersonic Flow

The pressure(s) measured by a Pitot tube or a P-S tube placed in a supersonic flow need a closer look. Bernoulli's equation is not applicable for compressible flows. The nose of the Pitot tube

AERODYNAMICS AND ITS APPLICATIONS

which is rounded creates a bow shock wave. Near the nose the shock may be assumed to be normal. Normal shock equations are then applied to relate the free stream Mach number to the measured pressures. The static pressure may be measured at the tunnel wall or a Pitot-static tube used to measure the static pressure. The error is quite small.

Exercises

1. Sketch a Pitot-static tube in supersonic flow. Draw and identify the main features of the flow around the P-s tube. Show locations of static, total, and stagnation quantities. Label each quantity.
2. A pitot-static tube is attached to an F-22 fighter aircraft flying at supersonic speeds at a height of 15 km above the earth's surface. The difference between the pitot and static pressures is measured and found to be 400 kPa. Analyze the flow around the p-s tube and estimate the Mach number and velocity of the flow. Determine the stagnation, static and dynamic pressures in the flow field.

Suggestions for further reading

1. Shapiro, A. H. (1953). *The Dynamics and Thermodynamics of Compressible Fluid Flow*, Vols. 1 and 2. New York: Ronald Press.

AERODYNAMICS AND ITS APPLICATIONS

2. Oosthuizen, P. H. & Carscallen, W. E. (1997). *Compressible Fluid Flow*, Singapore: McGraw-Hill.
3. Anderson, J. D. Jr. (2002). *Modern Compressible Flows with Historical Perspectives*, 3rd edition. New York: McGraw-Hill.

CHAPTER 5
OBLIQUE SHOCKS

Shocks which are straight (not curved) but are at an angle to the initial flow direction are known as oblique shocks. In general an oblique shock changes the direction of the incoming flow.

Since there is no change in momentum parallel to an oblique shock, the normal shock equations can be easily modified to analyze oblique shock waves.

Consider β as the angle made by the shock wave to the flow direction, and δ as the angle through which the flow turns away from its initial flow direction.

The velocity before the shock is V_1 and after the shock V_2 .

The normal shock equations can be used to analyze oblique shock waves by using the following substitutions in the equations for normal shock waves.

$$V_{1n} = V_1 \sin \beta$$

$$V_{2n} = V_2 \sin(\beta - \delta)$$

with these substitutions the governing continuity, momentum and energy equations for oblique shocks reduce to

$$\rho_1 V_1 \sin \beta = \rho_2 V_2 \sin(\beta - \delta)$$

$$p_1 - p_2 = \rho_2 (V_1 \sin \beta)^2 - \rho_1 [V_2 \sin(\beta - \delta)]^2$$

$$\frac{2\gamma}{\gamma - 1} \left[\frac{p_2}{\rho_2} - \frac{p_1}{\rho_1} \right] = (V_1 \sin \beta)^2 - [V_2 \sin(\beta - \delta)]^2$$

AERODYNAMICS AND ITS APPLICATIONS

Entropy considerations imply that a normal shock exists only if the upstream Mach number is >1 .

Hence an oblique shock will exist only if

$$M_1 \sin \beta \geq 1$$

The minimum value of $\sin \beta$ is therefore $1/M_1$, that is the minimum shock angle is the Mach angle.

The maximum value of β then is 90 degrees, a normal shock.

Since the flow behind a normal shock is subsonic i.e. $M_2 < 1$. For an oblique shock wave this condition is written as

$$M_2 \sin(\beta - \delta) \leq 1$$

Now M_2 can be supersonic!

A flow changes direction after going through an oblique shock. The angle (δ) through which the flow turns is computed using the following expression, derived using conservation of mass principle and the flow geometry:

$$\tan \delta = \frac{2 \cot \beta (M_1^2 \sin^2 \beta - 1)}{2 + M_1^2 (\gamma + \cos 2\beta)}$$

Here $\delta = 0$ when $\beta = 90^\circ$
and $\beta = \sin^{-1}(1/M_1)$

the upper limit being the case of a normal shock and the lower a weak Mach wave. In both these cases the flow does not change direction after the shock. The maximum value of δ lies in between. See the Appendix for a chart which shows the relationships between M_1 , β , and δ .

For $\delta < \delta_{\max}$ two values of the turning angle are possible. The solution corresponding to the larger value of β is termed the 'strong shock' solution. The other is termed the 'weak shock' solution.

Prandtl-Meyer Expansion

Steady supersonic flow over expansion corners (convex corner). Following geometrical reasoning, an oblique shock wave is not possible at a corner where the flow turns through a negative angle. It violates the second law of thermodynamics ($M_2 > M_1$). Applying the equations for conservation of mass, definition of speed of sound, the energy equation to a supersonic flow undergoing an infinitesimal change in direction $d\theta$, we obtain the following expressions for the corresponding change in velocity, pressure, temperature and density:

$$\frac{dV}{V} = \frac{-d\theta}{\sqrt{M^2 - 1}}$$

$$\frac{dp}{p} = \frac{\gamma M^2}{\sqrt{M^2 - 1}} d\theta$$

$$\frac{d\rho}{\rho} = \frac{M^2}{\sqrt{M^2 - 1}} d\theta$$

$$\frac{ds}{R} = 0$$

$$\frac{dM}{M} = \left[1 + \frac{\gamma - 1}{2} M^2 \right] \frac{(-d\theta)}{\sqrt{M^2 - 1}}$$

Supersonic flows over a compression corner (concave corner, $d\theta > 0$) result in:

Oblique shocks through convergence of Mach waves. Use oblique shock equations and charts.

Supersonic flows over an expansion corner (Convex corner, $d\theta < 0$) result in:

AERODYNAMICS AND ITS APPLICATIONS

Weak mach waves (expansion fan), with fully isentropic flow. Use isentropic flow equations and tables. The angles associated with the supersonic flow over an expansion corner are shown below:

Here α_1 is the Mach angle the first Mach wave makes w.r.t. the initial flow direction, α_2 is the Mach angle the last Mach wave makes with the final flow direction, δ is the flow turning angle, and β is the angle made by the last Mach wave w.r.t. the initial flow direction.

The angles are related to the Mach numbers as follows:

$$\sin\alpha_1 = \frac{1}{M_1}, \quad \sin\alpha_2 = \frac{1}{M_2}, \quad \beta = \alpha_2 - \delta$$

Exercises

1. An air stream flowing at a Mach number of 3.5 is expanded around a concave corner with an angle of 15° leading to the generation of an expansion wave. Some distance downstream of this the air flows around a concave corner leading to the generation of an oblique shock wave and returning the flow to its original direction. If the pressure in the initial flow is 80 kPa, find the static and stagnation pressure downstream of the oblique shock. Draw a diagram and show all physical processes.
2. An aircraft is flying at Mach 4, with an ambient pressure of 25 kPa and temperature of 250K. The air entering the engine is slowed to subsonic velocities by moving through two oblique shocks each of which turn the flow through angle of 12° and by then passing it through a normal shock wave. After the normal shock the flow is decelerated to a speed of Mach 0.15 before it enters the combustion zone. In another case of intake design for

AERODYNAMICS AND ITS APPLICATIONS

the same engine, the flow is decelerated through a single normal shock instead through a combination of oblique shocks and a normal shock.

(a) Draw a diagram for each case. Show and label important features.

(b) Compute the pressures (static and stagnation) and temperatures (static and stagnation) at the entrance to the combustion zone in both cases.

Suggestions for further reading

1. Shapiro, A. H. (1953). *The Dynamics and Thermodynamics of Compressible Fluid Flow*, Vols. 1 and 2. New York: Ronald Press.
2. Oosthuizen, P. H. & Carscallen, W. E. (1997). *Compressible Fluid Flow*, Singapore: McGraw-Hill.
3. Anderson, J. D. Jr. (2002). *Modern Compressible Flows with Historical Perspectives*, 3rd edition. New York: McGraw-Hill.

CHAPTER 6

FLOW THROUGH VARIABLE AREA DUCTS

Applying the conservation equations and the equation of state for steady, inviscid, compressible 1D flows, the equations which relate the change in flow properties to a finite change in area are given as:

$$\frac{d\rho}{\rho} = -M^2 \frac{dV}{V}$$

$$\frac{dA}{A} = (M^2 - 1) \frac{dV}{V}; \text{ for } M < 1, \text{ dA and dV have opposite signs; for } M > 1, \text{ dA and dV have same signs.}$$

$$\frac{dT}{T} = -\frac{V^2}{c_p T} \frac{dV}{V} = -(\gamma - 1) M^2 \frac{dV}{V}$$

and

$$\frac{dA}{A} = \frac{(M^2 - 1)}{1 + \left(\frac{\gamma - 1}{2}\right) M^2} \frac{dM}{M}; \text{ for } M < 1, \text{ dA and dM have opposite signs, for } M > 1 \text{ they have the same signs.}$$

For isentropic flow through nozzles

AERODYNAMICS AND ITS APPLICATIONS

The mass flow rate is given by :

$$\dot{m} = \rho_0 A_2 \left(\frac{p_2}{p_0} \right)^{\frac{1}{\gamma}} \left\{ \left(\frac{2\gamma}{\gamma-1} \right) \left(\frac{p_0}{\rho_0} \right) \left[1 - \left(\frac{p_2}{p_1} \right)^{\frac{\gamma-1}{\gamma}} \right] \right\}^{\frac{1}{2}}$$

The areas at two locations in the flow region are related to other flow properties as follows :

$$\frac{A_2}{A_1} = \left(\frac{p_1}{p_2} \right)^{\frac{1}{\gamma}} \left[\frac{1 - \left(\frac{p_1}{p_0} \right)^{\frac{\gamma-1}{\gamma}}}{1 - \left(\frac{p_2}{p_0} \right)^{\frac{\gamma-1}{\gamma}}} \right]^{\frac{1}{2}}$$

The critical flow properties are given as follows:

$$V^{*2} = \frac{2}{\gamma+1} a_0^2$$

$$\frac{p^*}{p_0} = \left(\frac{2}{\gamma+1} \right)^{\frac{\gamma}{\gamma-1}}$$

$$A^* = \frac{\dot{m}}{\sqrt{\rho_0} \rho_0} \left(\frac{2}{\gamma+1} \right)^{-\frac{\gamma+1}{2(\gamma-1)}}$$

Flow properties for isentropic flow through a nozzle are available in the isentropic flow tables.

These are given as a function of the local Mach number M.

Operating Characteristics of Nozzles

Assuming that the upstream stagnation properties ahead of the nozzle are kept constant, and the pressure downstream of the nozzle (termed back pressure) is varied.

The phenomenon of 'Choking' is observed.

Definition of Choking: mass flow rate remains constant for all back pressures below a certain critical pressure.

When $p_b > p^*$, the exit plane velocity, the exit plane pressure and the mass flow rate are given as follows:

$$p_e = p_b$$

$$V_e = \left\{ \left(\frac{2\gamma}{\gamma-1} \right) \left(\frac{p_0}{\rho_0} \right) \left[1 - \left(\frac{p_b}{p_0} \right)^{\frac{\gamma-1}{\gamma}} \right] \right\}^{\frac{1}{2}}$$

and

$$\dot{m} = \rho_0 A_e \left(\frac{p_b}{p_0} \right)^{\frac{1}{\gamma}} \left\{ \left(\frac{2\gamma}{\gamma-1} \right) \left(\frac{p_0}{\rho_0} \right) \left[1 - \left(\frac{p_b}{p_0} \right)^{\frac{\gamma-1}{\gamma}} \right] \right\}^{\frac{1}{2}}$$

When $p_b \leq p^*$:

$$\frac{p_e}{p_0} = \left(\frac{2}{\gamma+1} \right)^{\frac{\gamma}{\gamma-1}}$$

$$V_e = \sqrt{\left(\frac{2\gamma}{\gamma+1} \right) \frac{p_0}{\rho_0}}$$

39

$$\dot{m} = \sqrt{\gamma p_0} \rho_0 A_e \left(\frac{2}{\gamma+1} \right)^{\frac{\gamma+1}{2(\gamma-1)}}$$

all of these quantities being constants.

AERODYNAMICS AND ITS APPLICATIONS

The flow in a convergent divergent nozzle shows a range of very interesting behavior. Assuming the flow properties at the inlet of the nozzle to remain constant, and the back pressure to vary, the flow can be fully subsonic, subsonic-supersonic, with shocks and subsonic-supersonic isentropic (design condition).

For $p_b < p_{bcr}$, the flow remains fully subsonic throughout the nozzle, behaves like a venturi, Bernoulli's equation is not valid!

For $p_b > p_{bcr}$, the flow is subsonic in the converging section, sonic at the throat, and supersonic as well as subsonic in parts of the nozzle downstream of the throat.

At the design condition/ design back pressure, the nozzle contains no shocks inside, flow is subsonic in the converging section and supersonic in the entire diverging section. No shock waves inside or outside the nozzle.

'Over expanded nozzle': This condition exists when the back pressure higher is above the design back pressure but lower than the back pressure at which a normal shock appears at the exit plane. There are no normal shocks inside the nozzle. Outside the nozzle, oblique shock waves exist which interact with each other.

'Under expanded nozzle': This condition exists when the back pressure is reduced below the design back pressure. Expansion waves (Prandtl-Meyer flow) exist in the flow outside the nozzle exit plane.

AERODYNAMICS AND ITS APPLICATIONS

Exercises

1. Air is expanded through a convergent-divergent nozzle from a large reservoir in which the pressure and temperature are 300 kPa and 310 K respectively. A normal shock wave occurs at a point in the nozzle where the Mach number is 2.5. The air is then brought to rest in a second large reservoir.
2. Find the pressure and temperature in this second reservoir.
3. Clearly state and justify the assumptions you have made in arriving at the solution.
4. Draw the nozzle and the reservoirs, show the shock and label all flow quantities in the flow field.
- 5.

Suggestions for further reading

1. Shapiro, A. H. (1953). *The Dynamics and Thermodynamics of Compressible Fluid Flow*, Vols. 1 and 2. New York: Ronald Press.
2. Oosthuizen, P. H. & Carscallen, W. E. (1997). *Compressible Fluid Flow*, Singapore: McGraw-Hill.
3. Anderson, J. D. Jr. (2002). *Modern Compressible Flows with Historical Perspectives*, 3rd edition. New York: McGraw-Hill.

CHAPTER 7

INTRODUCTION TO AERODYNAMIC DRAG

The aerodynamic forces are lift and drag. Lift is the force which acts perpendicular to the incoming flow and drag is defined as aerodynamic force which resists the movement of the object through air. The aerodynamics forces are resulted from the combination of the shear and pressure forces.

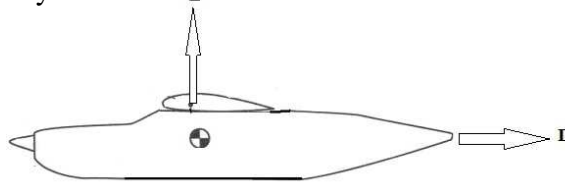


Figure 7.1 Aerodynamics Forces

Types of Drag

The drag force is divided into parasite drag, induced drag and wave drag. The parasite drag is also called zero lift drag which consists of form drag, skin friction drag, interference drag and shock induced separation drag. The induced drag also known as drag due to the lift and it includes trim drag and wave drag.

Form Drag

Form drag is defined as the drag due to the boundary layer normal pressure variation. This drag is due to the shape of the body and occurs when a separated wake is formed behind the body.

AERODYNAMICS AND ITS APPLICATIONS

Skin Friction Drag

Skin friction drag is drag due to the viscosity effects of the air. It results from the friction between solid surface and air. It is associated with growing of boundary layer region near the solid surface. The boundary layer region is defined as a low kinetic energy region where the local velocity of the flow is less than free stream velocity.

Interference Drag

The interference drag is drag due to flow interference between aircraft components such as wing/fuselage and tail/fuselage. The interference results in modification of pressure distribution on those surfaces and leads to higher parasite drag.

Shock Induced Separation Drag

It is defined as drag due to the flow separation by the formation of the shock wave, which leads to drag increase and reduction of the lift.

Induced Drag

It is defined as drag due to the formation of the tip vortices. Induced drag is generated as a result of lift. This drag force occurs in airplanes due to wings or a lifting surface.

Trim Drag

AERODYNAMICS AND ITS APPLICATIONS

It is the extra drag generated during the trimming operation of an aircraft. This is due to change in the values of the lift and drag resulting from the deflection of the trim tab.

Wave Drag Due to the Lift

Wave drag due to lift is for supersonic flight what induced drag is in subsonic flight. It highly depends on the angle of attack and sweep angle of the wing.

Equation of Drag

Drag is defined by the following relation:

$$D = \frac{1}{2} \rho V^2 C_D S \quad (7.1)$$

Where ρ is the air density, V is the relative free stream speed, C_D is the drag coefficient, and S is the surface area. The subsonic drag coefficient can be written as

$$C_D = C_{D,0} + C_{D,i} + C_{D,w} \quad (7.2)$$

$$\text{Where } C_{D,0} = C_{D,p} + C_{D,f} \quad (7.3)$$

And $C_{D,0}$, $C_{D,i}$, $C_{D,w}$, $C_{D,p}$ and $C_{D,f}$ are presenting respectively parasite, induced, wave, normal pressure and friction drag coefficients.

Relation between Drag and Body Shape

AERODYNAMICS AND ITS APPLICATIONS

The contribution of each drag type on the total drag is highly dependent on the geometry of the body. The drag for aerodynamically shaped (streamlined) body is dominated by skin friction drag; and normal pressure drag is dominant for bluff bodies. The Induced drag is considered only for three dimensional bodies. The contribution of the profile drag and skin friction drag on the parasite drag is dependent on the shape of the body. The airfoil shape has approximately 10% profile drag and 90% friction drag, while the circular or spherical shape has around 90% profile drag and 10% friction drag. Figure 7.2 shows the effect of streamlining on drag reduction. If same frontal area and velocity are used, a streamlined body will always give lower drag than a bluff body. Table 7.1 shows the drag coefficient of two dimensional bodies based on frontal area. It also shows the importance of the flow type on the drag coefficient for cylinder body. The importance of the body dimension on drag for three dimensional bodies is shown in table 7.2

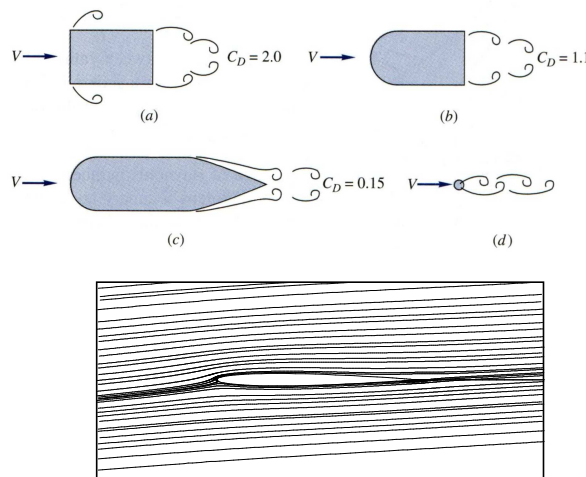
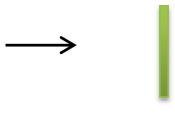











Figure 7.2: Effect of the streamlining on the drag coefficients




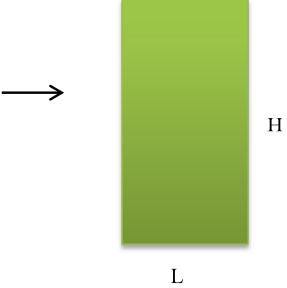




AERODYNAMICS AND ITS APPLICATIONS

Table 7.1: Drag coefficient of 2D body at $R_e \geq 10^4$ (1)

AERODYNAMICS AND ITS APPLICATIONS

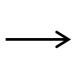

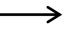

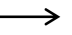

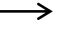

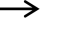

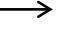

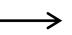

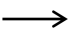
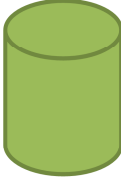
	Shape	CD based on frontal area
Plate		2.0
Thin plate normal to wall		1.4
Half - tube		1.2
		2.3
Half - Cylinder		1.2
		1.7
Equilateral triangle		2.0
		1.6
Hexagon		1.0
		0.7

AERODYNAMICS AND ITS APPLICATIONS

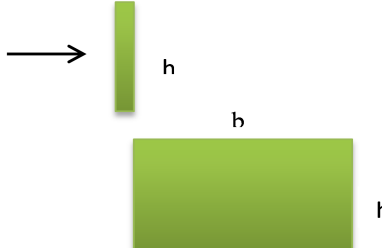

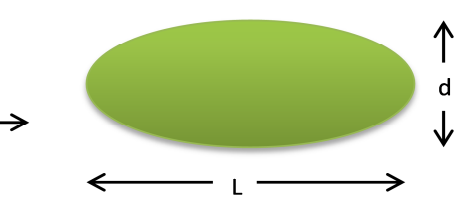
Shape		CD based on frontal area	
Square Cylinder		2.1	
		1.6	
Round Nosed Section		L/H	0.5 1 2 4 5
		C_D	1.16 .90 .70 .68 .64
Flat Nosed Section		L/H	0.1 0.4 0.7 1.2 2.0 2.5 3.0 6.0
		C_D	1.9 2.3 2.7 2.1 1.8 1.4 1.3 0.9
Elliptical Cylinders	1.1 	Laminar	Turbulent
	2.1 	1.2	0.3
	4.1 	0.6	0.2
	8.1 	0.35	0.15
		0.25	0.1

AERODYNAMICS AND ITS APPLICATIONS

Table 7.2 Drag of three dimensional Bodies at $R_e \geq 10^4$ (1)

Shape		CD based on frontal area									
Disk			1.17								
Cup			1.4								
			0.4								
Cube			1.07								
			0.81								
Cone			θ	10°	20°	30°	40°	60°	75°	90°	
			C_D	0.30	0.40	0.55	0.65	0.80	1.05	1.15	
Parachute			1.2								
Short Cylinder, laminar flow			L/D	1	2	3	5	10	20	40	∞
			C_D	.64	.68	.72	.74	.82	.91	.98	1.20

AERODYNAMICS AND ITS APPLICATIONS

Shape	Ratio	C_D based on frontal area		
Rectangular plate 	b/h	1	1.18	
		5	1.2	
		10	1.3	
		20	1.5	
		∞	2.0	
Flat-faced cylinder 	l/d	0.5	1.15	
		1	0.90	
		2	0.85	
		4	0.87	
		8	0.99	
Ellipsoid 	L/d		Laminar	Turbulent
		0.75	0.5	0.2
		1	0.47	0.2
		2	0.27	0.13
		4	0.25	0.1
8	0.2	0.08		

Flow separation

In aerodynamics flow separation is defined as a condition where the incoming air past a stationary body separates from the body's surface, generates a region of circulation (vortices) and forms wake region. Flow separation creates pressure drag. The separation is due to the growing of the viscous boundary layer at the surface of the body which is accompanied with an

AERODYNAMICS AND ITS APPLICATIONS

increase in pressure and reduction of the velocity in the direction of the flow. The velocity of the flow ranges from zero at the surface of the body (No slip condition) to 99% of free stream at the edge of the boundary layer.

Separation over airfoil highly depends on free stream Reynolds number, airfoil shape and angle of attack. Figure 7.3 shows flow separation over the top surface of NACA 0012 airfoil at $Re=1.6 \times 10^5$. At angle attack of 13° the flow is still attached to the airfoil and clear separation appears at trailing edge of the airfoil. At angle of attack of 18° massive flow separation occurs over the top surface which leads to higher pressure drag.

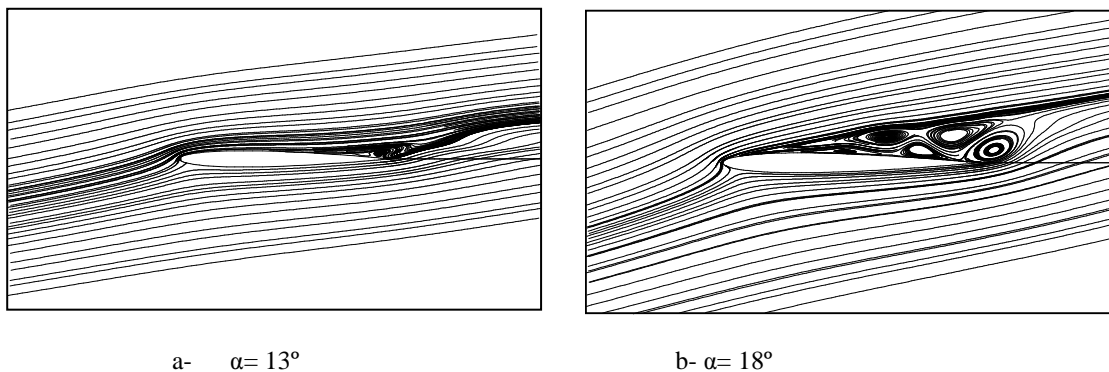
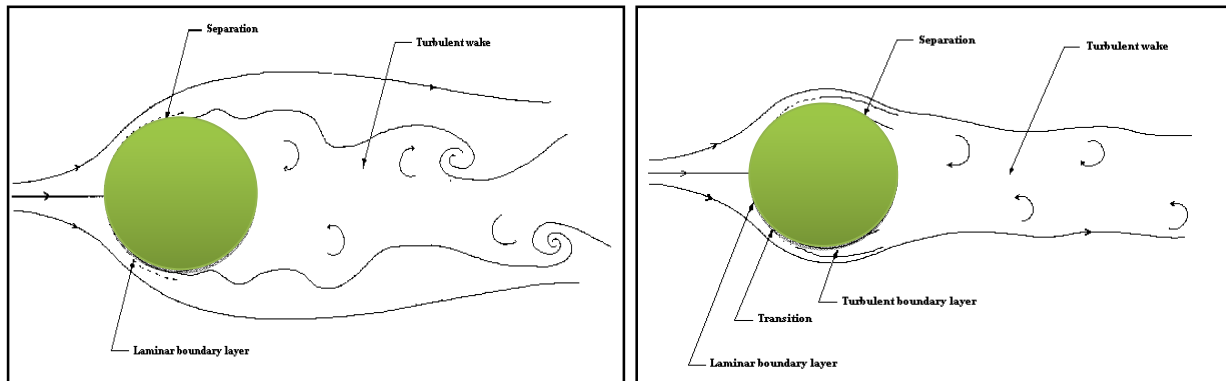


Figure 7.3 Stream Lines Over NACA 0012 Airfoil at $Re=1.6 \times 10^5$

For circular cylindrical body, the separation depends on the Re_{ed} of the body. As shown in figure 7.4(a) separation of the laminar flow is taking place at points on the front half of the cylinder, creating large wake and higher drag. Figure 7.4(b) shows that the separation under turbulent flow is taking place at rear half of the cylinder where the reduction of the wake width is seen. This

AERODYNAMICS AND ITS APPLICATIONS

reduction of the wake width is associated with a much lower drag. Pressure drag estimates for about 90% of the total drag, the remaining 10% is due to skin-friction drag. Most skin-friction drag is produced on the front half of the cylinder body.



(a) Laminar separation

(b) Turbulent separation

Figure 7.4 Separation over circular cylinder

References

- 1- Frank M. White, (2003), Fluid Mechanics, McGraw Hill

CHAPTER 8

TRANSONIC FLOW AND CRITICAL MACH NUMBER

Introduction

The critical Mach number (M_c) is defined as the free stream Mach at which the flow over an airfoil reaches the sonic speed. Flying at Mach higher than critical Mach number leads to formation of region of supersonic flow. As shown in figure 8.1, the first sonic Mach appears on the airfoil at minimum pressure point (suction point). Then the region of supersonic flow grows outwards and moves downstream as Mach number is increased. Flying at free stream Mach number slightly higher than critical Mach number creates a shock wave which causes higher drag, sudden loss of lift and rapid changes in the location of center of pressure. The increase in the drag is directly related to the strength of the shock waves. Predicting the critical Mach number of an airfoil is one of the most important problems in compressible flow.

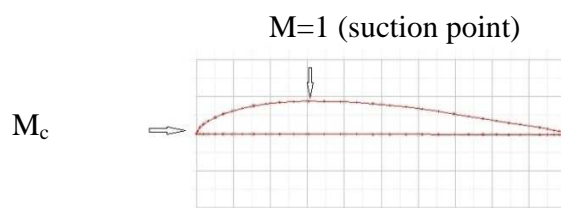


Figure 8.1 Critical Mach number

The value of M_c for any given airfoil depends on the airfoil shape and the angle of attack.

Equation of Motion

The equation of motion for 2 - D inviscid compressible flow is given as

$$(1 - M_\infty^2) \frac{\partial^2 \phi}{\partial x^2} + \frac{\partial^2 \phi}{\partial y^2} = 0 \quad (8.1)$$

Equation 8.1 was solved mathematically by Prandtl-Glauert. The resultant relation is

$$Cp_{comp} = \frac{C_{p_{incomp}}}{\sqrt{1 - M_\infty^2}} \quad (8.2)$$

Where Cp_{comp} , and Cp_{incomp} are the compressible and incompressible coefficients, respectively.

The factor $\sqrt{1 - M_\infty^2}$ in equation 8.2 is called Glauert's factor

For critical Mach number, equation 8.2 can be rewritten as

$$Cp_{crit.} = \frac{C_{p_{min}}}{\sqrt{1 - M_c^2}} \quad (8.3)$$

The value of M_c for an airfoil can be found from the value of the minimum pressure point, $C_{p_{min}}$.

If the low-speed data on the airfoil is available, the incompressible C_p values can be converted to values at a given subsonic Mach number using relation 8.2.

AERODYNAMICS AND ITS APPLICATIONS

In similar manner the lift coefficient of the incompressible subsonic flow can be related to the lift coefficient of the compressible flow as

$$C_{L_{comp}} = \frac{C_{L_{incomp}}}{\sqrt{1 - M_{\infty}^2}} \quad (8.4)$$

Where, C_{L_i} represents the incompressible lift coefficient.

For compressible flow over swept wing equation 8.4 can be rewritten as

$$C_{L_{comp}} = \frac{C_{L_{incomp}}}{\sqrt{1 - M_{\infty}^2 \cos^2 \Lambda}} \quad (8.5)$$

Where Λ is the sweep angle of the wing

Isentropic Relationships:

The isentropic relations are introduced as

$$C_{p_{crit}} = \left[\frac{p^*}{p_{\infty}} - 1 \right] \frac{2}{\gamma M_{crit}^2} \quad (8.6)$$

Where P^* is the sonic pressure and (p^*/p) is given as

$$\frac{p^*}{p_{\infty}} = \left(\frac{a^*}{a_{\infty}} \right)^{2\gamma/\gamma-1} \quad (8.7)$$

Where a^* and a represent the speed of sound and local sound speed, respectively and defined as.

$$\left(\frac{a^*}{a_\infty}\right)^2 = M_{crit}^2 \frac{\gamma-1}{\gamma+1} + \frac{2}{\gamma+1} \quad (8.8)$$

Equation 8.6 to equation 8.8 leads to the following relation

$$C_{p_{crit}} = \left[\left(\frac{\gamma-1}{\gamma+1} M_{crit}^2 + \frac{2}{\gamma+1} \right)^{\frac{\gamma}{\gamma-1}} - 1 \right] \frac{2}{\gamma M_{crit}^2} \quad (8.9)$$

Predication of Critical Mach

Equation 8.3 combined with equation 8.9 leads to the following relation

$$\frac{Cp_{min}}{\sqrt{1-M_c}} = \left[\left(\frac{\gamma-1}{\gamma+1} M_c^2 + \frac{2}{\gamma+1} \right)^{\frac{\gamma}{\gamma-1}} - 1 \right] \frac{2}{\gamma M_c^2} \quad (8.10)$$

Equation 8.10 can be used to predict the critical Mach number for any given airfoil if the incompressible flow minimum pressure point is known for that particular airfoil.

Predication of the compressible flow pressure distribution

The low speed pressure coefficient data over any given airfoil can be used in equation 8.2 to predict the compressible pressure distribution for that particular airfoil.

AERODYNAMICS AND ITS APPLICATIONS

Application

Example 1

Estimate the critical Mach number for NACA 0012 airfoil at 10° angle of attack. The pressure coefficient distribution over this airfoil, measured in wind tunnel at low speed is given in figure 8.2. Compute and draw the pressure distribution curve at Mach number of 0.75.

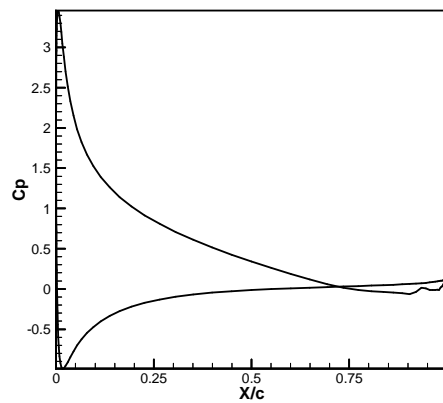


Figure 8.2: Pressure distribution over NACA0012 airfoil at angle of attack of 10°

Answer

AERODYNAMICS AND ITS APPLICATIONS

Part 1:

Equation 8.10 is used to estimate the critical Mach for the given airfoil. From figure 8.2 the minimum pressure point is -1. Eq. 8.10 can be written as

$$\frac{-1.0}{\sqrt{1-M_c}} = \left[\left(\frac{1.4-1}{1.4+1} M_c^2 + \frac{2}{1.4+1} \right)^{\frac{1.4}{1.4-1}} - 1 \right] \frac{2}{1.4 M_c^2} \quad (8.11)$$

Equation 8.11 is solved numerically using the guessing method. The M_c in the right hand side of the equation is guessed and then used to compute M_c in the other side of the equation. The difference (error) between the guessing and computed M_c is checked. If the difference is less than target error, the guessing M_c is the solution; otherwise new guessing M_c should be selected. The steps are repeated till the solution is found.

```

c*****
c  Program in Fortran to solve critical Mach Number Problem
c  (Gamma=1.4, Cpmin=-1, error=0.001)
c*****

open(1,file='data.in')
open(2,file='result.out')

read(1,*)
read(1,*)gamma,cp,am0,error0
write(2,100)
error1=10000
aa=gamma+1
bb=gamma-1

```

AERODYNAMICS AND ITS APPLICATIONS

```
cc=gama/(bb)
am=am0
c*****Right hand side of equation 2.11*****
5  rhs=cp/sqrt(1-am**2)
C*****Left hand side of equation 2.11*****
alhs=(((bb/aa)*am**2)+(2/aa)**cc-1)*(2/(gama*(am**2)))
c*****Difference (Error)*****
error=abs(rhs-alhs)
if(error.lt.error0)then
write(2,110)am,alhs,rhs,error
write(2,*)'Mcr=',am
stop
else
write(2,110)am,alhs,rhs,error
endif
if(error.lt.error1)then
am=am-0.001
else
am=am+.001
endif
error1=error
go to 5
100 format(7x, 'Mcr', 8x, 'LHS', 8X, 'RHS',7x,'error')
110 format(1x,4(1x,f10.5))
200 stop
End
```

AERODYNAMICS AND ITS APPLICATIONS

Program output

Mc	LHS	RHS	error
0.62700	-1.13188	-1.28367	0.15179
0.62600	-1.13754	-1.28234	0.14480
0.62500	-1.14323	-1.28103	0.13780
0.62400	-1.14894	-1.27972	0.13078
0.62300	-1.15468	-1.27841	0.12374
0.62200	-1.16044	-1.27711	0.11667
0.62100	-1.16623	-1.27582	0.10959
0.62000	-1.17205	-1.27453	0.10249
0.61900	-1.17789	-1.27325	0.09536
0.61800	-1.18377	-1.27198	0.08821
0.61700	-1.18967	-1.27071	0.08104
0.61600	-1.19559	-1.26945	0.07385
0.61500	-1.20155	-1.26819	0.06664
0.61400	-1.20753	-1.26694	0.05941
0.61300	-1.21354	-1.26569	0.05215
0.61200	-1.21958	-1.26445	0.04487
0.61100	-1.22565	-1.26322	0.03757
0.61000	-1.23175	-1.26199	0.03024
0.60900	-1.23787	-1.26077	0.02289
0.60800	-1.24403	-1.25955	0.01552
0.60700	-1.25021	-1.25834	0.00813
0.60600	-1.25642	-1.25713	0.00071

The answer is $M_c = 0.606$

Part 2:

AERODYNAMICS AND ITS APPLICATIONS

For pressure distribution at $M=0.75$, equation the following Eq. 8.4 can be used as

$$C_{p_{comp}} = \frac{C_{p_{incomp}}}{\sqrt{1-M_{\infty}^2}} = \frac{C_{p_{incomp}}}{\sqrt{1-0.75^2}} \quad (8.12)$$

Where $C_{p_{incomp}}$ can be obtained from figure 8.2 at various x/c . Examples of the results

At $x/c=0.25$, upper surface $C_{p_{incomp}}=-0.2$ leads to $C_{p_{comp}}= -0.457$

For lower surface $C_{p_{incomp}}=0.8$ leads to $C_{p_{comp}}= 1.83$

By selecting a few points along x/c for upper and lower surfaces, equation 8.12 can be used to obtain compressible pressure distribution at Mach number of 0.75.

CHAPTER 9

ESTIMATION OF SUPERSONIC AERODYNAMICS FORCES USING LINEARIZED THEORY

Introduction

Supersonic flow over body is associated with the formation of the shock waves. The properties of the flow across a shock wave show an extremely rapid rise in pressure, temperature and density. Supersonic flow over sharp leading edge airfoil produces two Mach waves and Prandtl-Meyer expansion around turning corner. Formation of shock waves cause load changes on the surface of the airfoil. Modification of the aerodynamic loads will change the lift, leads to a moving after of the center of pressure (pitching down moment) and rapid increase in drag force. Supersonic linearized theory as proposed by Ackeret can be used to predict the supersonic aerodynamic forces coefficients.

Equation of Motion

The equation motion for supersonic inviscid flow is derived from equation 8.1 and written as

$$(M_{\infty}^2 - 1) \frac{\partial^2 \phi}{\partial x^2} - \frac{\partial^2 \phi}{\partial y^2} = 0 \quad (9.1)$$

AERODYNAMICS AND ITS APPLICATIONS

This modification to equation 8.1 is necessary to avoid having negative square root for Glauert's factor. The mathematical solution of equation 9.1 as proposed by Ackeret results in the following relation

$$C_p = \frac{2\varepsilon}{\sqrt{M_\infty^2 - 1}} \quad (9.2)$$

Where ε is the local inclination of the surface to the direction of motion and it has positive value when the flow is being turned away from the free stream direction, and negative when it is being turned back.

Application

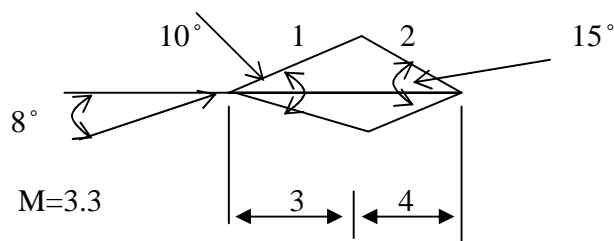
Equation 9.2 can be used to estimate the lift, wave drag, and moment coefficients of the supersonic flow over sharp edged airfoil, flat plate and double wedge at angle of attack.

1- Double Wedge airfoil

In double wedge airfoil, the value of ε is highly dependent on angle of attack and thickness. For symmetrical airfoil the contribution of the thickness is zero.

Example

For symmetrical double wedge airfoil as shown below,



AERODYNAMICS AND ITS APPLICATIONS

$$2c/3 \quad c/3$$

Compute

- i- Lift coefficient
- ii- Drag (wave) coefficient
- iii- Moment coefficient (about leading edge)
- iv- Center of pressure coefficient

Answer

$$\epsilon_1 = -8^\circ + 5^\circ = -3^\circ = -0.05236 \text{ radian}$$

$$\epsilon_2 = -3^\circ - 5^\circ - 7.5^\circ = -15.5^\circ = -0.2705 \text{ radian}$$

$$\epsilon_3 = 5^\circ + 8^\circ = 13^\circ = 0.2269 \text{ radian}$$

$$\epsilon_4 = 13^\circ - 5^\circ - 7.5^\circ = 0.5^\circ = 0.00873 \text{ radian}$$

i-

$$C_L = \frac{2}{\sqrt{M^2 - 1}} \left(\frac{2}{3} (0.2269 - (-0.05236)) + \frac{1}{3} (0.00873 - (-0.2705)) \right)$$

$$C_L = \frac{2}{\sqrt{M^2 - 1}} \left(\frac{2}{3} (0.2792) + \frac{1}{3} (0.2792) \right) = \frac{0.5584}{\sqrt{3.3^2 - 1}} = 0.1776 = \frac{4\alpha}{\sqrt{M^2 - 1}}$$

ii-

$$C_D = \frac{2}{\sqrt{M^2 - 1}} \int_0^1 (\epsilon_L^2 + \epsilon_U^2) d\left(\frac{x}{c}\right)$$

$$C_D = \frac{2}{\sqrt{M^2 - 1}} \left(\int_0^{2/3} ((-0.05236)^2 + (0.2269)^2) d\left(\frac{x}{c}\right) + \int_0^{1/3} ((-0.2705)^2 + (0.00873)^2) d\left(\frac{x}{c}\right) \right)$$

$$C_D = \frac{2}{\sqrt{M^2 - 1}} \left(\frac{2}{3} (0.05423) + \frac{1}{3} (0.07325) \right) = \frac{2}{6\sqrt{M^2 - 1}} (0.03615 + 0.02442) = 0.0385$$

AERODYNAMICS AND ITS APPLICATIONS

iii-

$$C_M = \frac{-2}{c^2 \sqrt{M^2 - 1}} \int_0^c (\epsilon_L - \epsilon_U) x dx$$

$$C_M = \frac{-2}{c^2 \sqrt{M^2 - 1}} \left(\int_0^{2c/3} (0.2269 - (-0.05236)) x dx + \int_{2c/3}^c (0.00873 - (-0.2705)) x dx \right)$$

$$C_M = \frac{-2}{\sqrt{M^2 - 1}} \frac{1}{c^2} \left(0.27923 \left| \frac{x^2}{2} \right|_0^{2c/3} + 0.27923 \left| \frac{x^2}{2} \right|_{2c/3}^c \right) = \frac{-2}{\sqrt{M^2 - 1}} \left(0.27923 \times \frac{4}{2 \times 9} + 0.27923 \times \left(\frac{1}{2} - \frac{4}{18} \right) \right)$$

$$C_M = -0.0888$$

iv-

$$k_{cp} = -\frac{C_M}{C_L} = \frac{0.0888}{0.1776} = 0.50$$

2- General sharp edged airfoil

For general airfoil case the contribution of the thickness, camber and angle of attack are considered in calculating the value of ϵ

Example

Aerofoil section made up of two unequal circular arcs profile. Measuring x from the leading edge, the local deflection from the free stream direction for upper and lower surface are given as:

AERODYNAMICS AND ITS APPLICATIONS

$$\varepsilon_U = 0.41\left(1 - \frac{x}{c}\right) - \alpha \text{ and } \varepsilon_L = 0.31\left(1 - \frac{x}{c}\right) + \alpha$$

The free stream Mach number is 1.65 and incidence angle of the free stream is 8° .

a- Prove that $C_L = \frac{4\alpha}{\sqrt{M^2-1}}$

b- Find

- i. Lift coefficient
- ii. Drag (wave) coefficient
- iii. Moment coefficient (about leading edge)
- iv. Center of pressure coefficient

Answer

Section a and b-i Lift Coefficient

$$C_L = \frac{-2}{c\sqrt{M^2-1}} \left[\int_0^c \varepsilon_U dx - \int_0^c \varepsilon_L dx \right]$$

$$C_L = \frac{-2}{c\sqrt{M^2-1}} \left[\int_0^c \left(0.41\left(1 - \frac{x}{c}\right) - \alpha\right) dx - \left(\int_0^c \left(0.31\left(1 - \frac{x}{c}\right) + \alpha\right) dx \right) \right]$$

$$C_L = \frac{-2}{c\sqrt{M^2-1}} \left[\int_0^c \left(-2\alpha + 0.10\left(1 - \frac{x}{c}\right) \right) dx \right] = \frac{-2}{c\sqrt{M^2-1}} \left(-2c\alpha + 0.10\left(c - \frac{c^2}{2c}\right) \right)$$

AERODYNAMICS AND ITS APPLICATIONS

$$C_L = \frac{-2}{c\sqrt{M^2 - 1}} \left[-2c\alpha + 0.10 \left(\frac{c}{2} \right) \right] = \frac{4 \times \frac{8 \times \pi}{180} - 0.1}{\sqrt{1.65^2 - 1}} = 0.349$$

ii- Drag Coefficient

$$C_{D_w} = \frac{2}{c\sqrt{M^2 - 1}} \int_0^c \left(\left(0.41 \left(1 - \frac{x}{c} \right) - \alpha \right)^2 + \left(0.31 \left(1 - \frac{x}{c} \right) + \alpha \right)^2 \right) dx$$

Now let's take

$$\int_0^c \left(\left(0.41 \left(1 - \frac{x}{c} \right) - \alpha \right)^2 \right) dx = \int_0^c \left(0.41 \left(1 - \frac{x}{c} \right) \right)^2 dx - \int_0^c 2 \times 0.41 \times \alpha \times \left(1 - \frac{x}{c} \right) dx + \int_0^c \alpha^2 dx$$

$$= (0.41)^2 \int_0^c \left(1 - \frac{2x}{c} + \frac{x^2}{c^2} \right) dx + \int_0^c \alpha^2 dx$$

$$= (0.41)^2 \left(c - \frac{2c^2}{2c} + \frac{c^3}{3c^2} \right) + \alpha^2 c = 0.41^2 c \left(1 - 1 + \frac{1}{3} \right) + \alpha^2 c$$

$$\int_0^c \left(\left(0.41 \left(1 - \frac{x}{c} \right) - \alpha \right)^2 \right) dx = c \left(\frac{0.41^2}{3} + \alpha^2 \right)$$

Similarly we can obtain

AERODYNAMICS AND ITS APPLICATIONS

$$\int_0^c \left(\left(0.31 \left(1 - \frac{x}{c} \right) + \alpha \right)^2 \right) = c \left(\frac{0.31^2}{3} + \alpha^2 \right)$$

Now rewrite drag coefficient as

$$C_D = \frac{2}{c\sqrt{M^2 - 1}} c \left(\frac{0.41^2 + 0.31^2}{3} + 2\alpha^2 \right)$$

$$C_D = \frac{2 \left(0.0881 + 2 \times \left(\frac{8 \times \pi}{180} \right)^2 \right)}{\sqrt{M^2 - 1}} = \frac{0.254}{\sqrt{1.65^2 - 1}} = 0.194$$

iii- Moment coefficient:

$$C_M = \frac{-2}{c^2\sqrt{M^2 - 1}} \int_0^c (\epsilon_L - \epsilon_U) x dx = \frac{-2}{c^2\sqrt{M^2 - 1}} \int_0^c \left(0.31 \left(1 - \frac{x}{c} \right) + \alpha - \left(0.41 \left(1 - \frac{x}{c} \right) - \alpha \right) \right) x dx$$

$$C_M = \frac{-2}{c^2\sqrt{M^2 - 1}} \int_0^c \left(-0.10 \left(1 - \frac{x}{c} \right) + 2\alpha \right) x dx = \frac{-2}{c^2\sqrt{M^2 - 1}} \left(-0.10 \left(\frac{x^2}{2} - \frac{x^3}{3c} \right) + 2 \frac{\alpha x^2}{2} \right)_0^c$$

$$C_M = \frac{-2}{c^2\sqrt{M^2 - 1}} c^2 \left(-0.10 \left(\frac{1}{2} - \frac{1}{3} \right) + \alpha \right) = \frac{-2}{\sqrt{M^2 - 1}} \left(-0.10 \times \frac{1}{6} + \alpha \right)$$

$$-C_M = \frac{2}{\sqrt{M^2 - 1}} (-0.017 + \alpha) = \frac{2}{\sqrt{1.65^2 - 1}} \left(-0.017 + \frac{8 \times \pi}{180} \right) = 0.187$$

AERODYNAMICS AND ITS APPLICATIONS

v- Location of Center pressure: $K_{CP} = \frac{-C_M}{C_L} = \frac{0.187}{0.349} = 0.536$

CHAPTER 10

FRICITION FORCE AND BOUNDARY LAYER DEVELOPMENT

Introduction

The flow is called viscous flow if the effects of the viscosity, thermal conduction, and mass diffusion are changing the properties (velocity, pressure and temperature) of the flow. The wall friction force (skin friction) is resulted from the effects of the viscosity on the surface. The magnitude of the skin frictional force is highly depends on the viscosity of the fluid, and velocity gradient in direction normal to the surface. Due to viscosity effects, region with flow velocity below free stream velocity is formed near the body surface. This region is called boundary layer (B-L). Prandtl divided the flow around body into two regions, inner and outer region. Inner region is very thin where the viscosity effects are concentrated and outer region is where the flow can be assumed inviscid.

Boundary layer

The boundary layer on the surface of flat plate grows from zero thickness, δ , (Figure 10.1) at the leading edge to the δ at trailing edge of the plate. The boundary layer is associated with large shearing force due to large velocity gradient in the direction normal to surface. This shearing force is greatest on the body surface and retards the layers of the fluid immediately adjacent to the surface.

AERODYNAMICS AND ITS APPLICATIONS

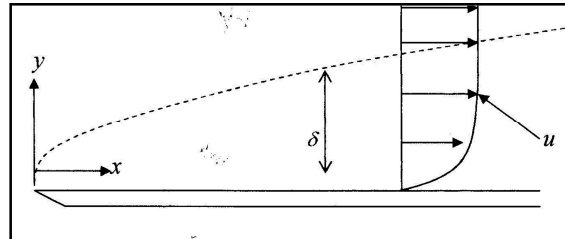


Figure 10.1: Boundary Layer Development

Velocity Profile

The fluid particle travel velocity for each layer varies with the distance normal to the surface. On the surface, the particle velocity is zero at the leading edge of the plate and reaches maximum at trailing edge of the flat plate. The shape of the velocity profile along the length depends on the type of the boundary layer (laminar or turbulent).

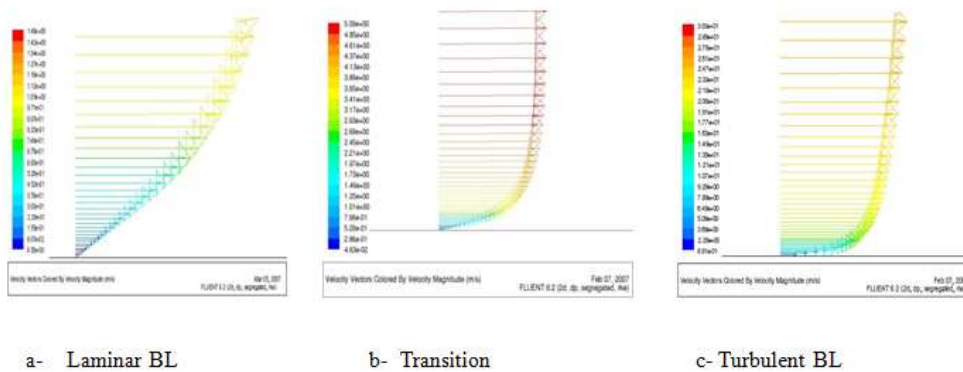


Figure 10.2: BL velocity profile

Laminar Boundary layer

As shown in figure 10.2(a), the velocity profile of laminar boundary layer changes uniformly in the direction normal to the wall. Laminar BL is thinner and the motion of the particles of fluid is very orderly with all particles moving in straight lines parallel to the wall with little interchange of fluid mass between layers.

Turbulent Boundary layer

Turbulent BL, shown in figure 10.2(c) is associated with velocity fluctuations in direction of the flow and in the direction perpendicular to it. There is large interchange of the fluid mass between the adjacent layers which results in large shearing stresses between the layers, so that energy from the mainstream easily transfers to fluid layers located closer to the surface. This causes the velocity of the layers close to surface not to be much less than free stream velocity. Since the velocity gradient $(\frac{\partial u}{\partial y})$ for turbulent BL is higher than laminar boundary layer, the surface friction stress under a turbulent boundary layer is 10 times or more great than laminar boundary layer friction.

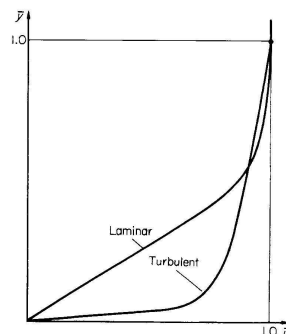


Figure 10.3: Laminar and Turbulent B-L

Favorable Pressure Gradient

The external pressure gradient is named favorable pressure gradient if the static pressure decreases ($dP/dx < 0$) along the surface and velocity along the edge of the B-L increases. In this case, the streamwise pressure forces help to reduce the effects of the shearing forces at the wall.

Unfavorable Pressure gradient (Adverse pressure gradient)

Unfavorable pressure occurs when the static pressure increases ($dP/dx > 0$) along the surface and velocity along the edge of the B-L decreases. In this case, the effect of the viscosity on the wall is reinforced by the streamwise pressure force. For a large pressure increase, the fluid particle may slow to zero velocity or even become reversed. The reversed flow is said to be separated from the surface. This is one of the most significant problems in aerodynamics. The flow separation modifies the pressure distribution along the surface which leads to lift reduction and high drag.

Laminar Turbulent Boundary Layer Transition

At higher Reynolds boundary layer transits from laminar to turbulent. This process is called transition. The transition is highly dependent on the Reynolds number and angle of attack. The effects of Reynolds number on the transition distance depends on many parameters such as pressure gradient, surface roughness, compressibility effects, surface temperature and turbulence level in free stream. Normally the transition takes place downstream not far from the point of

AERODYNAMICS AND ITS APPLICATIONS

minimum pressure. If the transition Re is reached, the transition process to full turbulent flow will pass through the following regions: stable laminar, unstable flow (T-S waves), 3-D unstable waves, vortex breakdown, fluctuating, turbulent spots, fully turbulent flow.

Boundary Layer Properties

Displacement thickness (δ^*)

The displacement thickness is defined as the distance by which the wall would have to be displaced outward into the free stream in order not to change the mass of the flow field and is given in equation 10.1

$$\frac{\delta^*}{\delta} = \int_0^1 \left(1 - \frac{u}{U_1}\right) d\bar{y} = \int_0^1 (1 - \bar{u}) d\bar{y}$$

Momentum Thickness (θ)

It has the same definition as displacement thickness except the momentum thickness is based on the total momentum of the fluid, rather than the total mass and it is given by equation 10.2

$$\frac{\theta}{\delta} = \int_0^1 \frac{u}{U_1} \left(1 - \frac{u}{U_1}\right) d\bar{y} = \int_0^1 \bar{u} (1 - \bar{u}) d\bar{y} \quad (10.2)$$

Kinetic energy thickness (δ^{**})

The kinetic energy thickness (δ^{**}) has same definition as momentum thickness and displacement, except that it is based on kinetic energy of the fluid instead of momentum or mass and it is defined by equation 10.3

$$\frac{\delta^{**}}{\delta} = \int_0^1 \frac{u}{U_1} \left[1 - \left(\frac{u}{U_1}\right)^2\right] d\bar{y} = \int_0^1 \bar{u} (1 - \bar{u}^2) d\bar{y}$$

$$(10.3)$$

Note that the ratios of the displacement, momentum and kinetic thicknesses to boundary layer thickness given in equation 10.1 to 10.3 can be easily obtained if the velocity profile is known.

Surface Friction Drag

Skin friction force (F) may be expressed in terms of a non-dimensional coefficient, C_F as

$$(10.4) \quad F = C_F \frac{1}{2} \rho_{\infty} U_{\infty}^2 S$$

Where S is the area of the surface

Total skin friction drag coefficient (C_{DF}) is defined by

$$D_F = C_{DF} \frac{1}{2} \rho_{\infty} U_{\infty}^2 S \quad (10.5)$$

Where D_F is total skin friction force on both surfaces of plate or airfoil. For a flat plate or symmetrical aerofoil, at zero incidence (top and bottom surfaces behave identically), $D_F=2F$.

$$(10.6) \quad \frac{2F}{\frac{1}{2} \rho_{\infty} U_{\infty}^2 S}$$

For *incompressible flow*, $\rho_1=\rho_{\infty}=\rho$, $\mu_1=\mu_{\infty}=\mu$ and $U_1=U_{\infty}=U$

The Momentum Integral Equation

The accurate evaluation of the quantities such as δ , δ^* , δ^{**} , and θ requires the numerical solution of the momentum integral equation. The boundary layer momentum integral equation was derived by Von Karman as:

$$\frac{d}{dx} (U_1^2 \theta) + \delta^* U_1 \frac{dU_1}{dx} + \rho U_1 V_s = \frac{\tau_w}{\rho} \quad (10.7)$$

Where V_s is suction or blowing on the wall and U_1 is flow velocity at outer edge of the boundary layer. The shear stress in equation 10.7 can be defined as

$$\tau_w = \mu \left(\frac{\partial u}{\partial y} \right) = C_f \frac{1}{2} \rho U_1^2 \quad (10.8)$$

Equation 10.7 is also called Von Karman's momentum integral equation. If the velocity profile is known, the the momentum integral equation (Eq. 10.4) can be solved to provide the variations of δ , δ^* , θ and C_f along the surface.

CHAPTER 11

FLAT PLATE BOUNDARY LAYER SKIN FRICTION DRAG

Introduction

The Momentum Integral Equation introduced in Chapter 10 can be used to obtain the solution of skin friction drag if the velocity profile is known. Expression for laminar boundary velocity profile is easy to obtain. Polynomial or sinusoid distribution can be used for the laminar boundary layer velocity profile. Number of the boundary conditions at the wall and outer edge of the laminar boundary layer should be specified for any proposed expression. The accuracy and the number of the boundary conditions depend on the degree of the expression. If the velocity profile is obtained, the values for ratios of the displacement thickness and momentum thickness to boundary layer thickness as described in chapter 10 can be easily obtained. These ratios will be used with the momentum integral to obtain an expression for boundary layer, displacement and momentum thicknesses. Expression for the skin friction drag can be also obtained.

Laminar Boundary Layer

Velocity Profile

From the literature the following expressions were used for the laminar boundary layer velocity profile

$$\bar{u} = \sin \frac{\pi}{2} \bar{y} \quad (11.1)$$

AERODYNAMICS AND ITS APPLICATIONS

$$\bar{u} = \frac{3}{2}\bar{y} - \frac{1}{2}\bar{y}^3 \quad (11.2)$$

$$\bar{u} = 2\bar{y} - \bar{y}^2 \quad (11.3)$$

Equation 11.1 present 1st order sinusoid expression and equations 11.2 and 11.3 are presenting 3rd and 2nd degree polynomial. The accuracy of each expression can be predicted by comparing their velocity profile distribution with Blasius velocity profile distribution.

Laminar Boundary Layer Relations

Expression presented by Equation 11.2 is used to obtain the following laminar boundary layer relations

$$I_1 = \frac{\delta^*}{\delta} = \frac{3}{8} \quad (11.4)$$

$$I = \frac{\theta}{\delta} = \frac{39}{280} \quad (11.5)$$

$$C_f = \frac{3\mu}{\rho U_1 \delta} \quad (11.6)$$

Momentum Integral Equation introduced in chapter 10 can be reduced to the following form

or
$$\tau_w = \rho U_1^2 \frac{d\theta}{dx} \quad C_f = 2I \frac{d\delta}{dx} \quad (11.7)$$

Using equation 11.7 with equations 11.4 to 11.6 lead to the following relations

$$\delta = \frac{4.64x}{(R_{e_x})^{1/2}} \quad (11.8)$$

$$\delta^* = 0.375\delta = \frac{1.74x}{(R_{e_x})^{1/2}} \quad (11.9)$$

$$\theta = 0.139\delta = \frac{0.646x}{(R_{e_x})^{1/2}} \quad (11.10)$$

Skin friction and drag coefficient can be also obtained as

$$C_F = \frac{1.293}{(R_{e_x})^{1/2}} \Rightarrow C_D = 2C_F = \frac{2.586}{(R_{e_x})^{1/2}} \quad (11.11)$$

Turbulent Boundary Layer

Velocity Profile

The mean velocity distribution in turbulent flow can be expressed by combining the analytical solution with experimental results. Prandtl suggested the use of Blasius's experimental results for circular pipe friction loss with skin friction empirical relationship to derive the turbulent Boundary layer velocity profile. This combination leads to the following turbulent boundary layer velocity profile

$$\frac{u}{U_1} = \left(\frac{y}{\delta}\right)^{1/7} \quad (11.12)$$

AERODYNAMICS AND ITS APPLICATIONS

$$\bar{u} = \bar{y}^{1/7} \quad (11.13)$$

Relation 11.12 or 11.13 is known as Prandtl's seventh root law.

Turbulent Boundary Layer Relations

Expression presented by Equation 11.12 or 11.13 is used to obtain the following turbulent boundary layer relations

$$I_1 = \frac{\delta^*}{\delta} = \frac{1}{8} \quad (11.14)$$

$$I = \frac{\theta}{\delta} = \frac{7}{72} \quad (11.15)$$

$$C_f = 0.0468 \left(\frac{v}{U\delta} \right)^{1/4} \quad (11.16)$$

Equations 11.14 to 11.16 are used with 11.7 leading to the following relations

$$\delta = \frac{0.383x}{(R_{e_x})^{1/5}} \quad (11.17)$$

$$\delta^* = 0.125\delta = \frac{0.0479x}{(R_{e_x})^{1/5}} \quad (11.18)$$

$$\theta = 0.0973\delta = \frac{0.0372x}{(R_{e_x})^{1/5}} \quad (11.19)$$

Skin friction and drag coefficient can be also obtained as

$$C_F = \frac{0.0744}{(R_{e_x})^{1/5}} \Rightarrow C_D = 2C_F = \frac{0.1488}{(R_{e_x})^{1/5}} \quad (11.20)$$

Equation 11.20 is valid for flow with $Re \leq 10^7$. For higher Reynolds number ($Re > 10^7$) semi-empirical expression presented by equation 11.21 can be used for the skin friction coefficient.

$$C_F = \frac{0.455}{(\log_{10} R_e)^{2.58}} \quad (11.21)$$

Mixed Boundary layer flow

Transition condition

If the Reynolds number (Re) is less than 3×10^5 the boundary layer can be considered entirely laminar. The transition Reynolds number depends on free stream and surface conditions. For a large range of Re the boundary layer is partly laminar and partly turbulent. The one condition which must be satisfied at the transition region is that the momentum thickness through the transition region should always remain constant.

$$\theta_{L_t} = \theta_{T_t} \quad (11.22)$$

AERODYNAMICS AND ITS APPLICATIONS

Where θ_{L_t} and θ_{T_t} are representing the momentum thickness for laminar and turbulent boundary layers at the transition region as shown in figure 11.1. Using equation 10.2 with Equation 11.22 leads to:

$$\delta_{L_t} \int_0^1 \bar{u}(1 - \bar{u}) d\bar{y} = \delta_{T_t} \int_0^1 \bar{u}(1 - \bar{u}) d\bar{y} \quad (11.23)$$

Using the values of I which is previously evaluated in equations 11.5 and 11.15 leads to

$$\frac{\delta_{T_t}}{\delta_{L_t}} = \frac{0.139}{0.0973} = 1.43 \quad (11.24)$$

Equation 11.24 indicates that on a flat plate the B-L increases in thickness by about 43% at transition.

Transition Distance

As shown in figure 11.1, at the beginning the boundary layer starts to develop as a laminar boundary layer and thickens as it moves towards trailing edge. If the plate length is long, the boundary layer will pass through short transition region. Immediately after transition region the turbulent boundary layer starts to form. The transition location depends on the transition Reynolds number which is defined as

$$R_{e_t} = U_1 L_t / \nu \quad (11.25)$$

AERODYNAMICS AND ITS APPLICATIONS

Using equation 11.22 the transition distance (L_{Tt}) can be expressed as

$$\rightarrow L_{Tt} = 35.5 \frac{\nu}{U_1} R_{e_t}^{5/8} \quad (11.26)$$

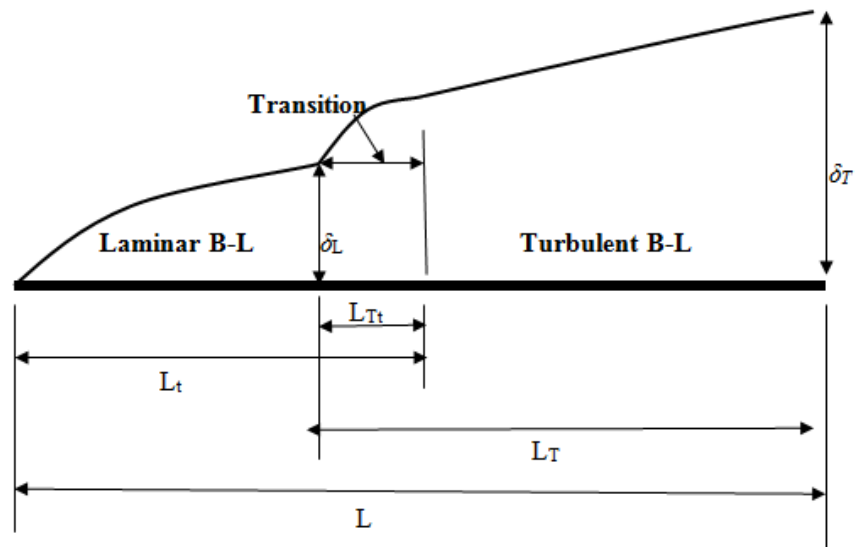


Figure 11.1: Mixed B-L flow on a flat plate

The total skin friction force for the whole plate shown in figure 11.1 can be found by calculating the skin friction force under turbulent layer acting over a length of L_T . Where L_T is defined as

$$L_T = L - L_t + L_{Tt}$$

The skin friction force of the turbulent boundary can be calculated using the following expression

$$C_F = \frac{0.0744}{R_e} \left(R_e - R_{e_t} + 3835 R_{e_t}^{5/8} \right)^{4/5}$$

(11.27)

Before solving any boundary layer problems the free stream Reynolds number (R_e) must be compared with the transition Reynolds (R_{e_t}), Equation 11.27 is not applicable for values of R_e less than R_{e_t} . For $R_e < R_{e_t}$, the boundary layer is considered as laminar B-L and equation 11.11 can be used for the skin friction. For accurate calculation, equation 11.27 for the laminar boundary layer skin friction can be applied for the portion $(L-L_T)$ and equation 11.27 can be applied for the turbulent boundary portion (L_T) . The total skin friction is the summation of the skin friction coefficient for both portions.

CHAPTER 12

SOLVED PROBLEMS IN BOUNDARY LAYER THEORY

Problem 1

One method of estimating the drag on a flat plate with some laminar and some turbulent flow is to assume that the flow is laminar up to the transition location, and then to assume that from there, the flow is turbulent. The turbulent layer does not start out with zero thickness at the transition location, but rather acts as though it started upstream of the transition and developed to have the same momentum thickness as the laminar layer at the transition point. Using the formulas for flat plate skin friction, estimate the drag coefficient of a flat plate at a Reynolds number of 2,000,000 with transition at 25%, 45%, and 90% of the chord. Discuss the results.

[Hint: Use transition Reynolds number for laminar boundary layer region].

Answer

$$R_e = 2 \times 10^6 = \frac{Uc}{\nu} \rightarrow \frac{U}{\nu} = \frac{R_e}{c} \quad (12.1)$$

$$R_{e_t} = \frac{Ux_t}{\nu} \rightarrow \frac{U}{\nu} = \frac{R_{e_t}}{x_t} \quad (12.2)$$

From Eq. 12.1 and 12.2

AERODYNAMICS AND ITS APPLICATIONS

$$\frac{R_e}{c} = \frac{R_{e_t}}{x_t} \rightarrow R_{e_t} = \frac{x_t}{c} R_e \quad (12.3)$$

a- $x_t = 0.25 c$

From Eq. (12.3)

$$R_{e_t} = \frac{x_t}{c} R_e = \frac{0.25c}{c} (2 \times 10^6) = 5 \times 10^5$$

If B-L assumed to be laminar until the end of transition

$$C_{D_t} = \frac{2.586}{R_{e_t}^{1/2}} = \frac{2.586}{(5 \times 10^5)^{1/2}} = 0.00366$$

$$C_F = \frac{0.0744}{R_e} (R_e - R_{e_t} + 35.5 R_{e_t}^{5/8})^{4/5}$$

$$C_F = \frac{0.0744}{2 \times 10^6} (2 \times 10^6 - 5 \times 10^5 + 35.5 \times (5 \times 10^5)^{5/8})^{4/5} = 0.00347$$

$$C_{D_t} = 2 \times 0.00347 = 0.00694$$

Total Drag:

$$C_D = C_{D_t} + C_{D_i} = 0.00366 + 0.00694 = 0.0106$$

b- $x_t = 0.45 c$

From Eq. (12.3)

$$R_{e_t} = \frac{x_t}{c} R_e = \frac{0.45c}{c} (2 \times 10^6) = 9 \times 10^5$$

AERODYNAMICS AND ITS APPLICATIONS

If B-L assumed to be laminar until the end of transition

$$C_{D_t} = \frac{2.586}{R_{e_t}^{1/2}} = \frac{2.586}{(9 \times 10^5)^{1/2}} = 0.00273$$

$$C_F = \frac{0.0744}{R_e} (R_e - R_{e_t} + 35.5 R_{e_t}^{5/8})^{4/5}$$

$$C_F = \frac{0.0744}{2 \times 10^6} (2 \times 10^6 - 9 \times 10^5 + 35.5 \times (9 \times 10^5)^{5/8})^{4/5} = 0.00287$$

$$C_{D_t} = 2 \times 0.00347 = 0.00574$$

Total Drag:

$$C_D = C_{D_t} + C_{D_i} = 0.00273 + 0.00574 = 0.00847$$

d- $x_t = 0.9c$

From Eq. (12.3)

$$R_{e_t} = \frac{x_t}{c} R_e = \frac{0.9c}{c} (2 \times 10^6) = 1.8 \times 10^6$$

If B-L assumed to be laminar until the end of transition

$$C_{D_t} = \frac{2.586}{R_{e_t}^{1/2}} = \frac{2.586}{(1.8 \times 10^6)^{1/2}} = 0.00193$$

$$C_F = \frac{0.0744}{R_e} (R_e - R_{e_t} + 35.5 R_{e_t}^{5/8})^{4/5}$$

$$C_F = \frac{0.0744}{2 \times 10^6} (2 \times 10^6 - 1.8 \times 10^6 + 35.5 \times (1.8 \times 10^6)^{5/8})^{4/5} = 0.00132$$

AERODYNAMICS AND ITS APPLICATIONS

$$C_{D_i} = 2 \times 0.00132 = 0.00265$$

Total Drag:

$$C_D = C_{D_f} + C_{D_i} = 0.00193 + 0.00265 = 0.00458$$

The results showed very clear that in order to reduce the drag the transition should be avoided at early stage and BL should be maintain laminar for long distance.

Problem 2

A laminar boundary layer velocity profile is approximated by the two straight line segments indicated in Figure problem 2. Derive an expression for the velocity profile and use the momentum integral equation to determine the boundary layer thickness, $\delta = \delta(x)$.

Answer

Velocity profile

$$1- \text{ B.C: } 0 \leq \bar{y} < \frac{1}{2}$$

$$\bar{u}_1 = a + b\bar{y}$$

$$\bar{y} = 0, \bar{u}_1 = 0 \rightarrow a = 0$$

$$\bar{y} = 1/2, \bar{u}_1 = 2/3 \rightarrow b = \frac{4}{3}$$

$$\bar{u}_1 = \frac{4}{3}\bar{y}$$

AERODYNAMICS AND ITS APPLICATIONS

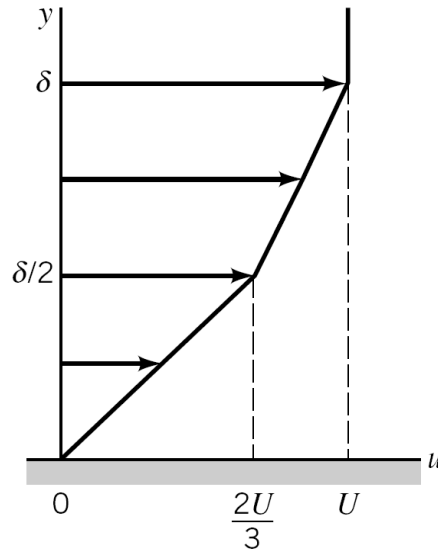


Figure Problem 2

2- B.C: $\frac{1}{2} \leq \bar{y} < 1$

$$\bar{u}_2 = a + b\bar{y}$$

$$\bar{y} = \frac{1}{2}, \bar{u}_2 = \frac{2}{3} \rightarrow \frac{2}{3} = a + \frac{1}{2}b$$

$$\bar{y} = 1, \bar{u}_2 = 1 \rightarrow 1 = a + b$$

$$\rightarrow a = \frac{1}{3}, b = \frac{2}{3}$$

$$\bar{u}_2 = \frac{1}{3} + \frac{2}{3}\bar{y}$$

Boundary Layer Thickness

$$\frac{\theta}{\delta} = \int \bar{u}(1-\bar{u})dy = \int_0^{1/2} \bar{u}_1(1-\bar{u}_1)d\bar{y} + \int_{1/2}^1 \bar{u}_2(1-\bar{u}_2)d\bar{y}$$

AERODYNAMICS AND ITS APPLICATIONS

$$\int_0^{1/2} \bar{u}_1(1-\bar{u}_1)d\bar{y} = \int_0^{1/2} \frac{4}{3}\bar{y}\left(1-\frac{4}{3}\bar{y}\right)d\bar{y} = \int_0^{1/2} \frac{4}{3}\bar{y}d\bar{y} - \int_0^{1/2} \frac{16}{9}\bar{y}d\bar{y} = \frac{4}{3}\left|\frac{\bar{y}^2}{2}\right|_0^{1/2} - \frac{16}{9}\left|\frac{\bar{y}^3}{3}\right|_0^{1/2}$$

$$= \frac{1}{6} - \frac{2}{27} = 0.093$$

$$\int_{1/2}^1 \bar{u}_1(1-\bar{u}_1)d\bar{y} = \int_{1/2}^1 \left(\frac{1}{3} + \frac{2}{3}\bar{y}\right)\left(1 - \left(\frac{1}{3} + \frac{2}{3}\bar{y}\right)\right)d\bar{y} = \frac{1}{3}|\bar{y}|_{1/2}^1 + \frac{2}{3}\left|\frac{\bar{y}^2}{2}\right|_{1/2}^1 - \frac{1}{9}|\bar{y}|_{1/2}^1 - \frac{4}{9}\left|\frac{\bar{y}^2}{2}\right|_{1/2}^1 - \frac{4}{9}\left|\frac{\bar{y}^3}{3}\right|_{1/2}^1$$

$$= 0.06481$$

$$\frac{\theta}{\delta} = 0.093 + 0.06481 = 0.1578 \text{ (p2.1)}$$

$$\text{Given } \frac{d\theta}{dx} = \frac{C_f}{2} = \frac{\pi}{2} \frac{v}{\delta U} \quad \text{(p2.2)}$$

We know from Eq. 2.1 that

$$\theta = 0.1578\delta \Rightarrow \frac{d\theta}{dx} = 0.1578 \frac{d\delta}{dx} \quad \text{(p2.3)}$$

From equations p2.2 and p2.3, we can write the following relation

$$0.1578 \frac{d\delta}{dx} = \frac{\pi}{2} \frac{v}{\delta U} \Rightarrow \delta d\delta = \frac{\pi}{2 \times 0.1578} \frac{v}{U} dx = 9.954 \frac{v}{U} dx$$

$$\Rightarrow \frac{1}{2} \delta^2 = 9.954 \frac{v}{U} x = 9.954 \frac{v}{Ux} x^2 \Rightarrow \left(\frac{\delta}{x}\right)^2 = \frac{2 \times 9.954}{R_{e_x}}$$

$$\Rightarrow \frac{\delta}{x} = \frac{4.462}{\sqrt{R_{e_x}}} \quad \text{(p2.4)}$$

Problem 3

AERODYNAMICS AND ITS APPLICATIONS

Develop an expression for the transition distance (L_{Tt}) of a flat plate of chord c and infinite span at zero incidence in a uniform stream of air, when transition occurs at a distance L_t from the leading edge (Figure Problem 3). Assume the following relationships for laminar and turbulent boundary layer velocity profile, respectively

$$\bar{u}_L = 2\left(\frac{y}{\delta}\right) - \left(\frac{y}{\delta}\right)^2, \quad \bar{u}_T = \bar{y}^{1/7}$$

b- For the flat plate shown in figure problem 3, develop an expression for the dependence of turbulent boundary layer skin friction coefficient on the Reynolds number.

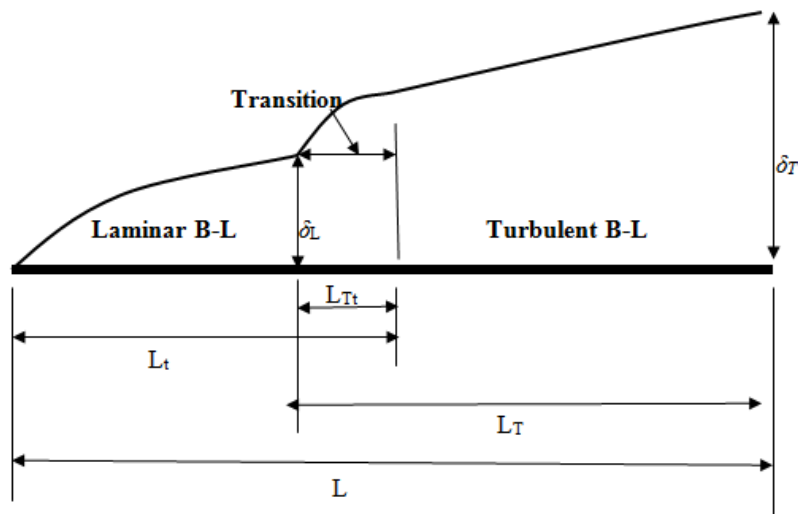


Figure Problem 3 Mixed B-L flow on a flat plate

Answer

At transition $\theta_{L_t} = \theta_{T_t}$

AERODYNAMICS AND ITS APPLICATIONS

a-

For laminar BL, The velocity profile as

$$\frac{u}{U} = \left[2 - \left(\frac{y}{\delta} \right) \right] \frac{y}{\delta} \rightarrow \bar{u} = 2\bar{y} - \bar{y}^2$$

$$C_f = 2 \frac{d\theta}{dx} \quad \text{Since } I = \frac{\theta}{\delta} \rightarrow C_f = 2I \frac{d\delta}{dx} \rightarrow \frac{d\delta}{dx} = \frac{C_f}{2I} \quad (\text{p3.1})$$

$$\frac{1}{2} \rho U^2 C_f = \tau_w = \mu \left(\frac{\partial u}{\partial y} \right)_w \rightarrow C_f = \frac{2\mu}{\rho U^2} \left(\frac{\partial u}{\partial y} \right)_w \quad (\text{p3.2})$$

$$\bar{u} = \frac{u}{U} \rightarrow u = \bar{u}U, \quad (\text{p3.3})$$

$$\bar{y} = \frac{y}{\delta} \rightarrow y = \bar{y}\delta$$

U is given as constant, then using equation p3.3 into equation p3.2 leads to

$$C_f = \frac{2\mu}{\rho U \delta} \left(\frac{\partial \bar{u}}{\partial \bar{y}} \right)_w \quad (\text{p3.4})$$

$$\frac{\partial \bar{u}}{\partial \bar{y}} = 2 - 2\bar{y} \text{ for wall } \bar{y} = 0, \text{ then}$$

$$\frac{\partial \bar{u}}{\partial \bar{y}} = 2 \quad (\text{p3.5})$$

Equation p3.5 with p3.4 leads to

$$C_f = \frac{2\mu}{\rho U \delta} (2) = \frac{4\mu}{\rho U \delta} \quad (\text{p3.6})$$

AERODYNAMICS AND ITS APPLICATIONS

$$I = \frac{\theta}{\delta} = \int_0^1 (\bar{u} - \bar{u}^2) d\bar{y} \quad (\text{p3.7})$$

$$\int_0^1 \bar{u} d\bar{y} = \int_0^1 (2\bar{y} - \bar{y}^2) d\bar{y} = \bar{y}^2 \Big|_0^1 - \frac{\bar{y}^3}{3} \Big|_0^1 = \frac{2}{3} \quad (\text{p3.8})$$

$$\int_0^1 \bar{u}^2 d\bar{y} = \int_0^1 (2\bar{y} - \bar{y}^2)^2 d\bar{y} = \int_0^1 (4\bar{y}^2 - 4\bar{y}^3 + \bar{y}^4) d\bar{y} = \frac{4}{3} - 1 + \frac{1}{5} = \frac{20 - 15 + 3}{15} = \frac{8}{15} \quad (\text{p3.9})$$

Equation p3.8 and p3.9 with p3.7 leads to

$$I = \frac{\theta}{\delta} = \int_0^1 (\bar{u} - \bar{u}^2) d\bar{y} = \frac{2}{3} - \frac{8}{15} = \frac{2}{15} \quad (\text{p3.10})$$

Sub Equation p3.6 and p3.10 into p3.1 leads to

$$\begin{aligned} \frac{d\delta}{dx} &= \frac{C_f}{2I} = \frac{4\mu}{2\rho U \delta \left(\frac{2}{15}\right)} = \frac{15\mu}{\rho U \delta} \rightarrow \delta d\delta = \frac{15\mu}{\rho U} dx \\ \rightarrow \frac{\delta^2}{2} &= \frac{15\mu}{\rho U} x \rightarrow \delta^2 = \frac{30\mu}{\rho U x} x^2 \rightarrow \delta = \frac{\sqrt{30x^2}}{\sqrt{R_{e_x}}} = \frac{5.477x}{\sqrt{R_{e_x}}} \end{aligned} \quad (\text{p3.11})$$

$$\text{Since } \frac{\theta}{\delta} = \frac{2}{15} \rightarrow \frac{\theta}{x} = \frac{2}{15} \times \frac{5.477}{\sqrt{R_{e_x}}}$$

$$\rightarrow \frac{\theta}{x} = \frac{0.7303}{\sqrt{R_{e_x}}} \quad (\text{p3.12})$$

Given for turbulent with velocity profile of $\bar{u} = \bar{y}^{1/7}$,

AERODYNAMICS AND ITS APPLICATIONS

$$\theta_T = 0.0973\delta = \frac{0.0372x}{(R_{e_x})^{1/5}} \quad (\text{p3.13})$$

At transition $\theta_{L_t} = \theta_{T_t}$, then

$$\theta_{L_t} = \frac{0.7303L_t}{(R_{e_t})^{1/2}} = 0.655\left(\frac{v}{U_1}\right)^{1/2} L_t^{1/2} = \theta_{T_t} = \frac{0.0372L_{T_t}}{(R_{e_x})_{T_t}^{1/5}} \quad (\text{p3.14})$$

Transition distance: $L_t = \frac{v}{U_1} R_{e_t}$

Substitute Transition into eq. p3.14 leads to

$$\theta_{L_t} = 0.7303\frac{v}{U_1}(R_{e_t})^{1/2} = \theta_{T_t} = \frac{0.0372L_{T_t}}{(R_{e_x})_{T_t}^{1/5}} \quad (\text{p3.15})$$

Solve Eq. p3.15 for transition distance leads to

$$0.7303L_t\left(\frac{v}{U_1L_t}\right)^{1/2} = 0.0372L_{T_t}\left(\frac{v}{U_1L_{T_t}}\right)^{1/5} \Rightarrow L_{T_t}^{4/5} = \frac{0.7303}{0.0372}\left(\frac{v}{U_1}\right)^{4/5} R_{e_t}^{1/2}$$

Substitute Transition into eq. p3.14 leads to

$$\rightarrow L_{T_t} = 41.32\frac{v}{U_1} R_{e_t}^{5/8} \quad (\text{p3.15})$$

b- The **Total skin friction force** for the **whole plate** may be found simply by **calculating the skin friction force** under **turbulent layer** acting over a length from

AERODYNAMICS AND ITS APPLICATIONS

the point at a distance L_{Tt} ahead of transition, to the trailing edge. **Total effective length** of turbulent layer is $L-L_t+L_{Tt}$

From the definition of **friction force**,

$$F = \int_0^{L-L_t+L_{Tt}} \tau_w dx = \frac{1}{2} \rho U_1^2 \int_0^{L-L_t+L_{Tt}} C_f dx$$

Given Eq. sheet for turbulent B-L

$$C_f = \frac{0.0595}{(R_{e_x})^{1/5}} = 0.0595 \left(\frac{\nu}{U_1} \right)^{1/5} x^{-1/5}$$

CHAPTER 13

INTRODUCTION TO HELICOPTERS

The Helicopter and Its Basic Components

A helicopter is a heavier than air flying machine. The lifting force is produced by a main rotor. By the rotation of the main rotor a thrust force is developed perpendicular to the plane of rotor rotation. If the main rotor rotates in the horizontal plane, then its thrust force T is directed vertically upwards (figure 13.1), that is, vertical flight is possible. The basic components of a helicopter are:

- Main rotor which is operated by engine.
- Fuselage for accommodation of crew, passengers, equipment and cargo.
- Landing gear used for movement on the ground.
- Tail rotor provides directional control of the helicopter.
- Propulsion system provides power to the lifting and tail rotors and auxiliary systems.
- Transmission transfers the torque from the power plant to the main and tail rotors.

The flight characteristics depend on the thrust force vector and the weight vector as follows:

- If thrust is vertical and in balance with the weight, the helicopter is motionless (hovering).
- If the thrust is vertical and greater than weight, the helicopter is making vertical

climb.

- If the thrust is inclined forward or backward, the helicopter can move forward or backward. The reason for this is that the thrust vector has two components; vertical component will be the lift force and the horizontal component will be the propulsive force.
- If the thrust is inclined rightward or leftward, the helicopter can move rightward or leftward. The reason for this is that the thrust vector has two components; vertical component will be the lift force and the horizontal component will be the sidewise force.

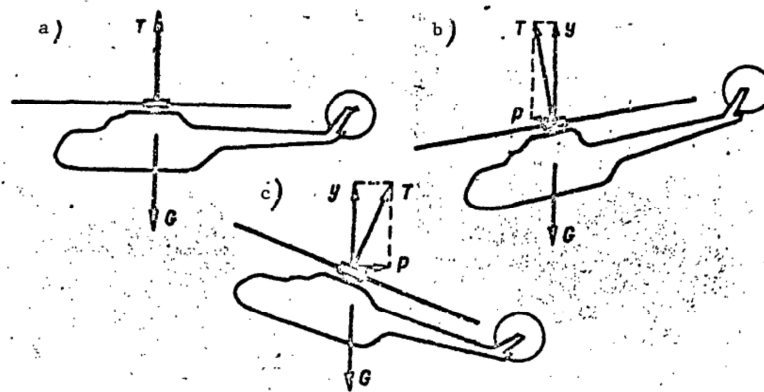


Figure 13.1: Principle of flight controls of a helicopter. (a) vertical flight; (b) horizontal flight forwards; (c) horizontal flight backwards (Bazof, 1969).

Classification of Helicopters

The basic classification of helicopters depends on the number of main rotors and their positions as follows: single rotor, dual rotor and multirotor helicopters.

AERODYNAMICS AND ITS APPLICATIONS

For single rotor helicopters, the main rotor is attached to the main fuselage and a tail rotor mounted on the tail structure. The advantage of single rotor helicopters is the simplicity of construction and the control system. This class of helicopters includes both light helicopters (weight about 500 kgf), and heavy helicopters (weight greater than 40 tons). Deficiencies of the single rotor helicopter are (Bazof, 1969):

- Large fuselage length
- A significant loss of power due to the tail rotor drive train (7 -10% of the full power of the engine);
- A limited range of permissible centering
- A higher level of vibration (the long transmission shafts, extending into the tail structure, are additional sources of spring oscillations).

Dual rotor helicopters appear in several arrangements. Rotors arranged in tandem; this is the most common arrangement (Figure13.2a), Rotors in a transverse arrangement (Figure13.2b); A cross connected rotor scheme (Figure13.2c); A coaxial rotor arrangement (Figure13.2d). Merits of helicopters with a tandem rotor arrangement are:

- Wider range of permissible centering;
- Large fuselage volume; which allows it to contain large-sized loads;
- Increased longitudinal stability;
- Large weight coefficient.

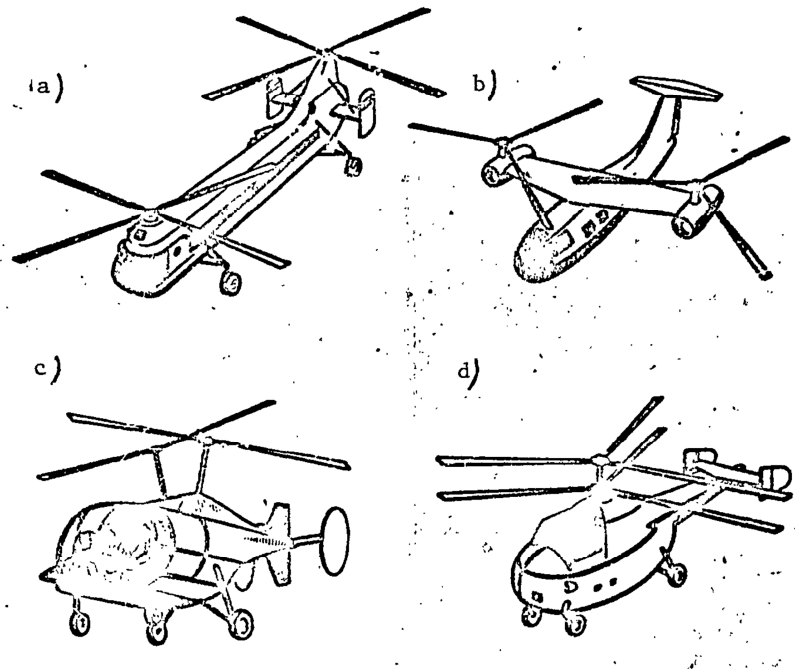


Figure13.2: Dual rotor helicopters. (a) tandem rotors; (b) transverse rotors; (c) cross connected rotors; (d) coaxial rotors (Bazof, 1969).

Helicopters with a tandem arrangement of rotors can have one or two engines, which are located in the forward or aft parts of the fuselage. These helicopters have the following deficiencies:

- A complicated system of transmission and control;
- Adverse mutual interaction between the main rotors which causes, in addition, a loss of power;
- Complicated landing techniques are required in the autorotation regime of main rotors.

AERODYNAMICS AND ITS APPLICATIONS

- Transverse arrangement of rotors has the following advantages:
- Convenient utilization of all parts of the fuselage for crew and passengers, since the engines are located outside the fuselage;
- Absence of harmful interaction of one rotor with the other;
- Higher lateral stability and controllability of the helicopter;
- The presence of an auxiliary wing, where the engines and main rotors are located, allows the helicopter to develop a high speed.

Deficiencies of these helicopters are as follows:

- A complicated system of control and transmission;
- An increase in size and structure weight due to the presence of the auxiliary wing.

Dual rotor helicopters with cross connected rotors have a considerable advantage over helicopters with transverse rotors; they do not have an auxiliary wing, which reduces the size and structure weight. But, at the same time, with these advantages there is a deficiency, a complicated transmission and control system.

The basic advantage of dual rotor helicopters with coaxial rotors is their small size. Their disadvantages:

- Complicated structure;
- Deficient directional stability;
- Danger of collision of the rotor blades;
- Considerable vibration.

AERODYNAMICS AND ITS APPLICATIONS

Multi-rotor helicopters are not widely used in view of their complex construction.

In all dual-rotor helicopters, the main rotors rotate in opposite directions. In this way the mutual reactive moments are balanced, and the necessity of having a tail rotor is eliminated. Thus the power loss from the engine is reduced.

References

1. Bazov, D. I. (1969). *Helicopter Aerodynamics*. Moscow: Transport press.
2. Bramwell, A., Done, G., & Balmford, D. (2001). *Bramwell's Helicopter Dynamics*. MA: Butterworth-Heinemann.
3. Gessow, A., & Myers, G. (1954). *Aerodynamics of the Helicopter*. New York: Frederick Ungar Publishing Company.
4. Seddon, J. (1990). *Basic Helicopter Aerodynamics*. London: BSP Professional Books.

CHAPTER 14

VERTICAL FLIGHT: MOMENTUM THEORY

Hover

In hovering, a vertical thrust is produced by pushing a column of air downwards through the rotor plane. Conservation laws of mass, momentum and energy can be used to calculate thrust produced. This approach is commonly referred to as the momentum theory for helicopters. This is similar to Glauert theory for aircraft propellers. When helicopter rotor is working, it is sucking air from above. This leads to pressure drop above the rotor. Across the rotor there will be a sudden increase in pressure (hence the name actuator disk) and then a fall to reach atmospheric value again below the rotor (see Figure 14.1). High above the rotor, the velocity is zero at 'upstream infinity', then it increases to a value V_i at the disc and continues to increase, reaching a value V_∞ at 'downstream infinity'. From the continuity equation for the streamtube shown in Figure 14.1, the velocity is continuous through the disc.

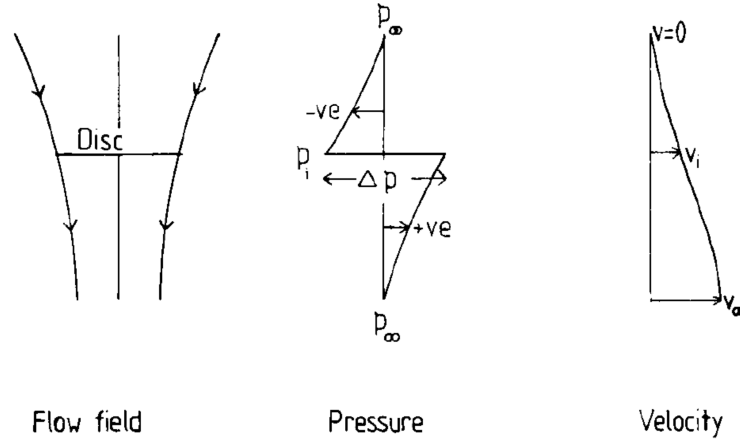


Figure 14.1: Actuator disc concept (Seddon, 1990).

Applying energy conservation for incompressible flow above the actuator disk, we get:

$$p_i + \frac{1}{2}\rho V_i^2 = p_\infty \quad (14.1)$$

Applying energy conservation for incompressible flow below the actuator disk, we get:

$$p_i + \Delta p + \frac{1}{2}\rho V_i^2 = p_\infty + \frac{1}{2}\rho_\infty V_\infty^2 \quad (14.2)$$

This leads to the pressure jump across the actuator disk to be:

$$\Delta p = \frac{1}{2}\rho_\infty V_\infty^2 \quad (14.3)$$

Using momentum equation, thrust T on the disc is equal to the overall rate of increase of axial momentum of the air, that is (dropping ∞ from density):

$$T = \rho A V_i V_\infty \quad (14.4)$$

Also, the pressure difference across the actuator disk can be calculated as

$$\Delta p = \frac{T}{A} = \rho V_i V_\infty \quad (14.5)$$

This leads to,

$$V_{\infty} = 2V_i \quad (14.6)$$

$$T = 2 \rho A V_i^2 \quad (14.7)$$

From which, the induced velocity is calculated as

$$V_i = \sqrt{\frac{T}{2 \rho A}} = \sqrt{\frac{w}{2 \rho}} \quad (14.8)$$

Where, w is the 'disc loading'. V_i is the 'induced velocity' or alternatively the 'downwash', using an analogy with aircraft wing flow which becomes more obvious when the helicopter is in forward flight.

For piston-engine helicopter, the disk loading is low (around 10 kg/m²). This is because the piston engines are heavy and a large rotor diameter must be used to achieve the required vertical lift. For gas turbine engines, which have higher power-to-weight ratios, smaller rotors can be used leading to high disc loadings (30-40 kg/m²).

Vertical Climb

Figure 13.2 shows a rotor in vertical climb with upward velocity V_e . Applying energy equation above the rotor, we get:

$$p_{\infty} + \frac{1}{2} \rho V_c^2 = p_i + \frac{1}{2} \rho (V_c + V_i)^2 \quad (14.9)$$

Below the rotor, we have

$$p_{\infty} + \Delta p + \frac{1}{2} \rho (V_c + V_i)^2 = p_{\infty} + \frac{1}{2} \rho (V_c + V_{\infty})^2 \quad (14.10)$$

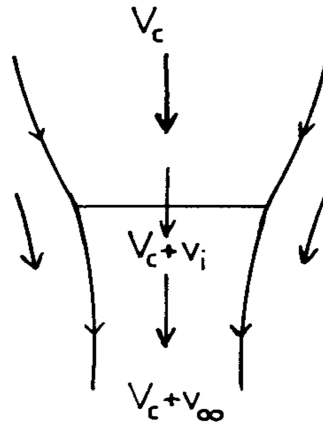


Figure 13.2: Rotor in Vertical climb (Seddon, 1990).

The thrust force is calculated using momentum equation as follows:

$$T = \rho A (V_c + V_i)V_\infty \quad (14.11)$$

$$V_\infty = 2V_i \quad (14.12)$$

$$T = 2 \rho A (V_c + V_i) V_i \quad (14.13)$$

Vertical descent

For vertical descent, V_c is negative (upward air stream), while the induced velocity V_i is positive (downward flow across the rotor). A vortical flow structure is formed due to the interaction between the upward flow around the rotor and the downward flow through it (see Figure 14.3). This results in unsteady flow behavior associated with rotor vibrations. The vortex rings periodically build up and then break spilling flow chaotically. This results in lift fluctuations and helicopter dynamic instability. The flight condition becomes dangerous at high descent rates (at three quarters of the hover induced velocity). The analysis of such flow needs consideration of energy dissipation in the unsteady flow.

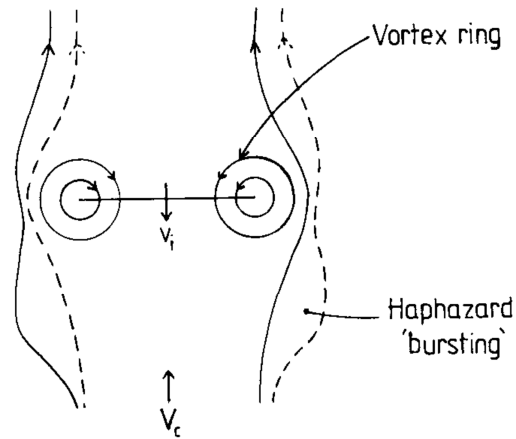


Figure 14.3: Vortex-ring state in vertical descent (Seddon, 1990).

When the descent rate approaches the level of the induced velocity, there is little or no net flow through the disc (see Figure 14.4). This case is similar to flow around bluff body (Turbulent-wake state). For large descent rates (V_c is greater than $2V_i$), the flow is everywhere upwards relative to the rotor, producing a *windmill-brake state*, in which power is transferred from the air to the rotor (see Figure 14.5).

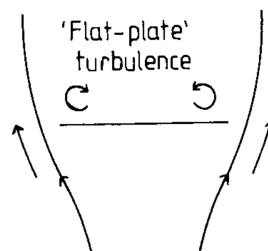


Figure 14.4: Turbulent-wake state in vertical descent.

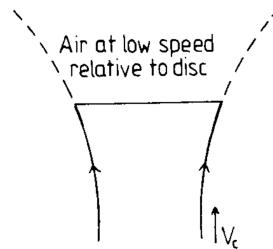


Figure 14.5: Windmill-brake state in vertical descent.

References

- Bazov, D. I. (1969). *Helicopter Aerodynamics*. Moscow: Transport press.
- Bramwell, A., Done, G., & Balmford, D. (2001). *Bramwell's Helicopter Dynamics*. MA: Butterworth-Heinemann.
- Gessow, A., & Myers, G. (1954). *Aerodynamics of the Helicopter*. New York: Frederick Ungar Publishing Company.
- Seddon, J. (1990). *Basic Helicopter Aerodynamics*. London: BSP Professional Books.

CHAPTER 15

VERTICAL FLIGHT: BLADE ELEMENT THEORY

Introduction

Blade element theory means the use of airfoil theory to determine the aerodynamic forces acting on the rotating blades. Figure shows the rotor disc viewed from above. The Blade rotation is anticlockwise with angular velocity Ω . An elementary blade section is taken at radius y , of chord length c and spanwise width dy . The velocity triangle and forces on the blade section are shown in Figure 15.2. The resultant velocity is given by

$$U = [(V_i + V_c)^2 + (\Omega y)^2]^{1/2} \quad (15.1)$$

$$\phi = \tan^{-1}[(V_i + V_c)/(\Omega y)] \quad (15.2)$$

$$\alpha = \theta - \phi \quad (15.3)$$

Where α is the angle of attack, θ is the pitch angle, and ϕ is the flow angle.

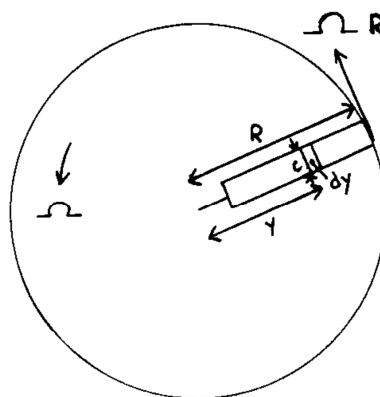


Figure 15.1: Rotor disc.

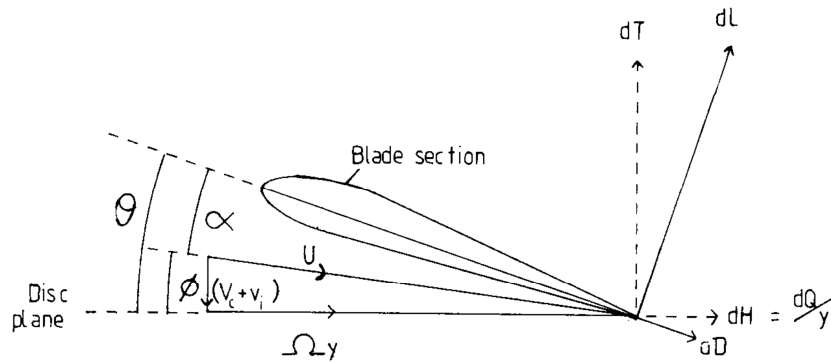


Figure 15.2: Blade section in vertical flight (Seddon, 1990).

The lift L , drag D , thrust T and torque Q can be calculated as follows:

First, we consider elemental forces and moments acting to an element dy of the blade, which can be obtained by:

$$dL = \frac{1}{2} \rho U^2 c dy C_L \quad (15.4)$$

$$dD = \frac{1}{2} \rho U^2 c dy C_D \quad (15.5)$$

$$dT = dL \cos \phi - dD \sin \phi \quad (15.6)$$

$$dQ = (dL \sin \phi + dD \cos \phi) y \quad (15.7)$$

The elemental thrust coefficient C_T is calculated as:

AERODYNAMICS AND ITS APPLICATIONS

$$dC_T = \frac{\frac{1}{2} \rho U^2 c dy C_L}{\rho \pi R^2 (\Omega R)^2} = \frac{1}{2} \frac{c}{\pi R} C_L r^2 dr \quad (15.8)$$

$$dC_T = \frac{1}{2} \frac{N c}{\pi R} C_L r^2 dr \quad (15.9)$$

Blade solidity σ is defined by

$$\sigma = \frac{\text{blade area}}{\text{disc area}} = \frac{N c}{\pi R} \quad (15.10)$$

To get the thrust coefficient, we integrate along blade as

$$C_T = \frac{1}{2} \sigma \int_0^1 C_L r^2 dr \quad (15.11)$$

Similarly, the torque coefficient can be obtained by

$$dC_Q = \frac{1}{2} \sigma (\phi C_L + C_D) r^3 dr \quad (15.12)$$

$$C_Q = \frac{1}{2} \sigma \int_0^1 (\lambda C_L r^2 + C_D r^3) dr \quad (15.13)$$

The power P and power coefficient C_P are calculated as

$$P = \Omega Q \quad (15.14)$$

$$C_P = \frac{P}{\rho A (\Omega R)^3} \quad (15.15)$$

To use previous equations, it is necessary to know the span-wise variation of the angle of attack, and C_L and C_D as a functions of angle of attack.

Blade mean lift coefficient

The *blade mean lift coefficient* is defined such that when applied along the blade span, would give the same total thrust as the actual lift distribution. Using mean lift coefficient \bar{C}_L , we have,

$$C_T = \frac{1}{2} \sigma \int_0^1 \bar{C}_L r^2 dr = \frac{1}{6} \sigma \bar{C}_L \quad (15.16)$$

Using the definition of the thrust coefficient and the solidity, we can write,

$$\frac{C_T}{\sigma} = \frac{T}{\rho A_b (\Omega R)^2} \quad (15.17)$$

where A_b is the total blade area. C_T/σ is the non-dimensional blade loading corresponding to the non-dimensional disc loading C_T . Blades usually operate in the C_L range 0.3 to 0.6, so typical values of C_T/σ are between 0.05 and 0.1. Typical values of C_T are an order of 10 smaller.

Power

The differential power coefficient is given by,

$$dC_P = \frac{1}{2} \sigma C_L \phi r^3 dr + \frac{1}{2} \sigma C_D r^3 dr = \lambda dC_T + \frac{1}{2} \sigma C_D r^3 dr \quad (15.18)$$

Assuming uniform inflow and a constant profile drag coefficient, we have the approximation

$$C_P = \lambda C_T + \frac{1}{8} \sigma C_D \quad (15.19)$$

A practical formula which includes an empirical factor κ is used as,

$$C_P = \kappa \lambda C_T + \frac{1}{8} \sigma C_D \quad (15.20)$$

A figure of merits M can be written as,

$$M = \frac{C_{P_ideal}}{C_{P_actual}} = \frac{C_T^{3/2}}{\kappa C_T^{3/2} + \frac{\sigma}{4\sqrt{2}} C_D} \quad (15.21)$$

which demonstrates that for a given thrust coefficient a high figure of merit requires a low value of σC_D . For low solidity, higher angles of attacks are required to produce the same thrust. This leads to an increase in the drag. So, a compromise is needed to decrease solidity without sacrificing drag.

Tip loss

To calculate forces and moments on blades, we integrated along span from hub to tip. Using actuator disc theory, the lift is linear from hub to tip. Disc theory assumes a well-defined stream tube to exist both above and below the rotor. In reality, the air is able to escape outward due to the rotor tip vortices. Hence, the total induced flow is lower and the thrust produced is less than the actuator disk theory. The deficiency is known as *tip loss* and is shown by a rapid falling off of lift over the last few per cent of span near the tip. A common method of analysis for this case is to assume that no lift is produced after certain radial station $r = BR$. The thrust integral

AERODYNAMICS AND ITS APPLICATIONS

becomes,

$$C_T = \frac{1}{2} \sigma a \int_0^B (\theta r^2 - \lambda r) dr = \frac{1}{2} \sigma a \left(\frac{1}{3} B^3 \theta - \frac{1}{2} B^2 \lambda \right) \quad (15.22)$$

References

- Bazov, D. I. (1969). *Helicopter Aerodynamics*. Moscow: Transport press.
- Bramwell, A., Done, G., & Balmford, D. (2001). *Bramwell's Helicopter Dynamics*. MA: Butterworth-Heinemann.
- Gessow, A., & Myers, G. (1954). *Aerodynamics of the Helicopter*. New York: Frederick Ungar Publishing Company.
- Seddon, J. (1990). *Basic Helicopter Aerodynamics*. London: BSP Professional Books.

CHAPTER 16

FORWARD FLIGHT: ROTOR MECHANISMS

Figure 16.1 shows a rotor disc in forward flight. Blade rotation is in a counter-clockwise sense with rotational speed, Ω . Forward flight velocity is V and the ratio $V/\Omega R$, R being the blade radius, is known as the *advance ratio* μ , and has a value normally within the range zero to 0.5. Azimuth angle ψ is measured from the downstream blade position. Advancing side of the rotor is defined by azimuth angle between 0° and 180° , while the retreating side is defined from 180° - 360° .

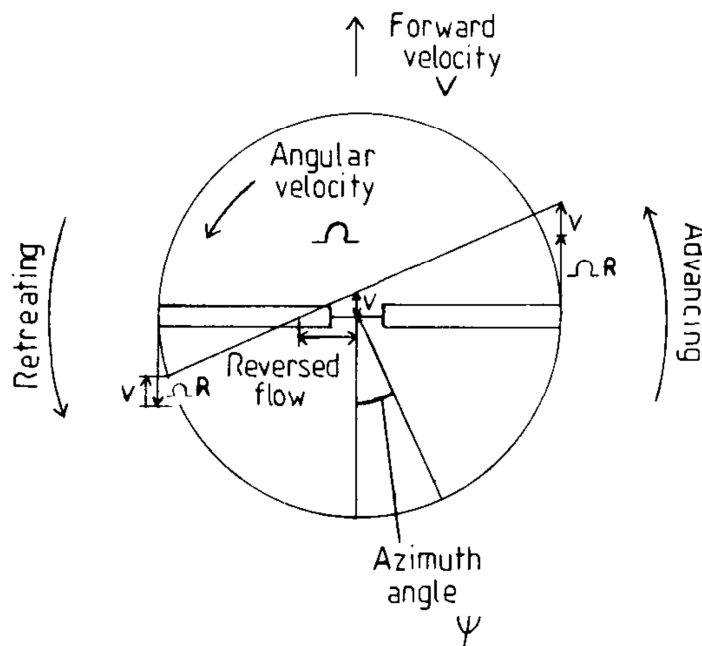


Figure 16.1: Rotor in forward flight (Seddon, 1990)

AERODYNAMICS AND ITS APPLICATIONS

For the blades shown in Figure 16.1 at 90° and 270° , the velocities at the tip are $(\Omega R + V)$ and $(\Omega R - V)$, respectively. If the angle of attack is the same for both blades, more lift would be generated on the advancing side than on the retreating side. Pressure contours for a fixed-incidence rotation with $\mu = 0.3$ are shown in Figure 16.2. About four-fifths of the total lift is produced on the advancing side. This would lead to large oscillatory bending stresses at the blade roots and a large rolling moment on the vehicle. Both structurally and dynamically it would be dangerous to fly such helicopter.

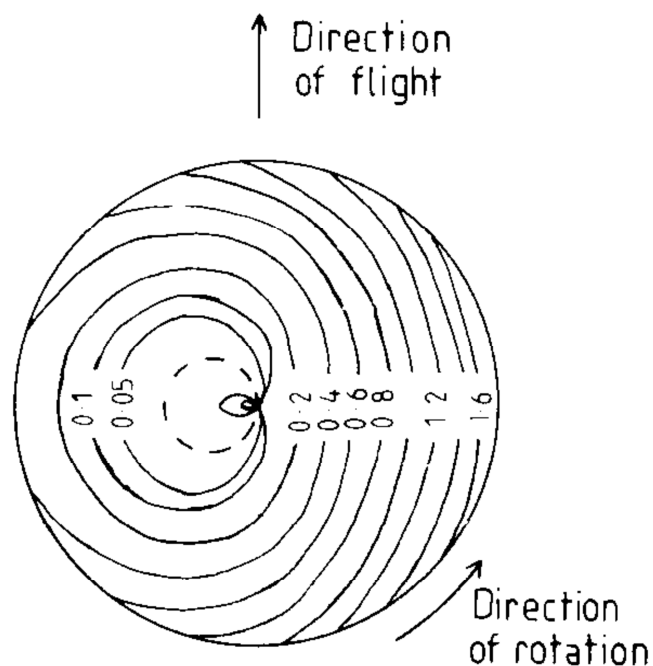


Figure 16.2: Pressure contours for unbalanced rotation

AERODYNAMICS AND ITS APPLICATIONS

To resolve this situation, a cyclical variation in blade incidence is needed to balance lift on the two sides. The widely adopted method for this purpose is the use of flapping hinges. These are free hinges near the root of the blade. It allows it to flap up and down during rotation. When the blade moves through the advancing side, the lift increases causing the blade to flap upward. The effective blade incidence is reduced and hence the lift reduces causing flap down again. On the retreating side the reverse process occurs. Free hinges also relieve the blade from root stresses and no rolling moment is produced.

Pressure contours for a roll-balanced lift distribution are shown in Figure . The lift on the advancing side is reduced, with only small compensation on the retreating side. The fore and aft sectors now carry the main lift load. The retreating blade is subjected to stall, while compressibility effects such as shock-induced flow separation will dictate the retreating side. Since load asymmetry across the disc increases with forward speed, the retreating-blade stall dictates the maximum flight speed.

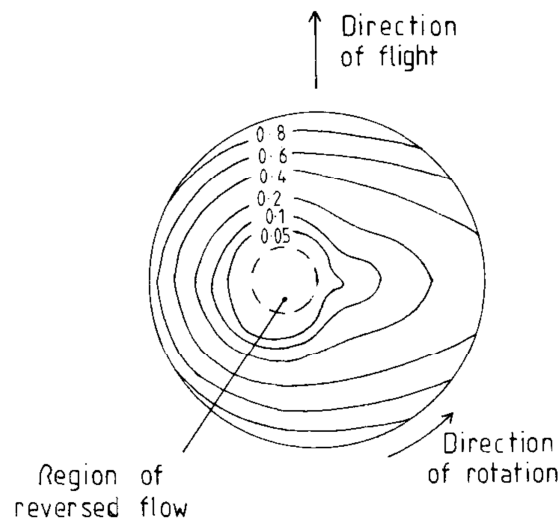


Figure 16.3: Pressure contours for roll-balanced rotation.

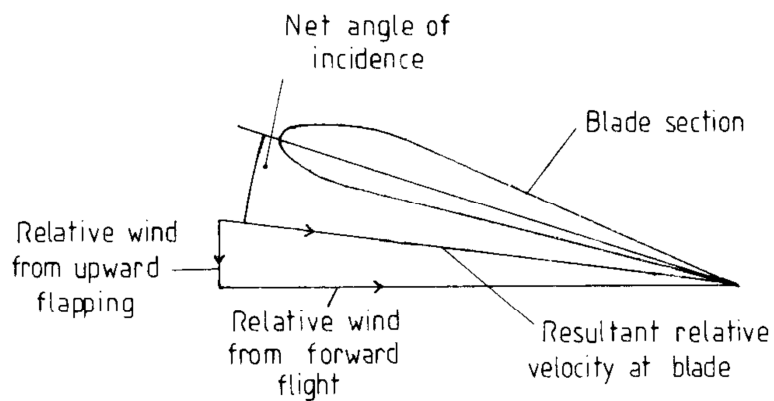


Figure 14.4: Blade flapping action

An additional feature of the asymmetry in velocity across the disc is that there exists a region on the retreating side where the flow over the blade is actually reversed. At 270° azimuth the resultant velocity at a point y of span is

AERODYNAMICS AND ITS APPLICATIONS

$$\mathbf{U} = \boldsymbol{\Omega} \mathbf{y} - \mathbf{V} \quad (16.1)$$

In nondimensional form,

$$\mathbf{u} = \frac{\mathbf{U}}{\boldsymbol{\Omega} R} = \mathbf{r} - \boldsymbol{\mu} \quad (16.2)$$

As shown in Figure 16.5, three hinge systems are used as follows:

- *Flapping hinge*, normal to blade span (in disc plane), to allow free flapping of blade.
- *Lead-lag hinge*, normal to the disc plane, to allow free in-plane motion. To relieve Coriolis moments.
- *Pitch bearing*, approximately normal to the flapping and lead-lag axes, is required for control of the blade incidence or pitch angle.

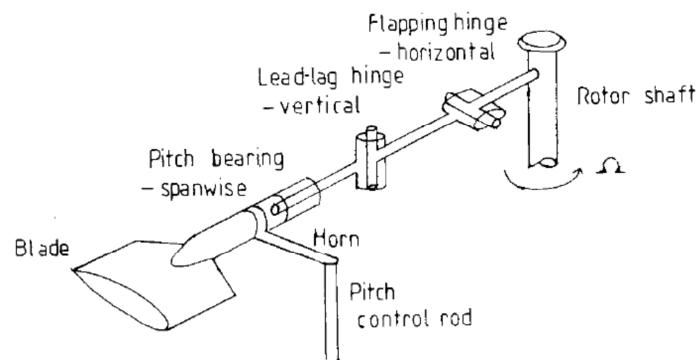


Figure 16.5: Rotor hinge system.

Flapping Motion

AERODYNAMICS AND ITS APPLICATIONS

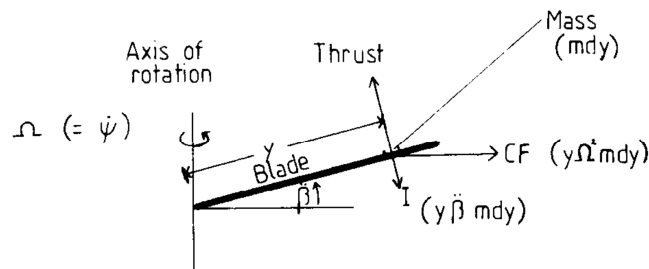


Figure 16.6: Blade forces in flapping.

Figure 16.6 shows flapping motion under conditions of dynamic equilibrium. The forces are the aerodynamic lift, the centrifugal force and the blade inertia. The oscillatory motion represents a dynamic system in resonance. The flapping moment equation is

$$\int_0^R y dT - \int_0^R m y^2 \ddot{\beta} dy - \int_0^R m \beta y^2 \Omega^2 dy = 0 \quad (16.3)$$

The centrifugal force is a stabilizing force. The degree of stability is highest in the hover condition (where the flapping angle is constant) and decreases as the advance ratio increases. Bramwell (Bramwell, 2001) concluded that the motion is dynamically stable for all realistic values of μ .

Maximum flapping velocities occur where the air velocity is maximum and minimum, that is at 90° and 270° azimuth. Maximum displacements occur 90° later, that is at 180° (upward) and 0° (downward). These displacements mean that the plane of rotation of the blade tips, the *tip-path plane* (TPP), is tilted backwards relative to the plane normal to the rotor shaft, the *shaft normal plane* (SNP).

AERODYNAMICS AND ITS APPLICATIONS

Since in any steady state of the rotor the flapping motion is periodic, the flapping angle can be expressed in the form of a Fourier series:

$$\beta = a_0 - a_1 \cos \psi - b_1 \sin \psi \quad (16.4)$$

Rotor Control

Control of the helicopter in flight involves changing the magnitude of rotor thrust or its line of action or both. This is achieved by tilting the rotor shaft, or the hub, relative to the fuselage. Since the rotor is driven by the engine, tilting the shaft is impracticable. Tilting the hub is possible with some designs but the large mechanical forces required restrict this method to very small helicopters. Use of the feathering mechanism to change the pitch angle of the blades, either collectively or cyclically, effectively changing the magnitude and direction of the rotor thrust.

Blade feathering, or pitch change, could be achieved using aerodynamic servo tabs, auxiliary rotors, fluidically controlled jet flaps, or pitch links from a control gyro as possible methods. The widely adopted method, however, is through a swashplate system, illustrated in Figure 16.7. It has two parallel plates, the lower of which does not rotate with the shaft but can be tilted in any direction by operation of the pilot's cyclic control column and raised or lowered by means of his collective lever. The upper plate is connected by control rods to the feathering hinge mechanisms of the blades and rotates with the shaft, while being constrained to remain parallel

AERODYNAMICS AND ITS APPLICATIONS

to the lower plate. Raising the collective lever thus increases the pitch angle of the blades by the same amount all round, while tilting the cyclic column applies a tilt to the plates and thence a cyclic pitch change to the blades, these being constrained to remain at constant pitch relative to the upper plate. An increase of collective pitch at constant engine speed increases the rotor thrust (short of stalling the blades), as for takeoff and vertical control generally. A cyclic pitch change alters the line of action of the thrust, since the tip-path plane of the blades, to which the thrust is effectively perpendicular, tilts in the direction of the swashplate angle.

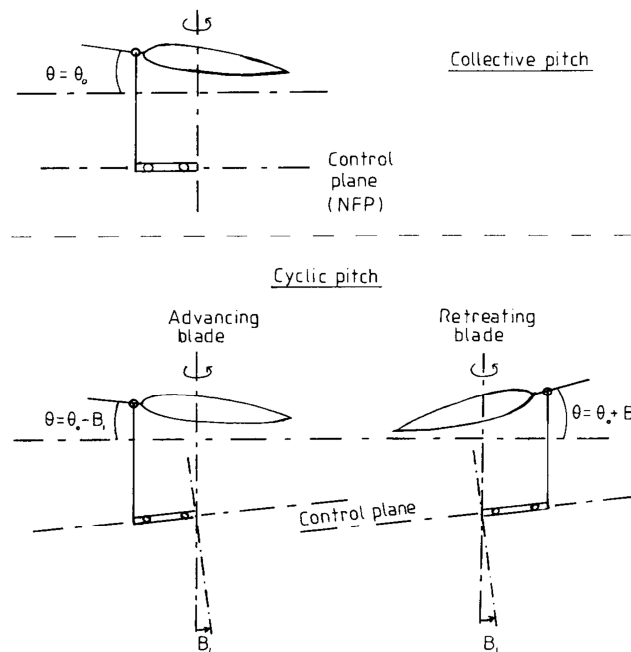


Figure 16.7: Swashplate system (Seddon, 1990).

References

AERODYNAMICS AND ITS APPLICATIONS

Bazov, D. I. (1969). *Helicopter Aerodynamics*. Moscow: Transport press.

Bramwell, A., Done, G., & Balmford, D. (2001). *Bramwell's Helicopter Dynamics*. MA: Butterworth-Heinemann.

Gessow, A., & Myers, G. (1954). *Aerodynamics of the Helicopter*. New York: Frederick Ungar Publishing Company.

Seddon, J. (1990). *Basic Helicopter Aerodynamics*. London: BSP Professional Books.

CHAPTER 17

FORWARD FLIGHT: ROTOR AERODYNAMICS

The aerodynamic situation in forward flight is complex. Here, the thrust vector has two components; one in the vertical direction to balance weight and the other in the horizontal plane to produce forward motion. We will examine both momentum theory and blade element theory in this chapter.

Momentum Theory

A modified Glauert actuator disc approach assuming a mean induced velocity as,

$$V_i = \frac{T}{2\rho A \hat{V}} \quad (17.1)$$

where

$$\hat{V} = \sqrt{V^2 + V_i^2} \quad (17.2)$$

V is the forward flight speed.

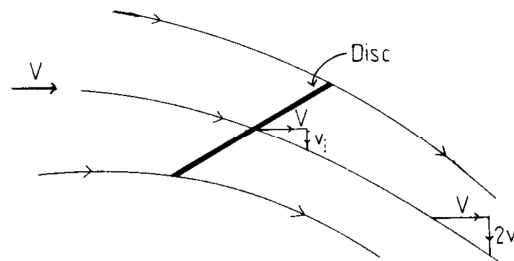


Figure 5: Interpretation of Glauert formula for momentum theory in forward flight (Seddon, 1990)

Figure 5 shows a helicopter rotor in forward flight. A jet of free stream velocity V , and area equals the rotor area, passes through the rotor and then it is deflected downwards at velocity V_i at the disc. The velocity reaches $2V_i$ downstream by similarity with hover flow discussed previously. Induced velocity reduces to that for hover, when V is zero. If V is large, the formula converts to that for the induced velocity of an elliptically-loaded fixed wing.

If V_h is the induced velocity in hover at the same thrust, we have

$$\left(\frac{V_i}{V_h}\right)^4 + \left(\frac{V}{V_h}\right)^2 \frac{V_i}{V_h} - 1 = 0 \quad (17.3)$$

In practice the induced velocity cannot be expected to be constant over the area of the disc. Standard aerofoil theory would suggest an upwash at the leading edge and a greater-than-mean downwash at the trailing edge.

Blade element theory

Using the same approach as the one used for hover analysis, we can determine the aerodynamic forces and moments acting on the rotor blade. Figure 6 shows a side view of the rotor disc. Helicopter is moving horizontally to the left. The angle between the disc edge plane (tip-path plane TPP) and flight direction is α_r . The advance ratio is:

$$\mu = \frac{V \cos \alpha_r}{\Omega R} \simeq \frac{V}{\Omega R} \quad (17.4)$$

AERODYNAMICS AND ITS APPLICATIONS

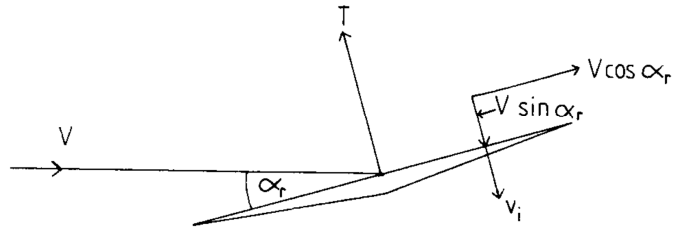


Figure 6: Rotor disc in forward flight.

Components U_T and U_R are defined as,

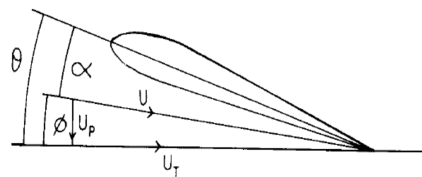
$$U_T = \Omega y + V \sin \psi \quad \text{and} \quad U_R = V \cos \psi \quad (17.5)$$

Using ΩR as a reference velocity, the components becomes,

$$u_T = r + \mu \sin \psi \quad \text{and} \quad u_R = \mu \cos \psi \quad (17.6)$$

We define the inflow factor λ as,

$$\lambda = \frac{V \sin \alpha_r + V_i}{\Omega R} = \mu \alpha_r + \lambda_i \quad (17.7)$$



AERODYNAMICS AND ITS APPLICATIONS

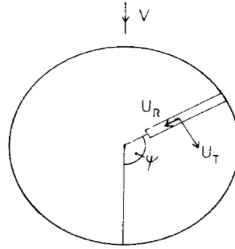


Figure 17.3: Velocity components

The component U_p is obtained by,

$$u_p = \lambda + \beta \mu \cos \psi + r \frac{d\beta}{d\psi} \quad (17.8)$$

Thrust

The differential thrust coefficient is given by,

$$dC_T = \frac{\frac{1}{2} \rho U^2 c dy C_L}{\rho \pi R^2 (\Omega R)^2} = \frac{1}{2} \frac{c}{\pi R} C_L r^2 dr \quad (17.9)$$

$$C_L = a \alpha = a \left(\theta - \frac{u_p}{u_T} \right) \quad (17.10)$$

$$dC_T = \frac{1}{2} \sigma a (\theta u_T^2 - u_T u_p) dr \quad (17.11)$$

$$C_T = \int_0^1 \frac{1}{2} \sigma a \left[\frac{1}{2\pi} \int_0^{2\pi} \theta u_T^2 - u_T u_p \right] d\psi dr \quad (17.12)$$

This is the formula for the lift coefficient of a rotor in forward level flight under the following

AERODYNAMICS AND ITS APPLICATIONS

assumptions:

- uniform induced velocity across the disc
- constant solidity along the span
- zero blade twist or a linearly twisted blade, with the value of θ taken to be that at three quarters radius.

In-plane H-force

In hover, the in-plane H force is the blade profile drag, while in forward flight the drag force on the advancing side exceeds the reverse drag force on the retreating side, leaving a net drag force on the blade, positive in the rearward direction. H force (normal to the blade span in the rearward direction) is

$$dH = (dD \cos \phi + dL \sin \phi) \sin \psi = dH_o + dH_i \quad (17.13)$$

Where, dH_o is the H force due to drag and dH_i is the H force due to lift.

The differential H forces becomes,

$$dH = dD \sin \psi = \frac{1}{2} \rho U_T^2 c dy C_{D0} \sin \psi \quad (17.14)$$

$$dC_{H0} = \frac{1}{2} \sigma C_{D0} (r + \mu \sin \psi)^2 \sin \psi dr \quad (17.15)$$

Integrating along the blade span, we get,

AERODYNAMICS AND ITS APPLICATIONS

$$C_{H0} = \frac{1}{4} \sigma \mu C_{D0} \quad (17.16)$$

The in-plane H force is

$$C_H = \frac{1}{4} \sigma \mu C_{D0} + C_{Hi} \quad (17.17)$$

The expression for the induced component C_{Hi} can be obtained in a similar way as in Bramwell, 2001.

Torque and power

The elementary torque is

$$dQ = dH y = y (dD \cos \phi + dL \sin \phi) \sin \psi = dQ_0 + dQ_i \quad (17.18)$$

where dQ_0 is the torque due to drag and dQ_i is the torque due to lift. The final expressions for these terms are

$$C_{Q0} = \frac{1}{8} \sigma C_{D0} (1 + \mu^2) \quad (17.19)$$

$$C_{Qi} = \lambda C_T - \mu C_{Hi} \quad (17.20)$$

The power equation with empirical coefficient κ is

$$C_P d = \kappa \lambda C_T + \frac{1}{8} \sigma C_{D0} (1 + k \mu^2) + \mu \frac{D}{W} C_T \quad (17.21)$$

AERODYNAMICS AND ITS APPLICATIONS

References

Bazov, D. I. (1969). *Helicopter Aerodynamics*. Moscow: Transport press.

Bramwell, A., Done, G., & Balmford, D. (2001). *Bramwell's Helicopter Dynamics*. MA: Butterworth-Heinemann.

Gessow, A., & Myers, G. (1954). *Aerodynamics of the Helicopter*. New York: Frederick Ungar Publishing Company.

Seddon, J. (1990). *Basic Helicopter Aerodynamics*. London: BSP Professional Books.

CHAPTER 18

HELICOPTER PERFORMANCE: HOVER, VERTICAL FLIGHT, FORWARD FLIGHT AND CLIMB IN FORWARD FLIGHT

Introduction

In this chapter, we will consider the helicopter as a vehicle. The aerodynamic forces and moments and the thrust power will be used to determine the performance. This includes various flight conditions in hover, vertical, and forward flight with or without climb.

A typical specification of a helicopter might include the following:

- Prescribed missions, such as a hover role, a payload/range task or a patrol/loiter task. A mission specification leads to a weight determination for payload plus fuel and thence to an all-up weight, see Figure 18.1:.
- Some specific atmosphere-related requirements, for example the ability to perform the mission at standard (ISA) temperature plus other temperatures; the ability to perform a reduced mission at altitude; the ability to fly at a particular cruise speed.
- Specified safety requirements to allow for an engine failure.
- Specified environmental operating conditions, such as to and from ships or oil rigs.
- Prescribed dimensional constraints for stowage, air portability etc.
- A prescribed power plant.

Vehicle performance calculations are needed both at the flexible design stage and after

AERODYNAMICS AND ITS APPLICATIONS

realization of design to compare with actual performance or enhance the performance.

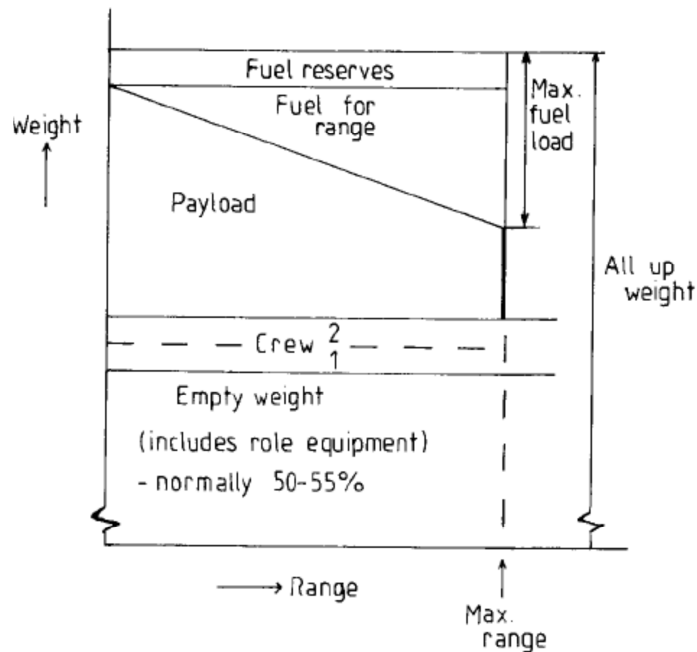


Figure 18.1: Determination of all-up weight for prescribed mission (Seddon, 1990).

To perform performance calculation, we need the power required in hover or forward flight and envelope of thrust limitations imposed by retreating-blade stall and advancing-blade compressibility drag rise. The thrust limitations will be the determining factor for level flight speed and maneuver capability.

Hover and vertical flight

The power required is the sum of induced power, related to blade lift, and profile power, related to blade drag. It is obtained as,

$$P = k (V_c + V_i) T + \frac{1}{8} C_D \rho A_b V_T^3 \quad (18.1)$$

Using momentum theory, we can write

$$V_c + V_i = \frac{1}{2} V_c + \sqrt{\left(\frac{1}{2} V_c\right)^2 + \frac{T}{2\rho A}} \quad (18.2)$$

In the profile term, A_b is the total blade area, and V_T is the tip speed, equal to ΩR . We calculate separately the power requirements of main and tail rotors. For the latter, V_c disappears and the level of thrust needed is such as to balance the main rotor torque in hover: this requires an evaluation of hover trim, based on the simple equation

$$T \ell = Q \quad (18.3)$$

Where, Q is the main rotor torque and ℓ is the moment arm from the tail rotor shaft perpendicular to the main rotor shaft.

Forward level flight

The empirical equation for power is used in the form

$$P = \kappa V_i T + \frac{1}{8} C_D \rho A_b V_T^3 \left[1 + k \left(\frac{V}{V_T}\right)^2 \right] + \frac{1}{2} \rho V^3 f \quad (18.4)$$

Where V_T is the rotor tip speed, V the forward-flight speed and f the fuselage-equivalent flat-plate area. The induced velocity V_i is given according to momentum theory as

AERODYNAMICS AND ITS APPLICATIONS

$$V_i^2 = -\frac{1}{2}V^2 + \frac{1}{2}\sqrt{V^4 + 4\left(\frac{T}{2\rho A}\right)^2} \quad (18.5)$$

The power equations shows the power coefficient to be a linear sum of three terms; induced power (rotor lift dependent), profile power (blade-section drag dependent) and parasite power (fuselage-drag dependent).

Extra power is needed for tail rotor and power to transmission and accessories (perhaps 15% of P at $V = 0$ and 8% at high speed). The thrust T may be assumed equal to the aircraft weight W for all forward speeds above 5 m/s (10 knots).

A typical breakdown of the total power as a function of flight speed is shown in Figure 18.2. In hover, induced power is the dominant term for low speed and its contribution diminishes as the speed increases. Profile power contribution is almost constant till the speed for compressibility drag rise, where it is increasing. Parasite power is zero in the hover. It increases as V^3 and it comprises the largest component at high speed. Adding all terms, the total power has a typical 'bucket' shape, high in the hover falling to a minimum at moderate speed and rising rapidly at high speed to levels above the hover value. Hence, the helicopter uses less power in forward flight than in hover except at high speeds.

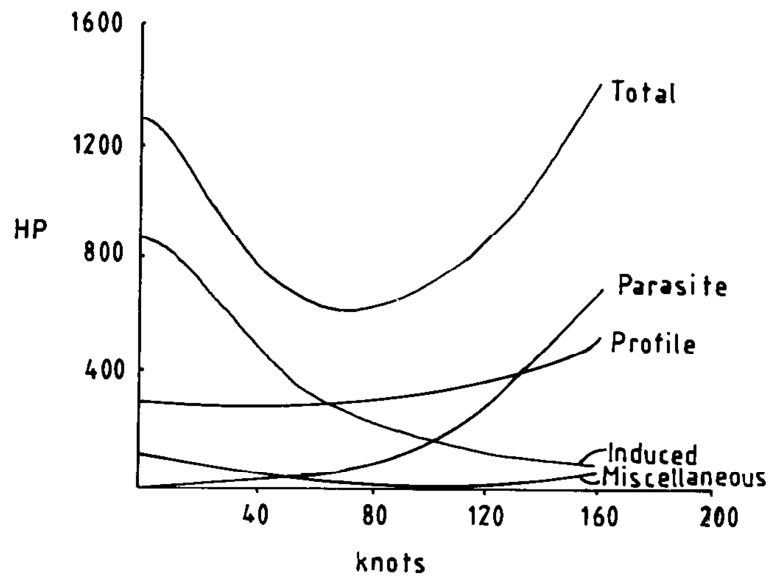


Figure 18.2: Typical power breakdown for forward level flight (Seddon, 1990).

Climb in forward flight

We assume that the profile power and parasite power remain the same as in level flight and only the induced power has to be calculated. The power is calculated as

$$C_P = \kappa \lambda_i C_T + \frac{1}{8} \sigma C_D [1 + k \mu^2] + \frac{1}{2} \mu^3 \frac{f}{A} + \lambda_c C_T \quad (18.6)$$

Minimum-power forward speed is usually used to calculate climb performance. In this case, V_i is small compared with V , its variation from level flight to climb can be neglected and the incremental power ΔP required for climb is simply $T V_c$. Thus the rate of climb is

$$V_c = \frac{\Delta P}{T} \quad (18.7)$$

During climb, the main rotor torque is increased which means the increase of tail rotor power to

AERODYNAMICS AND ITS APPLICATIONS

balance it. Hence, part of the incremental power available is used to supply extra power to the tail rotor which reduces the climb rate by as much as 30%.

For a given aircraft weight, the incremental power available for climb decreases with increasing altitude due to a decrease in the engine power available. When the incremental power becomes zero, the aircraft has reached its *absolute ceiling* at that weight. *Service ceiling* is defined as the height at which the climb rate is about 0.5 m/s (100 ft/min). Ceiling height reduces, if the helicopter weight increases.

References

- Bazov, D. I. (1969). *Helicopter Aerodynamics*. Moscow: Transport press.
- Bramwell, A., Done, G., & Balmford, D. (2001). *Bramwell's Helicopter Dynamics*. MA: Butterworth-Heinemann.
- Gessow, A., & Myers, G. (1954). *Aerodynamics of the Helicopter*. New York: Frederick Ungar Publishing Company.
- Seddon, J. (1990). *Basic Helicopter Aerodynamics*. London: BSP Professional Books.

CHAPTER 19

HELICOPTER PERFORMANCE: OPTIMUM SPEEDS, MAXIMUM LEVEL SPEED, ROTOR LIMITS ENVELOPE

Optimum speeds

The optimum efficiency for level-flight corresponds to the minimum power speed point (point A in Figure 7). This point also represents the *minimum rate of descent* in autorotation. Speed A' is the speed for *maximum rate of climb* considering parasite drag correction.

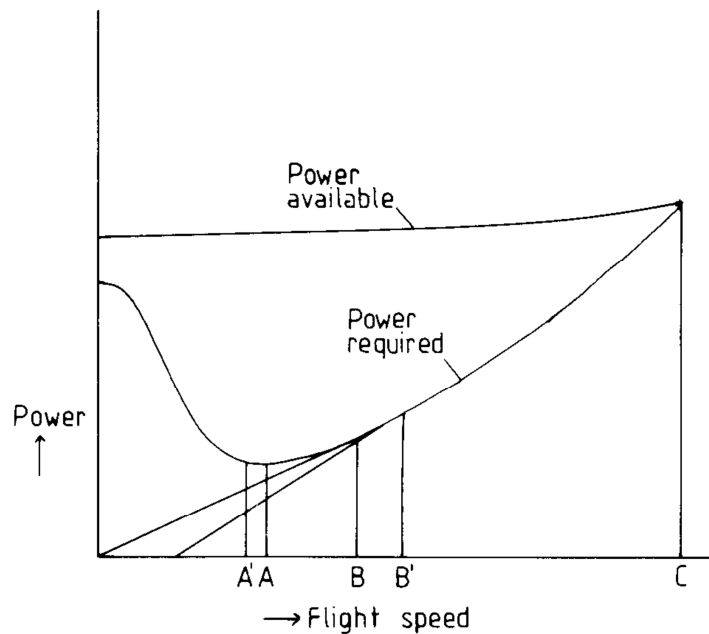


Figure 7 Optimum speeds and maximum speed (Seddon, 1990).

AERODYNAMICS AND ITS APPLICATIONS

Point A also defines the speed for *maximum endurance* or loiter time. *Maximum glide distance* in descent is achieved at speed B, defined by a tangent to the power curve from the origin. Here the ratio of power to speed is a minimum: the condition corresponds to that of gliding a fixed-wing aircraft at its maximum lift-to-drag ratio. Point B is also the speed for *maximum range* in zero wind. For headwind best-range speed is at B' obtained by striking the tangent from a point on the speed axis corresponding to the wind strength. For a tailwind the tangent is taken from a point on the negative speed axis, leading to a lower best-range speed than B

Maximum level speed

The *maximum speed* for level flight is limited by the envelope of retreating-blade stall and advancing-blade drag rise. It is defined by the intersection of the curves of power required and power available, (C in Figure 7). Power available is assumed to be greater than that required for hover (out of ground effect) and, typically, to be nearly constant with speed, increasing a slight at high speed from the effect of ram pressure in the engine intakes. The power required curve takes the bucket shape. It is the sum of the induced drag, profile drag and miscellaneous additional drag. At maximum speed, the power required is almost double the parasite power P_p , hence,

$$P_{av} = 2 P_p = \rho V_{max}^3 f \quad (19.1)$$

$$V_{max} = \left(\frac{P_{av}}{\rho f}\right)^{1/3} \quad (19.2)$$

Increasing density altitude reduces the power available and may either increase or decrease the

AERODYNAMICS AND ITS APPLICATIONS

power required. Generally the reduction of available power dominates and V_{max} decreases. Increasing weight increases the power required (through the induced power P_i) without changing the power available, so again V_{max} is reduced.

Rotor limits envelope

Rotor limits envelope is determined by stall at high angle of attack and compressibility effects at high Mach number. Also, the limits of the available power for the rotor will affect its operation. Typical envelope is sketched in Figure 19.2.

In hover, the stall will limit the thrust available since conditions are uniform at any radial position. As forward speed increases, maximum thrust on the retreating blade decreases because of the drop in dynamic pressure and this limits the thrust achievable throughout the forward-speed range. On the contrary, maximum thrust on the advancing side increases but it is unrealizable because of the retreating blade restriction. At higher speeds, the shock waves will result in flow separation, which leads to drag divergence and loss in lift. Eventually the maximum speed is limited. Thus, the envelope represents a limit on thrust from retreating-blade stall and a limit on forward speed from advancing-blade Mach effects.

Calculation of the limits envelope is usually done by computer allowing the inclusion of other factors, such as a non-uniform induced velocity distribution, a compressibility factor on lift slope and a representation of blade dynamic stall characteristics.

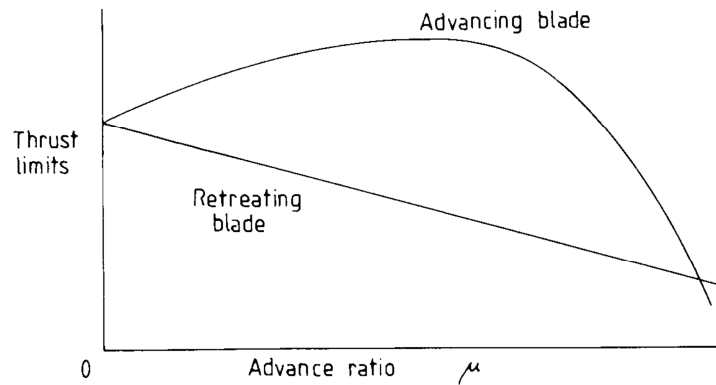


Figure 19.2: Rotor thrust limits (Seddon, 1990).

Accurate performance prediction

Usually using numerical methods will relieve some of the assumptions needed for analytical analysis. Hence, modern performance analysis relies heavily in numerical methods to produce accurate results that can be compared with actual flight tests.

Special cases usually need accurate predictions. For example, the stress analysis of the rotor is so critical and complicated such that it needs accurate methods. Another case is the determination of the behavior of a helicopter flying in a bad aerodynamic environment.

Some terms needs special attention such as parasite drag. To determine the total drag of the helicopter, it is broken down into manageable groupings, such as streamlined and non-streamlined components, fuselage angle of attack, surface roughness, leakage and cooling-air loss.

To improve induced and profile drag predictions, we should use a realistic distribution of

AERODYNAMICS AND ITS APPLICATIONS

induced velocity over the disc area, accurate blade section lift and drag characteristics including dynamic effects. The rotor is analyzed for various angles of attack and Mach numbers of all blade sections varying from root to tip and round the azimuth as the blade rotates. Usually, iterative methods are required among the basic equations of thrust, collective and cyclic pitch and the flapping angles.

References

- Bazov, D. I. (1969). *Helicopter Aerodynamics*. Moscow: Transport press.
- Bramwell, A., Done, G., & Balmford, D. (2001). *Bramwell's Helicopter Dynamics*. MA: Butterworth-Heinemann.
- Gessow, A., & Myers, G. (1954). *Aerodynamics of the Helicopter*. New York: Frederick Ungar Publishing Company.
- Seddon, J. (1990). *Basic Helicopter Aerodynamics*. London: BSP Professional Books.

CHAPTER 20

INTRODUCTION TO AIRCRAFT CONCEPTUAL DESIGN PROCESS

Introduction

In designing remote controlled home build aircraft, conceptual design process is sufficient enough to provide all configuration details such as wing, tail and fuselage dimensions. The design process must start with initial requirements and mission profile. The designer needs to guess the target weight of the designed aircraft. The design process then will continue with weight estimation, wing, tail and fuselage sizing. After the configuration layout is completed, the total drag of the aircraft must be predicted in order to estimate engine power. Stability analysis, location of center of gravity and the performance of the aircraft should be considered. If any design problem appears in this stage, it can be corrected through optimization process or repeating of the components calculation process. The optimization of the components dimension can be also carried out during fabrication process or before conducting the flight test. Figure 20.1 shows suggested flow chart to develop new RC home build aircraft.

In this stage set of specific design requirements will be established by the designer. The initial requirements the aircraft should be related to the mission profile of the aircraft. Aircraft design requirements should include the following details: target weight, range, altitude, engine type, maximum speed, endurance and takeoff and landing distance.

AERODYNAMICS AND ITS APPLICATIONS

Takeoff Weight

Estimation of the aircraft takeoff is considered as one of the most important parameter where the historical data base is used to estimate unknown parameters.

Airfoil selection

Lift to drag ratio is the most important parameter in selecting the suitable airfoil type for the wing section but selection of the airfoil also highly depends on the type of the aircraft.

Wing and Tail Geometry Parameters

The most important wing geometry parameters for homebuilt RC aircraft are area (S), chord (c), aspect ratio (AR), taper ratio (λ), span (b), sweep angle (Λ), incidence angle (i), dihedral angle (Γ), wing vertical location, and wing tip type. Some of those parameters such as wing area, span and chord can be calculated using the design relations.

Fuselage Geometry Parameters

The historical data can be used to find the suitable ratio of the fuselage length to maximum diameter of the fuselage. The selection of the fuselage cross section type is highly dependent on the use of the aircraft.

Wing Loading

The design wing loading is defined as the takeoff weight of the aircraft divided by the wing area. The wing loading is very important design parameter and must be predicated in early stage of the

AERODYNAMICS AND ITS APPLICATIONS

design. The wing loading affect the aircraft performance, small wing loading can leads to large wing area and high drag but large wing loading can increase the aircraft weight. The best way to predict the design wing is to estimate the wing loading for all the mission segments and then the lowest wing loading must be selected as design wing loading but very low wing loading is also not acceptable. If problem with unacceptable design wing loading was faced, the designer should modify the initial requirements in order to improve the wing loading value.

AERODYNAMICS AND ITS APPLICATIONS

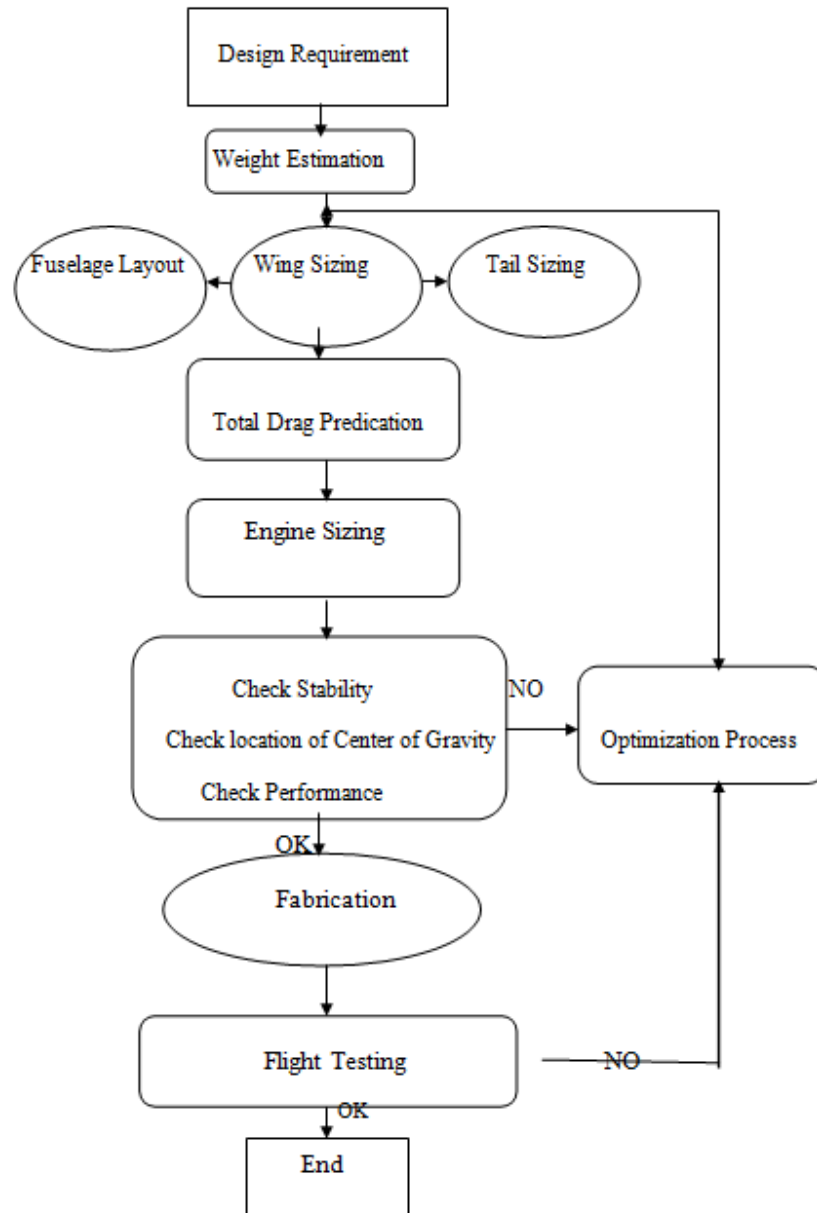


Figure 20.1 Conceptual Design Process of RC Home builds aircraft

Estimation of Drag for New Designed Subsonic Aircraft

Parasite Drag

Estimation of total aircraft drag is important factor in estimating the aircraft power required. The drag of low speed aircraft is divided into two types, mainly, parasite drag and drag due to lift. Rough estimation of profile drag can be achieved by using component build method. In component build method, the flat plate skin friction coefficient of each component is used to calculate the component parasite drag. The interference (F_i) and separation (F_s) drag factors are also included in the component buildup methods for each component. Drag due to any special geometry feature ($C_{D_{spf}}$), manufacture defects, holes and gaps ($C_{D_{mhg}}$) is also roughly estimated and will be added to the parasite drag. The component buildup method can be expressed as

$$C_{D_0} = \frac{1}{S_{Ref}} \sum_N^1 (C_f F_i F_s S)_n + C_{D_{spf}} + C_{D_{mhg}} \quad (20.1)$$

Where S_{Ref} is presenting the reference area, N is total components number, and n is component number.

The skin friction coefficient can be calculated using flat plate relations as

For laminar flow:

AERODYNAMICS AND ITS APPLICATIONS

$$C_f = \frac{1.33}{\sqrt{R_e}} \quad (20.2)$$

For turbulent flow:

$$C_f = \frac{0.455}{1.1(\log_{10} R_e)^{2.58}} \quad (20.3)$$

Where the Reynolds number can be obtained from the following relations

For smooth surface:

$$R_e = \frac{V\bar{C}}{\nu} \quad (20.4)$$

For turbulent flow, the Reynolds number of the rough surface must be consider as

$$R_e = 38.2 \left(\frac{l}{k} \right)^{1.053} \quad (20.5)$$

Where l is presenting the maximum length and k is the skin roughness value which is presented in table 20.1

Table 20.1: Skin Roughness Value

Surface	$K (ft) \times 10^{-5}$
Smooth Paint	2.08

AERODYNAMICS AND ITS APPLICATIONS

Smooth molded composite	0.17
-------------------------	------

The lowest value of the Reynolds number from equation 20.4 and 20.5 will be used in equation 20.3. The average skin friction coefficient can be estimated from the calculation of the laminar and turbulent skin friction coefficients. Then the average skin friction coefficient will be used in equation 20.1.

The interference drag (F_i) factor for the wing and tail can be expressed as

$$F_i = \left[1 + 2\left(\frac{t}{c}\right) + 100\left(\frac{t}{c}\right)^4 \right] \left[1.34M^{0.18} (\cos \Lambda_m)^{0.28} \right] \quad (20.6)$$

And for fuselage as

$$F_i = \left(1 + \frac{60}{f^3} + \frac{f}{400} \right) \quad (20.7)$$

Where Λ_m is refer to the sweep of the maximum thickness line and f is defined as

$$f = \frac{l}{d} \quad (20.8)$$

Table 20.2 shows the estimation value of the separation (F_s) drag factor

Table 20.2 Separation (F_s) drag factor

Type	F_s
Engine mounted directly on the fuselage	1.5
High and mid wing	1.0
Low wing	1.25
Fuselage	1.0
V-Tail	1.03
H-Tail	1.08
Conventional Tail	1.05

Drag due to any special geometry feature ($C_{D_{spf}}$) is predicted using drag area (D/q). The historical data is normally used to estimate the component drag area. Raymer(1992) gives the guide line of estimating $C_{D_{spf}}$. Drag due to manufacture defects, holes and gaps ($C_{D_{mhg}}$) can be estimated for homebuilt aircraft as about 5-10% of the parasite drag.

Induced Drag

AERODYNAMICS AND ITS APPLICATIONS

The induced drag can be estimated using the following relation

$$C_{D_i} = \frac{C_L^2}{\pi e AR} \quad (20.9)$$

Raymer (1992) present relation used to estimate Oswald efficiency factor as

$$e = 1.78(1 - 0.045AR^{0.68}) - 0.64 \quad (20.10)$$

If the wing is equipped with winglet or endplates, equation for the effective aspect ratio must be used in equation 20.10.

CHAPTER 21

LIGHTER THAN AIR VEHICLES

Lighter-than-air (LTA) vehicles represent a unique and promising platform for many applications that involve a long-duration airborne presence. Achieving their lift through buoyancy, these vehicles require much less power than traditional aircraft. An airship is a large lighter-than-air gas balloon that can be navigated by using engine-driven propellers. The airship evolved from the spherical balloon first successfully flown by the Montgolfier brothers in 1783. Airships are basically large, controllable balloons that have an engine for propulsion, use rudders and elevator flaps for steering, and carry passengers in a gondola suspended under the balloon.

There are three types of airship systems.

1. **Non-rigid Airships:** Non-rigid airships are airships which, like balloons, keep their exterior shape through the pressure of the lifting gas inside the envelope. There is no interior supporting structure. The gondola and tail units are mounted on the airship envelope. So-called catenaries curtains or cable mechanisms transfer force to the upper envelope sections and thereby ensure the even distribution of weight on top of the envelope section. The engines of non-rigid airships are mounted directly on to or even underneath the gondola. They are also equipped with ballonets.
2. **Semi-rigid Airships/Keeled Airships:** These airships differ from pressure airships through their rigid keel structure below the airship envelope or a partial structure inside the envelope. The rigid structure helps to ensure even distribution of force to the envelope and as a reinforcement of the entire system. These aircraft - just like non-rigid airships - get their shape from gas

AERODYNAMICS AND ITS APPLICATIONS

pressure gas pressure inside the envelope. Therefore ballonets are needed for semi-rigid airships to keep the envelope pressure constant. Furthermore, all attachments (engines, tail units and gondola) are firmly connected to the interior support structure, which also acts to absorb stress. With this type, optimal low weight and greater efficiency for larger airships can be achieved.

3. Rigid Airships: With this type of airship, the exterior form is determined by its rigid skeletal structure. The attachments (tail unit and gondola) are either part of the structure or connected to it. Within the skeletal structure of large rings fastened to longitudinal girders are gases bags filled with lifting gas. The skeletal structure of old Zeppelins was made from aluminum alloys. It is simply covered with a material that gives the airship a smooth surface and protects the gas bags. These are suspended from the structure in a way that compensate for any volume fluctuations of the lifting gas with increasing or decreasing altitude which means for any expansion or contraction of the gas bags. Thus, rigid airships do not need any additional ballonets. With this design, the motors can be placed very efficiently. (www.globalsecurity.com)

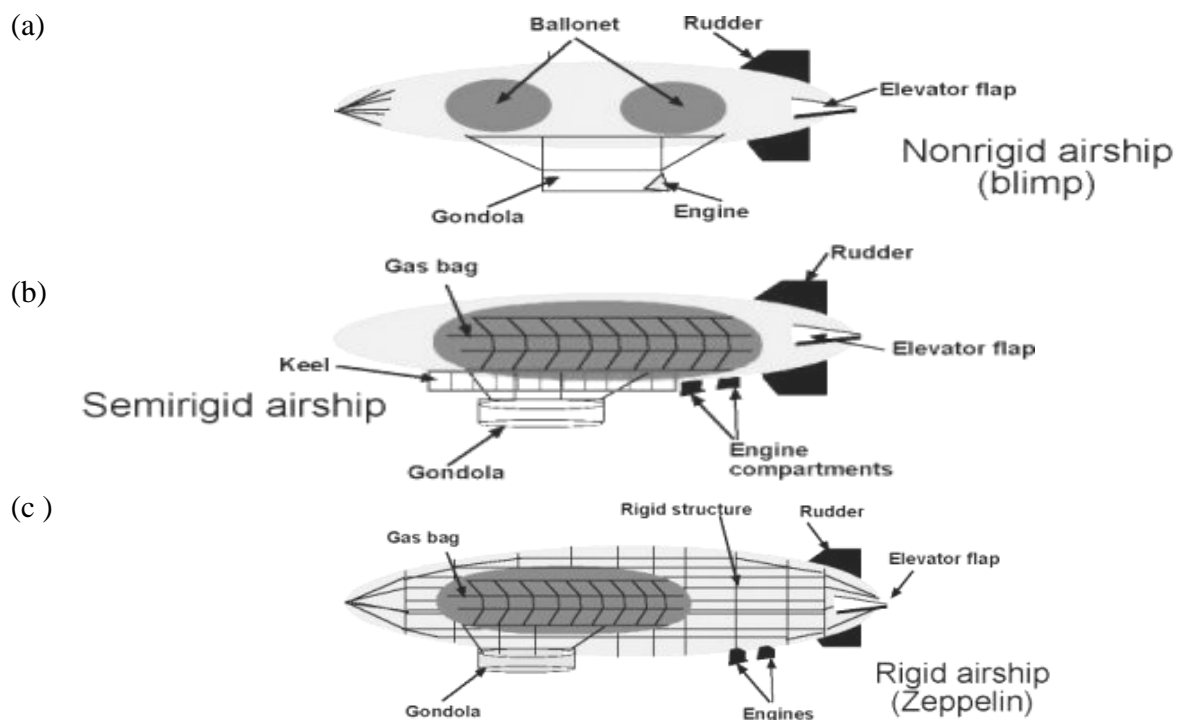


Figure 21.1:(a) Non-rigid airship, (b) Semi-rigid airship, (c) Rigid airship (Wikipedia)

AERODYNAMICS AND ITS APPLICATIONS

LITERATURE REVIEW

Airships are designed to carry cargo or passengers. They fly just low enough to avoid having to pressurize the cabin like an airplane. They don't require long runways like jets or a large crew on the ground. They also don't need to be stored in a hangar.

Any gas or gas mixture that is "lighter than air", and therefore has a lower density (weight per cubic meter) is suitable as a lifting gas. Under standard conditions, air has a density of 1.28 kg/m³.

Hydrogen is a low-density gas and easy to produce. However, together with oxygen, hydrogen is flammable and in a certain mixing ratio with air can form oxyhydrogen which is highly explosive. Therefore, hydrogen is no longer used for commercial airship operations.

Helium is an inert gas and therefore chemically inert, not flammable and appears as a single atom He. It is found in the earth's crust and is a by-product of natural gas extraction. Because of the small size of the helium atom, it was a problem for a long time to manufacture gas-tight envelope materials. With modern materials it is now possible to better confine the diffusion within the envelope material.

Buoyant lift is the influence on the weight of a body created when the body density differs from that of the medium surrounding it. This buoyancy lift is utilized in airship aviation. The balloon envelope is filled with a gas, which has a lower density than air. Buoyancy force is equal to the weight of fluid displaced, $B = V \times \rho_a$.

AERODYNAMICS AND ITS APPLICATIONS

The lift created through flow around bodies is called positive lift. One example is the lifting surface of an airplane. Because of the special profile with a more prominent curvature on the upper side an air particle has to cover a greater distance, and therefore flow around the profile at a higher speed. This creates force which in turn works on the profile i.e. the body. In pre-war airship aviation, positive lift, especially with rigid airships, did not play a big role. Today positive lift is applied selectively. Most airships today start "heavier than air" and also use positive lift for take-off. (www.globalsecurity.com)

The airship is essentially a low-speed vehicle. Higher speeds generate a rapid escalation of weight and fuel consumption, structure weight increase to meet the higher aerodynamic loading, and the power plant weight increases with output. The aerodynamic drag is also increase; the drag of the hull by itself is usually less than that due to the attached gondola and installations, which interfere with the flow over the envelope as well as contributing their own drag components.

History

The history of airships begins, like the history of hot air balloons, in France. After the invention of the hot air balloon in 1783, a French officer named Meusnier visualized an airship that utilized the design of the hot air balloon, but was able to be navigated. In 1784, he designed an airship that had an elongated envelope, propellers, and a rudder, not unlike today's airship. Although he documented his idea with extensive drawings, Meusnier's airship was never built.

In 1852, another Frenchman, an engineer named Henri Giffard, built the first practical airship. Filled with hydrogen gas, it was driven by a 3 hp steam engine weighing 350 lb (160 kg),

AERODYNAMICS AND ITS APPLICATIONS

and it flew at 6 mi/hr (9 km/hr). Even though Giffard's airship did achieve liftoff, it could not be completely controlled.

The first successfully navigated airship, *La France*, was built in 1884 by two more Frenchmen, Renard and Krebs. Propelled by a 9 hp electrically-driven airscrew, *La France* was under its pilots' complete control. It flew at 15 mi/hr (24 km/hr).

Military airships

In 1895, the first distinctly rigid airship was built by German David Schwarz. His design led to the successful development of the zeppelin, a rigid airship built by Count Zeppelin. The zeppelin utilized two 15 hp engines and flew at a speed of 25 mi/hr (42 km/hr). Their development and the subsequent manufacture of 20 such vessels gave Germany an initial military advantage at the start of World War I.

It was Germany's successful use of the zeppelin for military reconnaissance missions that spurred the British Royal Navy to create its own airships.

AERODYNAMICS AND ITS APPLICATIONS

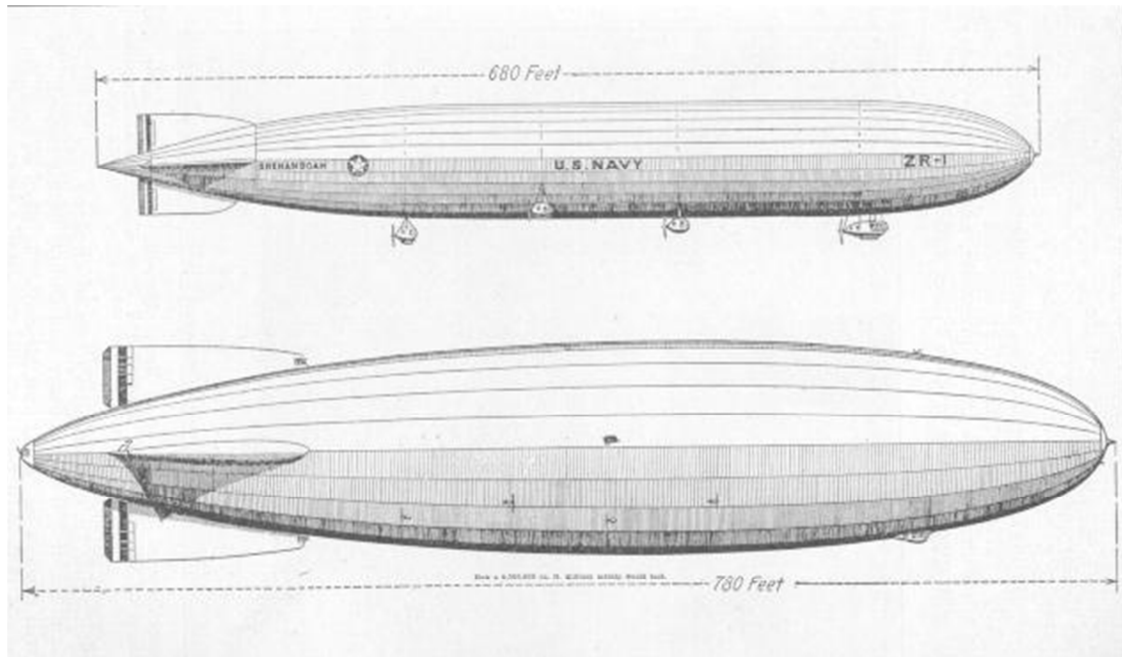


Figure 21.2: Military airships (Wikipedia)

Passenger-carrying airships

During the 1920s and 1930s, Britain, Germany, and the United States focused on developing large, rigid, passenger-carrying airships. Unlike Britain and Germany, the United States primarily used helium to give their airships lift. The first passenger-carrying non-rigid airship was invented in 1898 by Alberto Santos Dumont, a citizen of Brazil living in Paris. Under a sausage-shaped balloon with a ballonet or collapsible air bag inside, Dumont attached a propeller to his motorcycle's engine. He used both air and hydrogen, not helium, to lift the airship.

There are some advantages of rigid type airship. It is the one that lends itself most easily to large structures and which is also the safest of the three types of airships. Rigid airships have

AERODYNAMICS AND ITS APPLICATIONS

made longer single flights than other types and have flown more hours and miles without refueling than any other form. The rigid airship is said to be the fastest large vehicle of transportation that engineering ability of man has yet evolved. The rigid airship, owing to its large size and light weight can carry more load than any other type of aircraft.



Figure 21.3: Innovation of rigid airship (Airliners.net)

The future

Propulsive efficiency will be improved by using lightweight, two-stroke aviation diesel engines, gas turbines, or solar energy. New bow and stem thrusters will be developed to improve maneuverability. New lightweight composites might change the hull design. More lightweight, high strength materials will probably be developed and inevitably improve the overall design and function of the airship. The Pentagon and the U.S. Navy have renewed interest in developing blimps for various defense, missile surveillance, radar-surveillance platforms, and reconnaissance purposes. (from www.experiencefestival.com – zeppelin encyclopedia)

AERODYNAMICS AND ITS APPLICATIONS

Further Reading

1. Khoury, G. A. & Gillette, D. (1999). *Airship Technology*, United Kingdom, Cambridge University Press.
2. Konstantinov, L. *The Basics of Gas and Heat Airship Theory*.

Website: www.aeronautics.com/airship

CHAPTER 22

INTRODUCTION TO COMPUTATIONAL FLUID DYNAMICS

This and the next few chapters provide an introduction to computational fluid dynamics and a powerful commercial CFD solver known as FLUENT. These chapters are intended to provide a new user of FLUENT a step by step guide though a simple problem in aerodynamics namely flow pas an airfoil NACA 0012.

Computational Fluid Dynamics (CFD) is one of the popular methods to estimate the forces and moments on a body in a flow field. CFD is useful in a wide variety of applications especially in the industry. . However, one must note that complex flow simulations are challenging and error-prone and it takes a lot of engineering expertise to obtain validated solutions.

FLUENT is a computational fluid dynamics (CFD) software package to simulate fluid flow problems. It provides the capability to use different physical models such as incompressible or compressible, inviscid or viscous, laminar or turbulent flow. Geometry and grid generation is done using GAMBIT which is a preprocessor bundled with FLUENT.

THEORETICAL BACKGROUND

The Strategy of CFD

Broadly, the strategy of CFD is to replace the continuous problem domain with a discrete domain using a grid. In the continuous domain, each flow variable is defined at every point in the

AERODYNAMICS AND ITS APPLICATIONS

domain. For instance, the pressure p in the continuous 1D domain shown in the Fig. 22.1 below would be given as

$$p = p(x), \quad 0 < x < 1$$

In the discrete domain, each flow variable is defined only at the grid points. So, in the discrete domain shown below, the pressure would be defined only at the N grid points.

$$p_i = p(x_i), \quad i = 1, 2, \dots, N$$

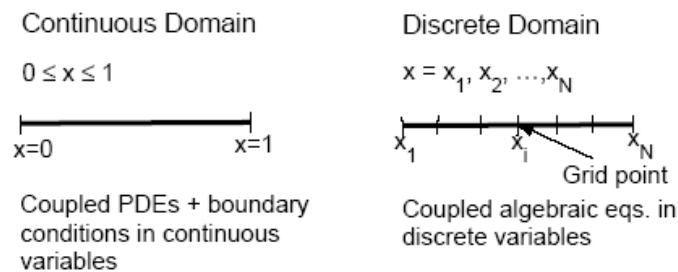


Figure 22-1: Continuous and Discrete Domain

In a CFD solution, one would directly solve for the relevant flow variables only at the grid points. The values at other locations are determined by interpolating the values at the grid points.

The governing partial differential equations and boundary conditions are defined in terms of the continuous variables p, \vec{V} etc. One can approximate these in the discrete domain in terms of the discrete variables p_i, \vec{V}_i etc. The discrete system is a large set of coupled, algebraic equations in the discrete variables. Setting up the discrete system and solving it involves a very large number of repetitive calculations and is done by the digital computer. This idea can be

AERODYNAMICS AND ITS APPLICATIONS

extended to any general problem domain. The following Fig. 22.2 shows the grid used for solving the flow over an airfoil.

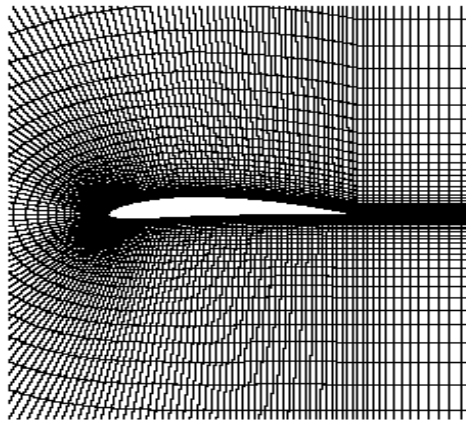


Figure 22-2 Grid over an airfoil

To keep the details simple, here are the illustrations of the fundamental ideas underlying CFD by applying them to the following simple 1D equation:

$$\frac{\partial u}{\partial x} + u^m = 0 \quad ; \quad 0 \leq x \leq 1 \quad ; \quad u(0) = 1 \quad (22.1)$$

We will first consider the case where $m = 1$ when the equation is linear. We will later consider the $m = 2$ case when the equation is nonlinear.

We will derive a discrete representation of the above equation with $m = 1$ on the following grid (Fig. 22.3):

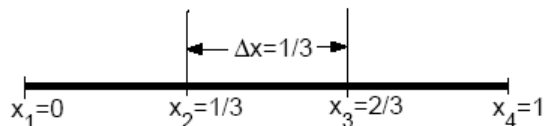


Figure 22-3: An equally spaced grid

AERODYNAMICS AND ITS APPLICATIONS

This grid has four equally-spaced grid points with Δx being the spacing between successive points. Since the governing equation is valid at any grid point, we have

$$\left(\frac{\partial u}{\partial x}\right)_i + u_i = 0 \quad (22.2)$$

where the subscript i represents the value at grid point x_i . In order to get an expression for $(du/dx)_i$ in terms of u at the grid points, we expand u_{i-1} in a Taylor's series:

$$u_{i-1} = u_i - \Delta x \left(\frac{du}{dx}\right)_i + O(\Delta x^2)$$

Rearranging gives

$$\left(\frac{du}{dx}\right)_i = \frac{u_i - u_{i-1}}{\Delta x} + O(\Delta x^2) \quad (22.3)$$

The error in $(du/dx)_i$ due to the neglected terms in the Taylor's series is called the truncation error. Since the truncation error above is $O(\Delta x)$, this discrete representation is termed first-order accurate.

Using (3) in (2) and excluding higher-order terms in the Taylor's series, we get the following

discrete equation:
$$\frac{u_i - u_{i-1}}{\Delta x} + u_i = 0 \quad (22.4)$$

Note that we have gone from a differential equation to an algebraic equation.

This method of deriving the discrete equation using Taylor's series expansions is called the finite-difference method.

Discretization Using The Finite-Volume Method

If we look closely at the airfoil grid shown earlier, we will see that it contains of quadrilaterals. In the finite-volume method, such a quadrilateral is commonly referred to as a “cell” and a grid point as a “node”. In 2D, one could also have triangular cells. In 3D, cells are usually hexahedrals, tetrahedrals, or prisms. In the finite-volume approach, the *integral form* of the conservation equations are applied to the control volume defined by a cell to get the discrete equations for the cell. For example, the integral form of the continuity equation was given earlier. For steady, incompressible flow, this equation reduces to

$$\int_S \vec{V} \cdot \hat{n} dS = 0 \tag{22.5}$$

The integration is over the surface S of the control volume and \hat{n} is the outward normal at the surface. Physically, this equation means that the net volume flow into the control volume is zero.

Consider the rectangular cell shown below in Fig.22.4.

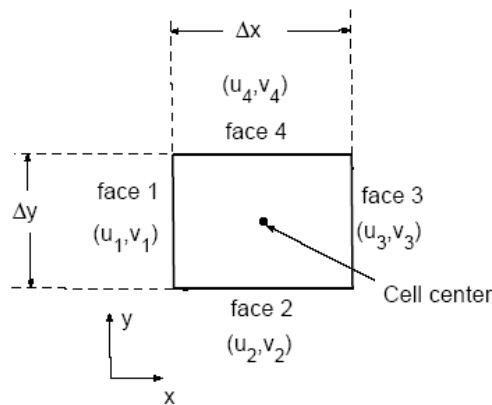


Figure 22-4 Rectangular Cell

AERODYNAMICS AND ITS APPLICATIONS

The velocity at face i is taken to be $\vec{V}_i = u_i \hat{i} + v_i \hat{j}$. Applying the mass conservation equation (22.5) to the control volume defined by the cell gives

$$-u_1 \Delta y - v_2 \Delta x + u_3 \Delta y + v_4 \Delta x = 0$$

This is the discrete form of the continuity equation for the cell. It is equivalent to summing up the net mass flow into the control volume and setting it to zero. So it ensures that the net mass flow into the cell is zero i.e. that the mass is conserved for the cell. Usually the values at the cell centers are stored. The face values u_1, v_2 , etc. are obtained by suitably interpolating the cell-center values for adjacent cells.

Similarly, one can obtain discrete equations for the conservation of momentum and energy for the cell. One can readily extend these ideas to any general cell shape in 2D or 3D and any conservation equation. These equations are solved to obtain the unknown flow variables.

Assembly of Discrete System and Application of Boundary Conditions

Recall that the discrete equation that we obtained using the finite-difference method was

$$\frac{u_i - u_{i-1}}{\Delta x} + u_i = 0$$

Rearranging, we get

$$-u_{i-1} + (1 + \Delta x)u_i = 0$$

Applying this equation to the 1D grid shown earlier at grid points $i = 2, 3, 4$ gives

$$-u_1 + (1 + \Delta x)u_2 = 0 \quad (i = 2) \quad (22.6)$$

$$-u_2 + (1 + \Delta x)u_3 = 0 \quad (i = 3) \quad (22.7)$$

$$-u_3 + (1 + \Delta x)u_4 = 0 \quad (i = 4) \quad (22.8)$$

The discrete equation cannot be applied at the left boundary ($i = 1$) since u_{i-1} is not defined here.

Instead, we use the boundary condition to get

$$u_1 = 1 \quad (22.9)$$

Equations (6)-(9) form a system of four simultaneous algebraic equations in the four unknowns u_1, u_2, u_3, u_4 . It is convenient to write this system in matrix form:

$$\begin{bmatrix} 1 & 0 & 0 & 0 \\ -11 + \Delta x & 0 & 0 & 0 \\ 0 & -1 & 1 + \Delta x & 0 \\ 0 & 0 & -1 & 1 + \Delta x \end{bmatrix} \begin{bmatrix} u_1 \\ u_2 \\ u_3 \\ u_4 \end{bmatrix} = \begin{bmatrix} 1 \\ 0 \\ 0 \\ 0 \end{bmatrix} \quad (22.10)$$

In a general situation, one would apply the discrete equations to the grid points (or cells in the finite-volume method) in the interior of the domain. For grid points (or cells) at or near the boundary, one would apply a combination of the discrete equations and boundary conditions. In the end, one would obtain a system of simultaneous algebraic equations with the number of equations being equal to the number of independent discrete variables.

FLUENT, like other commercial CFD codes, offers a variety of boundary condition options such as velocity inlet, pressure inlet, pressure outlet, etc. it is very important that we specify the proper boundary conditions in order to have a well-defined problem.

Suggested Reading

AERODYNAMICS AND ITS APPLICATIONS

1. Anderson, John D., Jr. (2001). *Fundamentals of Aerodynamics*. New York, McGraw-Hill.
2. Bhaskaran, R. (2003). *Fluent Tutorials*. New York, Cornell University.
3. Currie, I.G. (1993). *Fundamental Mechanics of Fluids*. New York, McGraw-Hill Inc.

CHAPTER 23

FLOW PAST AN AIRFOIL

CREATION OF AIRFOIL GEOMETRY IN GAMBIT

The first step towards the implementation of the CFD concept is by tackling the problem of flow over an airfoil.

Flow over an airfoil

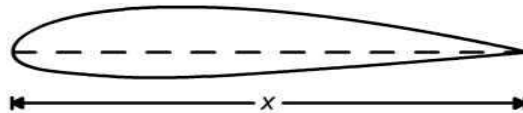


Figure 23-1: An airfoil geometry

Consider air flowing over the given airfoil. The first airfoil that we will be using here is NACA 0012, a symmetric airfoil although the picture above is not showing a symmetric airfoil. In this example, the free stream velocity is 50 m/s and the angle of attack is 5° . Here we discuss NACA0012 for the sake of explaining step by step of creating the geometry in GAMBIT and analyzing it in FLUENT.

Assume standard sea-level values for the free stream properties: Pressure = 101,325 Pa, Density = 1.2250 kg/m^3 , Temperature = 288.16 K, Dynamic viscosity $\mu = 1.7894 \times 10^{-5} \text{ kg/m-s}$. We will determine the lift and drag coefficients under these conditions using FLUENT. Before proceeding any further, here is the list of steps that we need to follow in order to solve the airfoil problem using FLUENT.

AERODYNAMICS AND ITS APPLICATIONS

1. Create Geometry in GAMBIT, 2. Mesh Geometry in GAMBIT, 3. Specify Boundary Types in GAMBIT, 4. Set Up Problem in FLUENT, 5. Solve!, 6. Analyze Results

Step 1: Create Geometry in GAMBIT

The creation of geometry of the airfoil has the same principle as all other geometry making in GAMBIT. The main objective is to create the mesh.

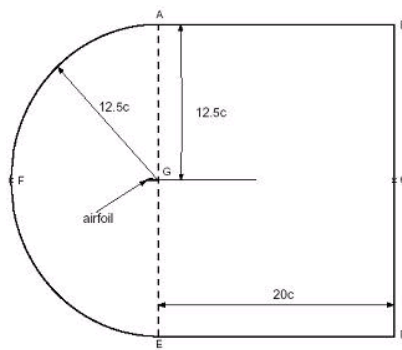


Figure 23-2 The farfield boundary

This chapter will lead you through the steps for generating a mesh in GAMBIT for an airfoil geometry. This mesh can then be read into FLUENT for fluid flow simulation. In an external flow such as that over an airfoil, we have to define a farfield boundary and mesh the region between the airfoil geometry and the farfield boundary. It is a good idea to place the farfield boundary well away from the airfoil since we will use the ambient conditions to define the boundary conditions at the farfield. The farfield boundary we will use is the line ABCDEFA in the figure above. c is the chord length. For the purpose of simplicity, here the chord length is 1m.

Start GAMBIT

Create a new directory called *NACA0012* and start *GAMBIT* from that directory by typing `gambit -id NACA0012` at the command prompt. Alternatively, many computers that have the software *FLUENT*, will have a direct shortcut to *GAMBIT* and students can define their filename once they run *GAMBIT* and click *File>New...* or the newer version has a *GAMBIT Startup* that prompt the user the filename and the working directory.

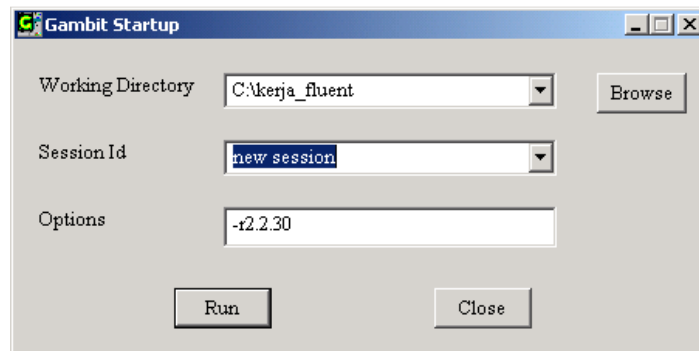


Figure 23-3: Gambit Startup

Under **Main Menu**, select **Solver > FLUENT 5/6** since the mesh to be created is to be used in *FLUENT 6*.

Import Edge

To specify the airfoil geometry, we will import a file containing a list of vertices along the surface and have *GAMBIT* join these vertices to create two edges, corresponding to the

AERODYNAMICS AND ITS APPLICATIONS

upper and lower surfaces of the airfoil. We'll then split these edges into 4 distinct edges to help us control the mesh size at the surface.

Students can get the airfoil vertices data from many websites at the internet like UIUC Airfoil Data Site - <http://uxh.cso.uiuc.edu/~selig/ads.html>. Alternatively, they can get the data from softwares like NACA4GEN and Profili. It takes some alteration in order to make the data similar to the one below. The data at first is in percentage; therefore it has to be divided with 100. Plus, the coordinates are in two dimensions and has only x and y coordinates for each point. Therefore, you have to add a zero (0) for each point for the z coordinate before importing it into GAMBIT. Let's take a look at the NACA0012.txt file:

```
66      2
0      0      0
0.0005839  0.0042603  0
0.0023342  0.0084289  0
..... (Continue)
0.9994161  0.0013419  0
1      0      0
0      0      0
169
```

AERODYNAMICS AND ITS APPLICATIONS

0.0005839 -0.0042603 0

0.0023342 -0.0084289 0

..... (Continue)

0.9976658 -0.001587 0

0.9994161 -0.0013419 0

1 0 0

The first line of the file represents the number of points on each edge (66) and the number of edges (2). The first 66 set of vertices are connected to form the edge corresponding to the upper surface; the next 66 are connected to form the edge for the lower surface. Make sure that each edge will coincide each other at the trailing and leading edge. This is done by checking the end vertices for each edge are the same. For example, upper surface and lower surface has (0 0 0) and (1 0 0) at each end. This step is important in order to avoid any error while creating the surfaces and meshing in GAMBIT. The chord length c for the geometry in NACA0012.txt file is 1, so x varies between 0 and 1. If you are using a different airfoil geometry specification file, note the range of x values in the file and determine the chord length c . You will need this later on.

Main Menu > File > Import > ICEM Input ...

AERODYNAMICS AND ITS APPLICATIONS

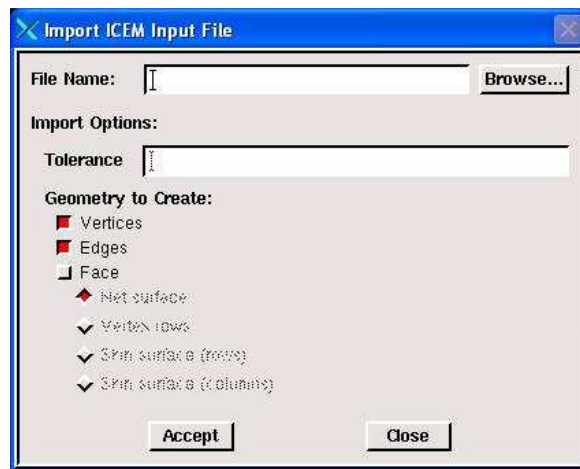


Figure 23-4 Import ICEM Input File

For **File Name**, browse and select the NACA0012.txt file. Select both **Vertices** and **Edges** under **Geometry to Create**: since these are the geometric entities we need to create. Deselect **Face**. Click **Accept**. The result will be something like in the Fig.8.

AERODYNAMICS AND ITS APPLICATIONS

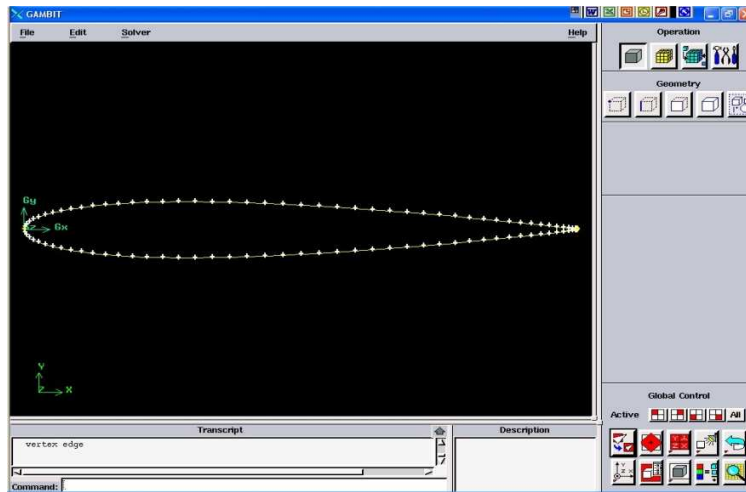


Figure 23-5 Airfoil edge and vertices

When we zoomed in the trailing edge, we should see that the point (1 0 0) connects the two upper and lower surface of the airfoils.

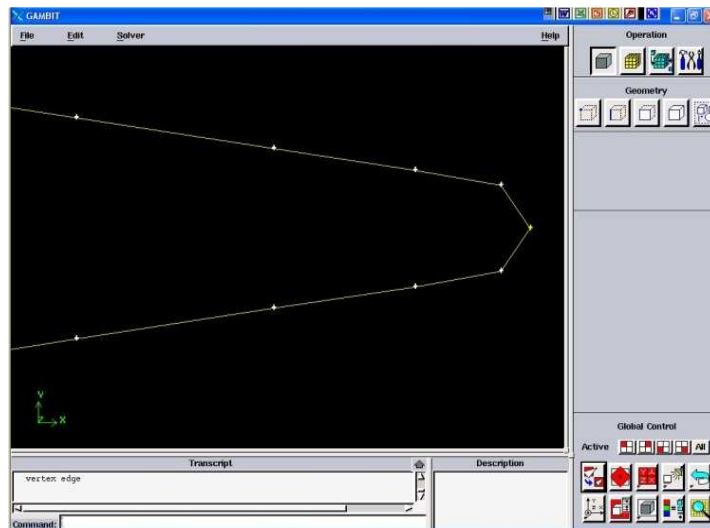


Figure 23-6 Trailing edge

Split Edges

AERODYNAMICS AND ITS APPLICATIONS

Next, we will split the top and bottom edges into two edges each as shown below.

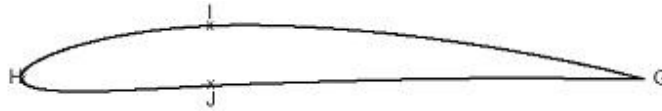


Figure 23-7 Split edge of airfoil

We need to do this because a non-uniform grid spacing will be used for $x < 0.3c$ and a uniform grid spacing for $x > 0.3c$. To split the top edge into HI and IG, select

Operation Toolpad > Geometry Command Button > Edge Command Button > Split/Merge Edge

Make sure Point is selected next to Split With in the *Split Edge* window.

Select the top edge of the airfoil by Shift-clicking on it. The selected edge will become red in color. We'll use the point at $x=0.3c$ on the upper surface to split this edge into HI and IG. To do this, enter 0.3 for x: under Global. If your c is not equal to one, enter the value of $0.3*c$ instead of just 0.3. For instance, if $c=4$, enter 1.2. From here on, whenever you are asked to enter (some factor)* c , calculate the appropriate value for your c and enter it.

You should see that the white circle has moved to the correct location on the edge.

AERODYNAMICS AND ITS APPLICATIONS

Click **Apply**. You will see a message saying ``Edge edge.1 was split, and edge edge.3 created" in the *Transcript* window.

Note the yellow marker in place of the white circle, indicating the original edge has been split into two edges with the yellow marker as its dividing point. Repeat this procedure for the lower surface to split it into HJ and JG. Use the point at $x=0.3c$ on the lower surface to split this edge.

Further Reading

1. Anderson, John D., Jr. (2001). *Fundamentals of Aerodynamics*. New York, McGraw-Hill.
2. Bhaskaran, R. (2003). *Fluent Tutorials*. New York, Cornell University.
3. Currie, I.G. (1993). *Fundamental Mechanics of Fluids*. New York, McGraw-Hill Inc.

CHAPTER 24

CREATING FAR FIELD BOUNDARY IN GAMBIT

Creation of Far field Boundary

Next we will create the far field boundary by creating vertices and joining them appropriately to form edges. The following commands in GAMBIT are required to create the far field boundary.

Operation Toolpad > Geometry Command Button > Vertex Command Button > Create

Vertex

Create the following vertices by entering the coordinates under **Global** and the label under **Label**:

AERODYNAMICS AND ITS APPLICATIONS

Table 24-1 Farfield boundary vertices

Label	x -coordinate	y -coordinate	z -coordinate
A	C	12.5c	0
B	21c	12.5c	0
C	21c	0	0
D	21c	-12.5c	0
E	C	-12.5c	0
F	-11.5c	0	0
G	C	0	0

AERODYNAMICS AND ITS APPLICATIONS

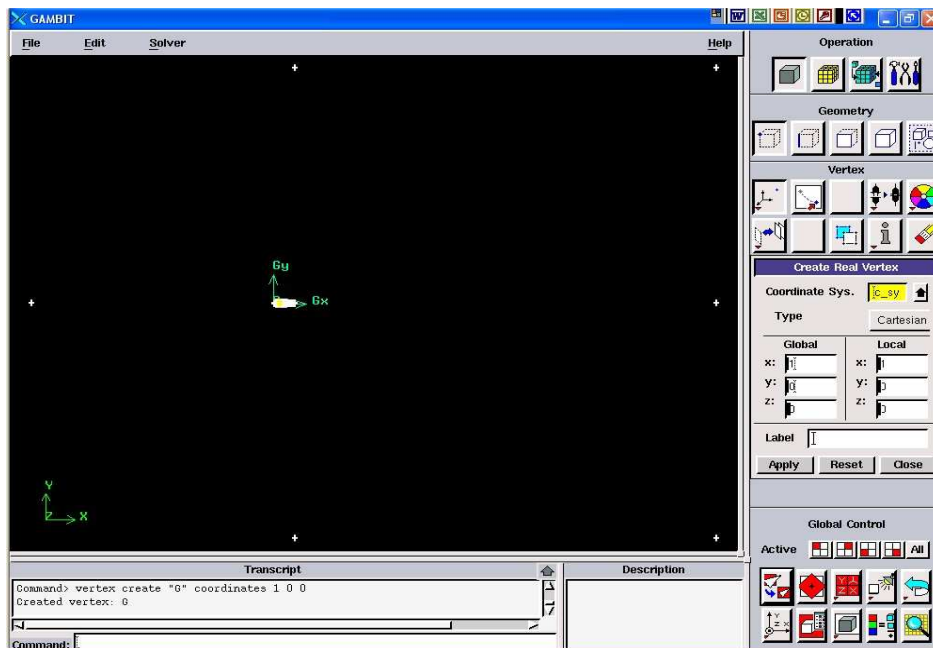


Figure 24-1 Boundary vertices

Click the *FIT TO WINDOW* button to scale the display so that you can see all the vertices.

As you create the edges for the farfield boundary, keep the picture of the farfield nomenclature given at the top of this step handy.

Operation Toolpad > Geometry Command Button > Edge Command Button > Create Edge

Create the edge AB by selecting the vertex A followed by vertex B. Enter AB for **Label**. Click Apply. GAMBIT will create the edge. You will see a message saying something like "Created edge: AB" in the *Transcript* window.

AERODYNAMICS AND ITS APPLICATIONS

Similarly, create the edges BC, CD, DE, EG, GA and CG. Note that you might have to zoom in on the airfoil to select vertex G correctly.

Next we will create the circular arc AF. Right-click on the Create Edge button and select Arc.

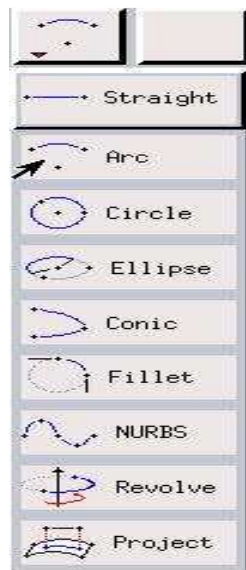


Figure 24-2 Create edge options

In the *Create Real Circular Arc* menu, the box next to **Center** will be yellow. That means that the vertex you select will be taken as the center of the arc. Select vertex G and click Apply.

Now the box next to **End Points** will be highlighted in yellow. This means that you can now select the two vertices that form the end points of the arc. Select vertex A and then vertex F. Enter AF under **Label**. Click **Apply**.

AERODYNAMICS AND ITS APPLICATIONS

If you did this right, the arc AF will be created. If you look in the transcript window, you'll see a message saying that an edge has been created.

Similarly, create an edge corresponding to arc EF.

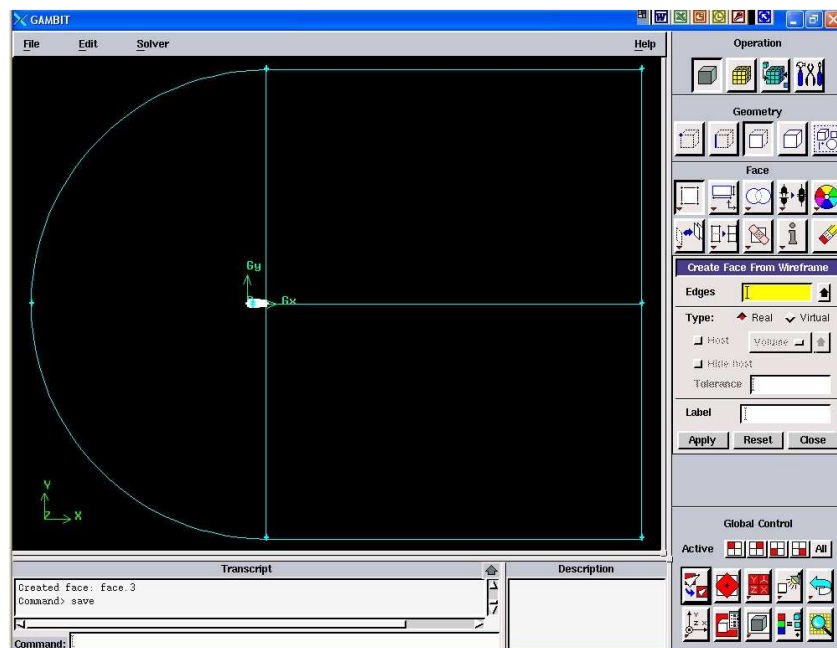


Figure 24-3: Farfield Boundary

Create Faces

The edges can be joined together to form faces (which are planar surfaces in 2D). We'll create three faces: ABCGA, EDCGE and GAFEG+airfoil surface. Then we will mesh each face.

Operation Toolpad > Geometry Command Button > Face Command Button > Form Face

AERODYNAMICS AND ITS APPLICATIONS

This brings up the *Create Face From Wireframe* menu. Recall that we had selected vertices in order to create edges. Similarly, we will select edges in order to form a face.

To create the face ABCGA, select the edges AB, BC, CG, and GA and click **Apply**. GAMBIT will tell you that it has "Created face: face.1" in the transcript window.

Similarly, create the face EDCGE.

To create the face consisting of GAFEG + airfoil surface, select the edges in the following order: AG, AF, EF, EG, and JG, HJ, HI and IG (around the airfoil in the clockwise direction). Click **Apply**.

Further Reading

1. Anderson, John D., Jr. (2001). *Fundamentals of Aerodynamics*. New York, McGraw-Hill.
2. Bhaskaran, R. (2003). *Fluent Tutorials*. New York, Cornell University.
3. Currie, I.G. (1993). *Fundamental Mechanics of Fluids*. New York, McGraw-Hill Inc.

CHAPTER 25

MESH GENERATION IN GAMBIT

Mesh Geometry in GAMBIT

Mesh Faces

We'll mesh each of the 3 faces separately to get our final mesh. Before we mesh a face, we need to define the point distribution for each of the edges that form the face i.e. we first have to mesh the edges. We'll select the mesh stretching parameters and number of divisions for each edge based on three criteria:

1. We'd like to cluster points near the airfoil since this is where the flow is modified the most; the mesh resolution as we approach the farfield boundaries can become progressively coarser since the flow gradients approach zero.
2. Close to the surface, we need the most resolution near the leading and trailing edges since these are critical areas with the steepest gradients.
3. We want transitions in mesh size to be smooth; large, discontinuous changes in the mesh size significantly decrease the numerical accuracy.

The edge mesh parameters we will use for controlling the stretching are *successive ratio*, *first length* and *last length*. Each edge has a direction as indicated by the arrow in the graphics

window. The *successive ratio* R is the ratio of the length of any two successive divisions in the arrow direction as shown below.

Operation Toolpad > Mesh Command Button > Edge Command Button > Mesh Edges

Select the edge GA. The edge will change color and an arrow and several circles will appear on the edge. This indicates that you are ready to mesh this edge. Make sure the arrow is pointing upwards. You can reverse the direction of the edge by clicking on the **Reverse** button in the *Mesh Edges* menu. Enter a ratio of 1.15. This means that each successive mesh division will be 1.15 times bigger in the direction of the arrow. Select **Interval Count** under **Spacing**. Enter 45 for **Interval Count**. Click **Apply**. GAMBIT will create 45 intervals on this edge with a successive ratio of 1.15.

For edges AB and CG, we will set the *First Length* (i.e. the length of the division at the start of the edge) rather than the *Successive Ratio*. Repeat the same steps for edges BC, AB and CG with the following specifications:

AERODYNAMICS AND ITS APPLICATIONS

Table 25-1 Mesh specification of edges

Edges	Arrow Direction	Successive Ratio	Interval Count
GA and BC	Upwards	1.15	45

Edges	Arrow Direction	First Length	Interval Count
AB and CG	Left to Right	$0.02c$	60

Note that later we'll select the length at the trailing edge to be $0.02c$ so that the mesh length is continuous between IG and CG, and HG and CG.

AERODYNAMICS AND ITS APPLICATIONS

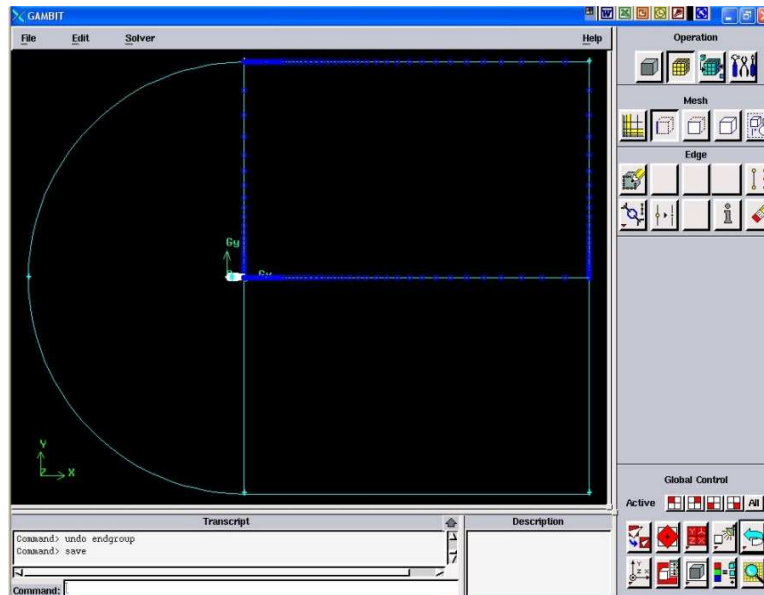


Figure 25-1 Meshed edges

Now that the appropriate edge meshes have been specified, mesh the face ABCGA:

Operation Toolpad > Mesh Command Button > Face Command Button > Mesh Faces

Select the face ABCGA. The face will change color. You can use the defaults of Quad (i.e. quadrilaterals) and Map. Click **Apply**.

The meshed face should look as follows:

AERODYNAMICS AND ITS APPLICATIONS

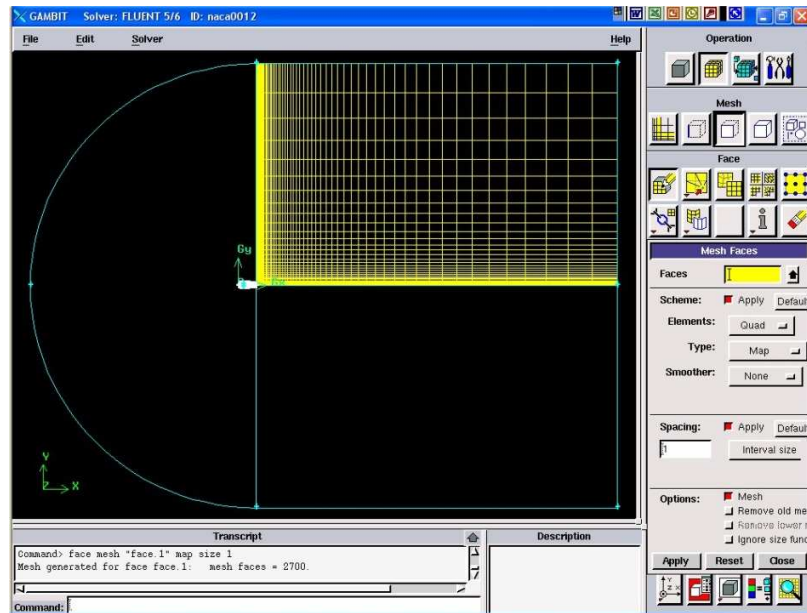


Figure 25-2 Meshed face

Next mesh face EDCGE in a similar fashion. The following table shows the parameters to use for the different edges:

Table 25-2 Mesh specification of edges

Edges	Arrow Direction	Successive Ratio	Interval Count
EG and CD	Downwards	1.15	45

Edges	Arrow Direction	First Length	Interval Count
DE	Left to Right	0.02c	60

AERODYNAMICS AND ITS APPLICATIONS

The resultant mesh should be symmetric about CG as shown in the figure below.

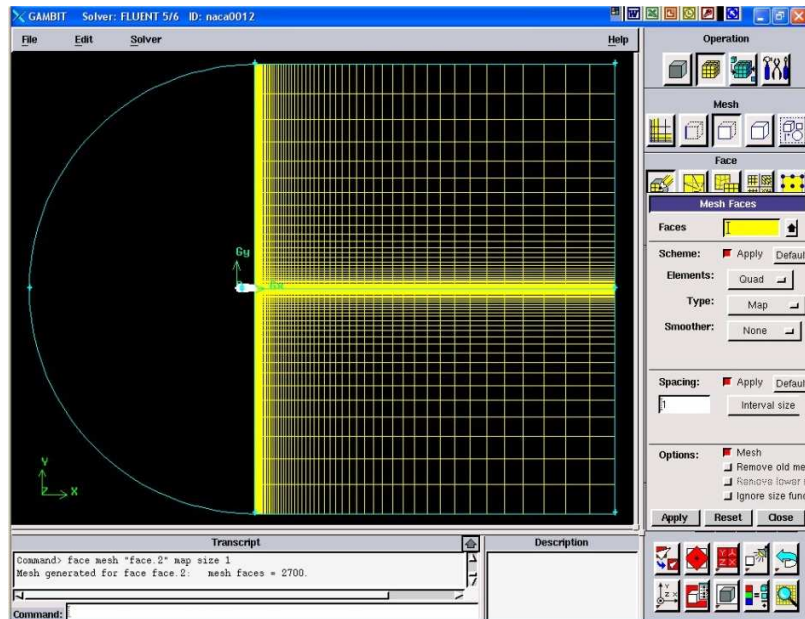


Figure 25-3 Meshed two faces

Finally, let's mesh the face consisting of GAFEG and the airfoil surface. For edges HI and HJ on the front part of the airfoil surface, use the following parameters to create edge meshes:

Table 25-3 Mesh specification of edges

Edges	Arrow Direction	Last Length	Interval Count
HI	From H to I	0.02 <i>c</i>	40

AERODYNAMICS AND ITS APPLICATIONS

HJ	From H to J	$0.02c$	40
----	-------------	---------	----

For edges IG and JG, we'll set the divisions to be uniform and equal to $0.02c$. Use *Interval Size* rather than *Interval Count* and create the edge meshes:

Table 25-4 Edge mesh specification

Edges	Arrow Direction	Successive Ratio	Interval Size
IG and JG	Left to Right	1	$0.02c$

For edge AF, the number of divisions needs to be equal to the number of divisions on the line opposite to it i.e. the upper surface of the airfoil

Operation Toolpad > Mesh Command Button > Edge Command Button > Summarize Edge Mesh

Select edge IG and then Elements under Component and click Apply. This will give the total number of nodes (i.e. points) and elements (i.e. divisions) on the edge in the *Transcript* window. The number of divisions on edge IG is 35. (If you are using a different geometry, this number will be different; I will refer to it as N_{IG}). So the *Interval Count* for edge AF is $N_{HI} + N_{IG} = 40 + 35 = 75$.

AERODYNAMICS AND ITS APPLICATIONS

Similarly, determine the number of divisions on edge JG. This also comes out as 35 for the current geometry. So the *Interval Count* for edge EF also is 75.

Create the mesh for edges AF and EF with the following parameters:

Table 25-5 Mesh specification of edges

Edges	Arrow Direction	First Length	Interval Count
AF	From A to F	$0.02c$	$40+N_{IG}$
EF	From E to F	$0.02c$	$40+N_{JG}$

Mesh the face. The resultant mesh is shown below.

AERODYNAMICS AND ITS APPLICATIONS

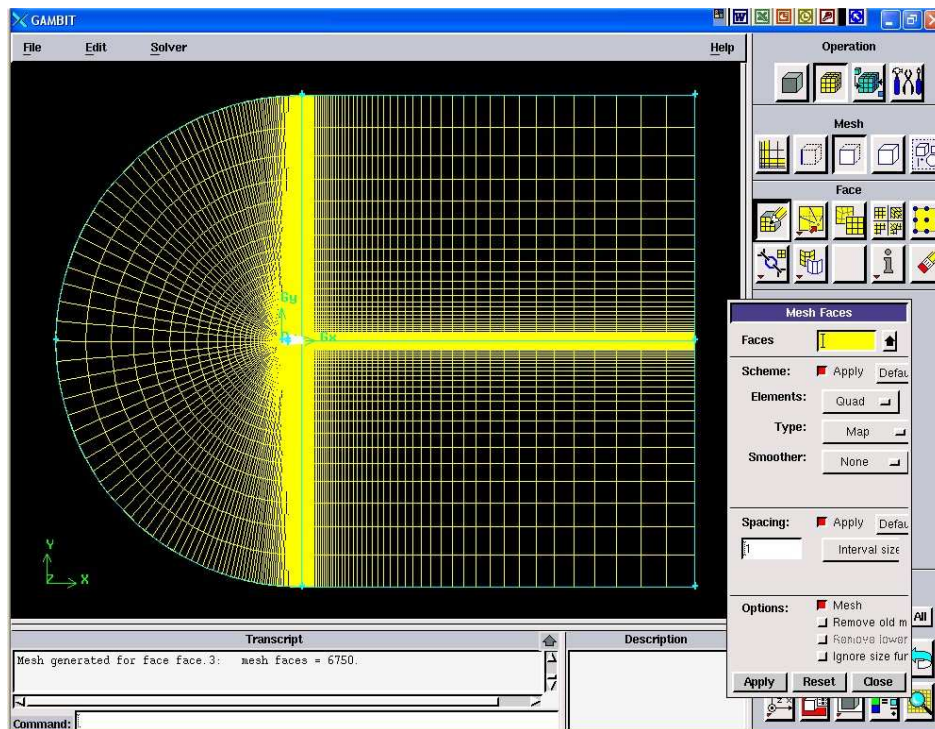


Figure 25-4 Meshed faces (final)

Further Reading

1. Anderson, John D., Jr. (2001). *Fundamentals of Aerodynamics*. New York, McGraw-Hill.
2. Bhaskaran, R. (2003). *Fluent Tutorials*. New York, Cornell University.
3. Currie, I.G. (1993). *Fundamental Mechanics of Fluids*. New York, McGraw-Hill Inc.

CHAPTER 26

CREATING BOUNDARIES IN GAMBIT

Specify Boundary Types in GAMBIT

We will label the boundary AFE as *farfield1*, ABDE as *farfield2* and the airfoil surface as *airfoil*. Recall that these will be the names that show up under boundary zones when the mesh is read into FLUENT.

Group Edges

We'll create groups of edges and then create boundary entities from these groups. First, we will group AF and EF together.

Operation Toolpad > Geometry Command Button > Group Command Button > Create Group

Select Edges and enter *farfield1* for Label, which is the name of the group. Select the edges AF and EF. Note that *GAMBIT* adds the edge to the list as it is selected in the GUI.

AERODYNAMICS AND ITS APPLICATIONS

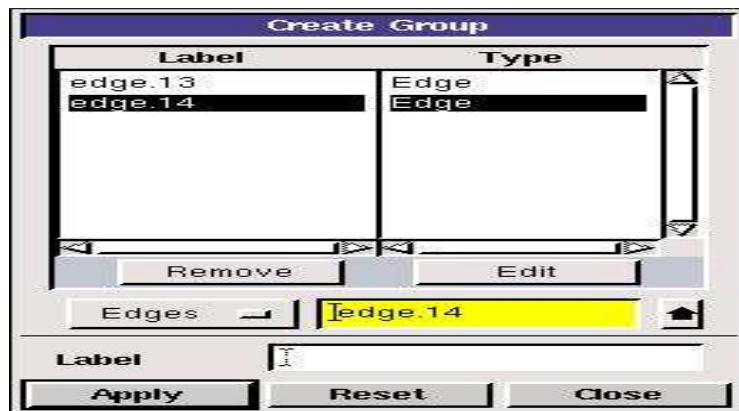


Figure 26-1 Create group

Click **Apply**.

In the transcript window, you will see the message “Created group: farfield1 group”.

```
Command> group create edge "edge.13" "edge.14"  
Created group: group.1  
Command> group delete "group.1" lowertopology  
Command> group create "farfield1" edge "edge.13" "edge.14"  
Created group: farfield1
```

Figure 26-2 Transcript window

Similarly, create the other two farfield groups. You should have created a total of three groups:

AERODYNAMICS AND ITS APPLICATIONS

Table 26-1 Group name

Group Name	Edges in Group
farfield1	AF,EF
farfield2	AB,DE
farfield3	BC,CD
Airfoil	HI,IG,HJ,JG

Define Boundary Types

Now that we have grouped each of the edges into the desired groups, we can assign appropriate boundary types to these groups.

Operation Toolpad> Zones Command Button > Specify Boundary Types

Under Entity, select Groups

Select any edge belonging to the airfoil surface and that will select the airfoil group. Next to Name:, enter airfoil. Leave the Type as WALL.

AERODYNAMICS AND ITS APPLICATIONS

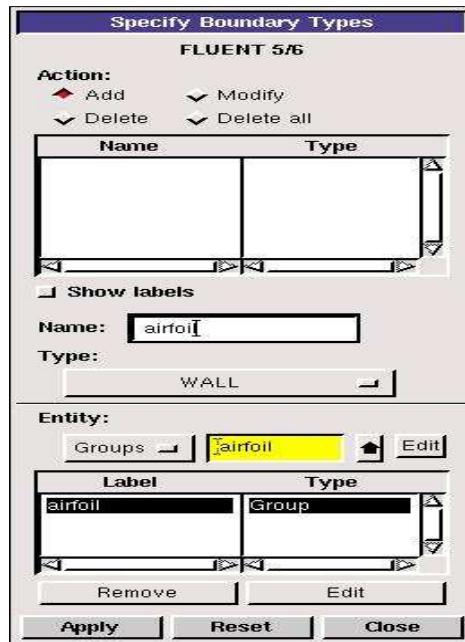


Figure 26-3 Specify Boundary Types

Click Apply.

In the *Transcript Window*, you will see a message saying "Created Boundary entity: airfoil".

Similarly, create boundary entities corresponding to *farfield1*, *farfield2* and *farfield3* groups. Set the Type to Pressure Farfield in each case.

Save Your Work

Main Menu > File > Save

Export Mesh

Main Menu > File > Export > Mesh...

AERODYNAMICS AND ITS APPLICATIONS

Save the file as NACA0012.msh.

Make sure that the Export 2d Mesh option is selected.

Check to make sure that the file is created.

Further Reading

1. Anderson, John D., Jr. (2001). *Fundamentals of Aerodynamics*. New York, McGraw-Hill.
2. Bhaskaran, R. (2003). *Fluent Tutorials*. New York, Cornell University.
3. Currie, I.G. (1993). *Fundamental Mechanics of Fluids*. New York, McGraw-Hill Inc.

CHAPTER 27

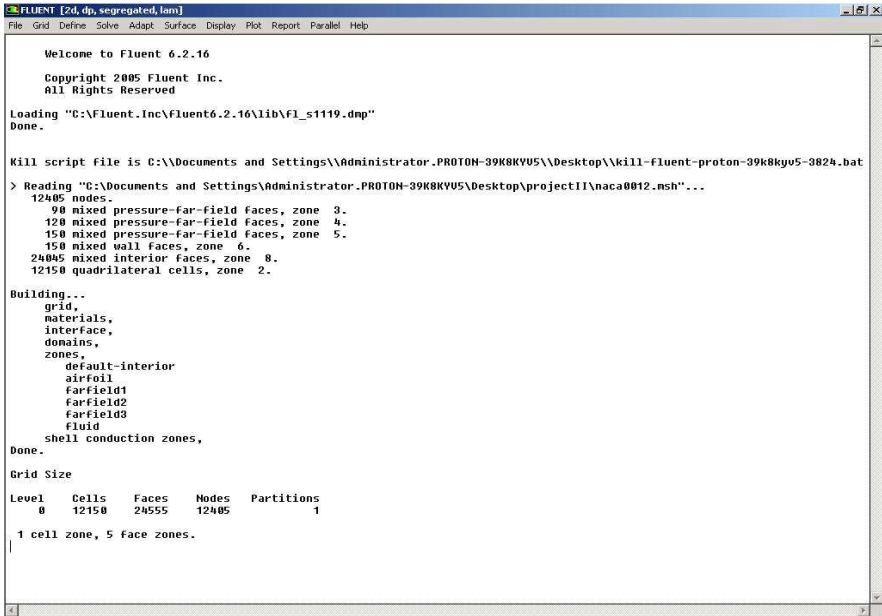
SETTING UP PROBLEM IN FLUENT

In order to run a CFD problem in FLUENT the following steps must be followed.

Set Up Problem in FLUENT; Launch FLUENT Start> Programs > Fluent Inc> FLUENT 6.0;
then Select 2ddp from the list of options and click Run.

Import File; then on Main Menu > File > Read > Case...

Navigate to your working directory and select the NACA0012.msh file. Click OK. The following should appear in the FLUENT window:



```

Welcome to Fluent 6.2.16

Copyright 2005 Fluent Inc.
All Rights Reserved

Loading "C:\Fluent.Inc\Fluent6.2.16\lib\fl_s1119.dmp"
Done.

Kill script file is C:\Documents and Settings\Administrator.PROTON-39K8KV05\Desktop\kill-fluent-proton-39k8ky5-3824.bat

> Reading "C:\Documents and Settings\Administrator.PROTON-39K8KV05\Desktop\project11\naca0012.msh"...
12405 nodes.
 90 mixed pressure-far-field faces, zone 3.
120 mixed pressure-far-field faces, zone 4.
150 mixed pressure-far-field faces, zone 5.
150 mixed wall faces, zone 6.
24005 mixed interior faces, zone 8.
12150 quadrilateral cells, zone 2.

Building...
grid,
materials,
interface,
domains,
zones,
default-interior
airfoil
farfield1
farfield2
farfield3
fluid
shell conduction zones,
Done.

Grid Size

Level  Cells    Faces    Nodes    Partitions
0      12150   24555   12405    1

1 cell zone, 5 face zones.
    
```

Figure 27-1 Fluent window

AERODYNAMICS AND ITS APPLICATIONS

Check that the displayed information is consistent with our expectations of the airfoil grid.

Analyze Grid then Display > Grid



Figure 27-2 Grid Display

Note what the surfaces *farfield1*, *farfield2*, etc. correspond to by selecting and plotting them in turn.

AERODYNAMICS AND ITS APPLICATIONS

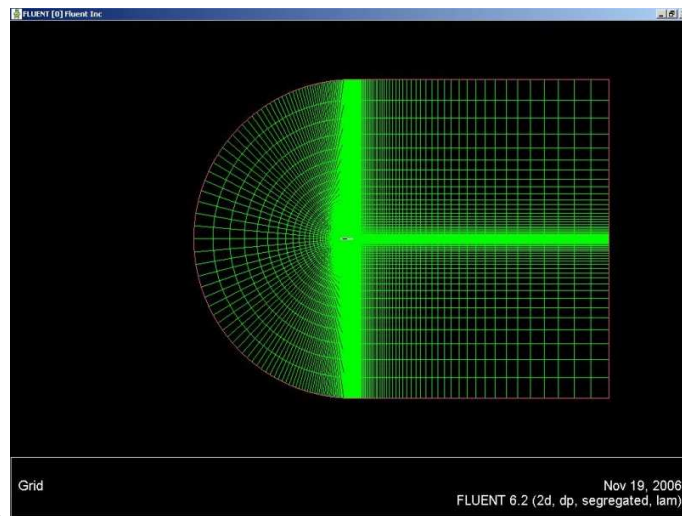


Figure 27-3 Airfoil grid

Zoom into the airfoil.

AERODYNAMICS AND ITS APPLICATIONS

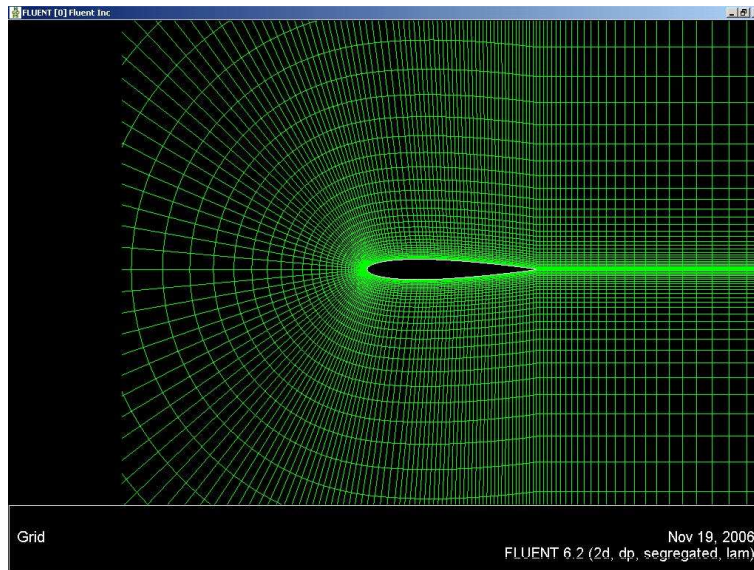


Figure 27-4 Zoomed airfoil

Define Properties then Define > Models > Solver...

Under the Solver box, select *Segregated*.

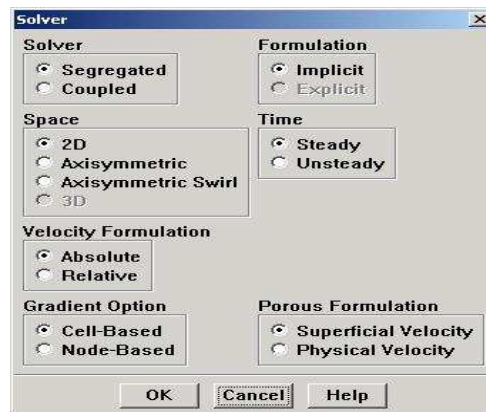


Figure 27-5 Solver

AERODYNAMICS AND ITS APPLICATIONS

Click **OK**.

Define > Models > Viscous

Select *Laminar* under Model.

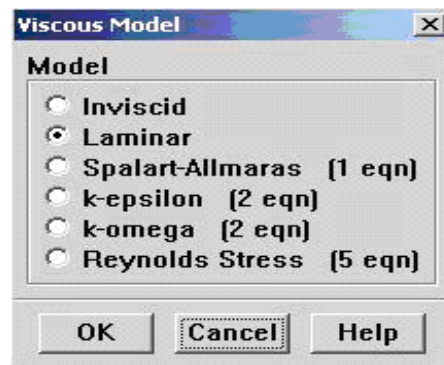


Figure 27-6 Viscous model

Click **OK**. Then **Define > Models > Energy**

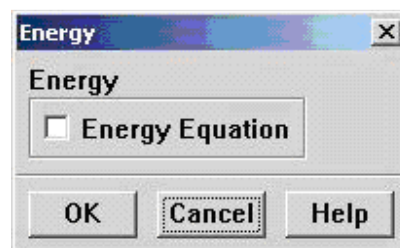


Figure 27-7 Energy equation

AERODYNAMICS AND ITS APPLICATIONS

The speed of sound under SSL conditions is 340 m/s so that our free stream Mach number is around 0.15. This is low enough that we'll assume that the flow is incompressible. So the energy equation can be turned off. Make sure there is no check in the box next to Energy Equation and click OK.

Define > Materials

Make sure air is selected under *Fluid Materials*. Set *Density* to constant and equal to 1.225 kg/m³.

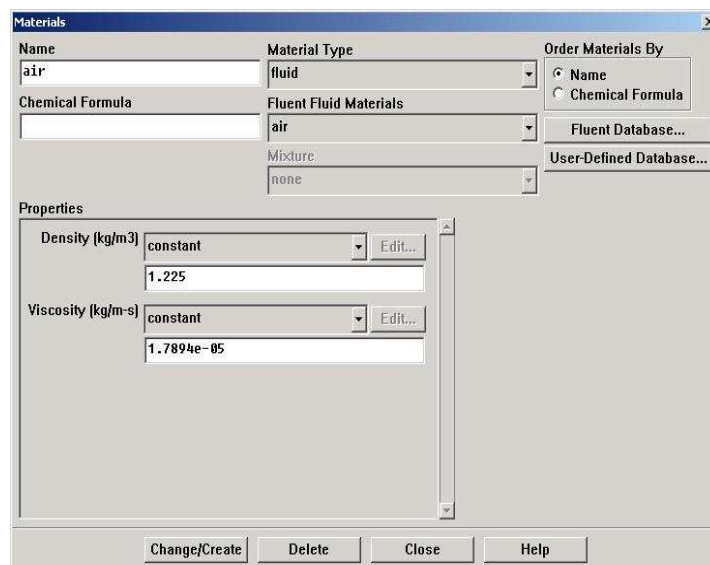


Figure 27-8 Defining materials

Click *Change/Create*.

Define > Operating Conditions

We'll work in terms of gauge pressures in this example. So set *Operating Pressure* to the ambient value of 101,325 Pa.

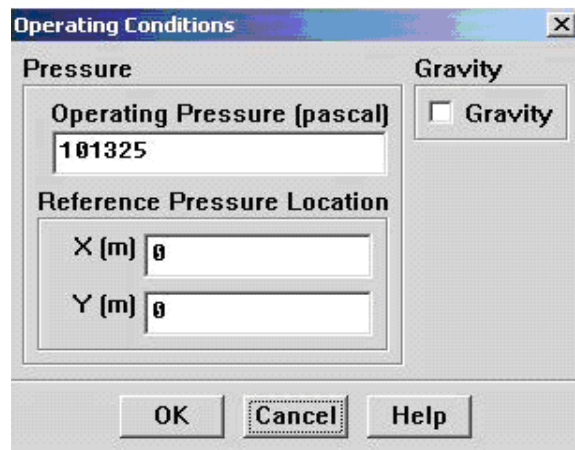


Figure 27-9 Operating conditions

Click OK.

Define > Boundary Conditions

Set *farfield1* and *farfield2* to the *velocity-inlet* boundary type.

For each, click **Set...** Then, choose *Components* under *Velocity Specification Method* and set the x- and y-components to that for the freestream. For instance, the x-component is $50 \cdot \cos(5^\circ) = 49.81$.

AERODYNAMICS AND ITS APPLICATIONS

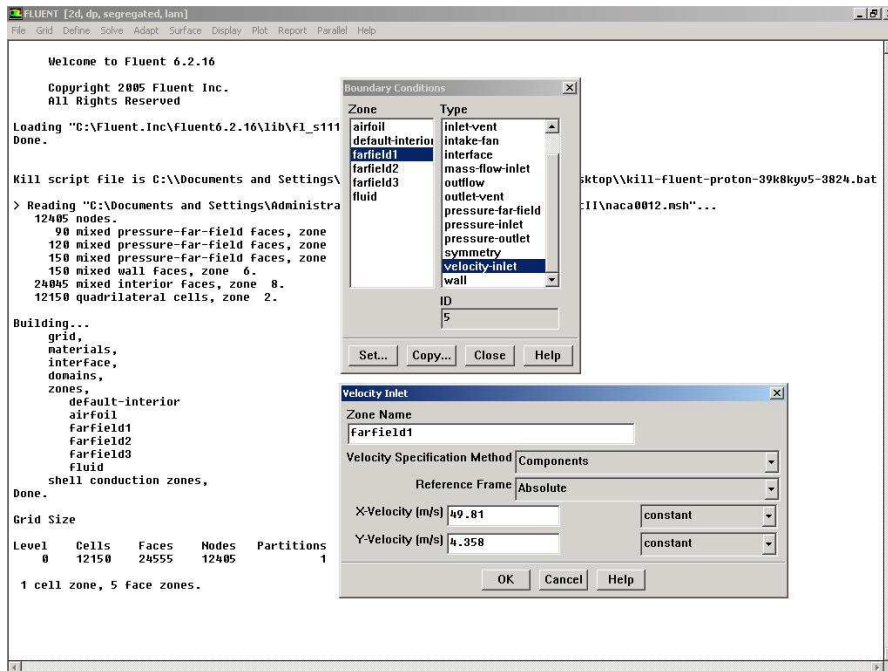


Figure 27-10 Defining Boundary Conditions

Click OK.

AERODYNAMICS AND ITS APPLICATIONS

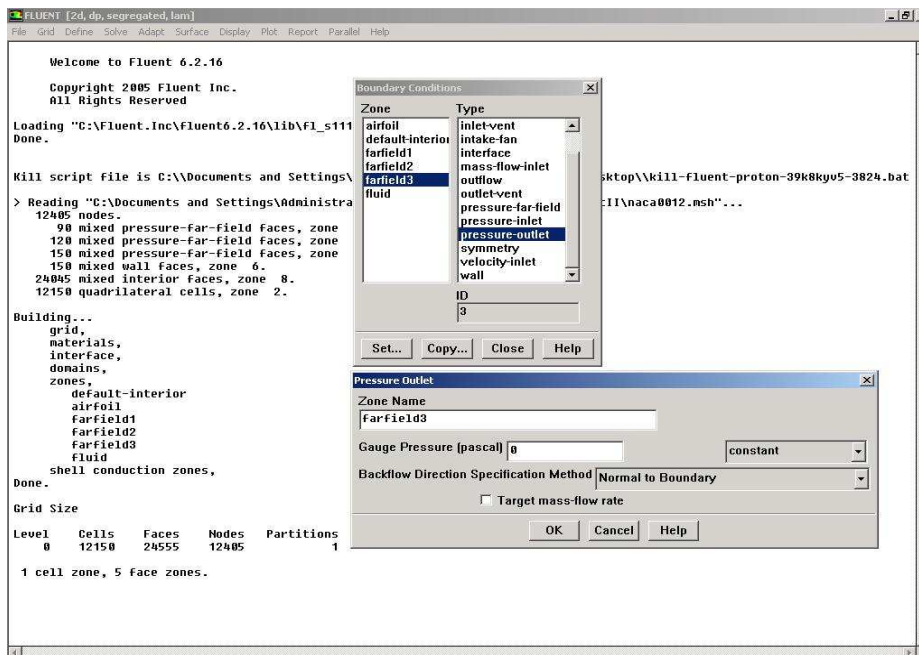


Figure 27-11 Defining Boundary Conditions

Set *farfield3* to *pressure-outlet* boundary type, click Set... and set the Gauge Pressure at this boundary to 0. Click OK. Then click Close.

Further Reading

1. Anderson, John D., Jr. (2001). *Fundamentals of Aerodynamics*. New York, McGraw-Hill.
2. Bhaskaran, R. (2003). *Fluent Tutorials*. New York, Cornell University.
3. Currie, I.G. (1993). *Fundamental Mechanics of Fluids*. New York, McGraw-Hill Inc.

CHAPTER 28

SOLVING PROBLEM IN FLUENT

Solve!

Solve > Control > Solution; Take a look at the options available.

Under **Discretization**, set Pressure to **PRESTO!** and **Momentum** to **Second-Order Upwind**.

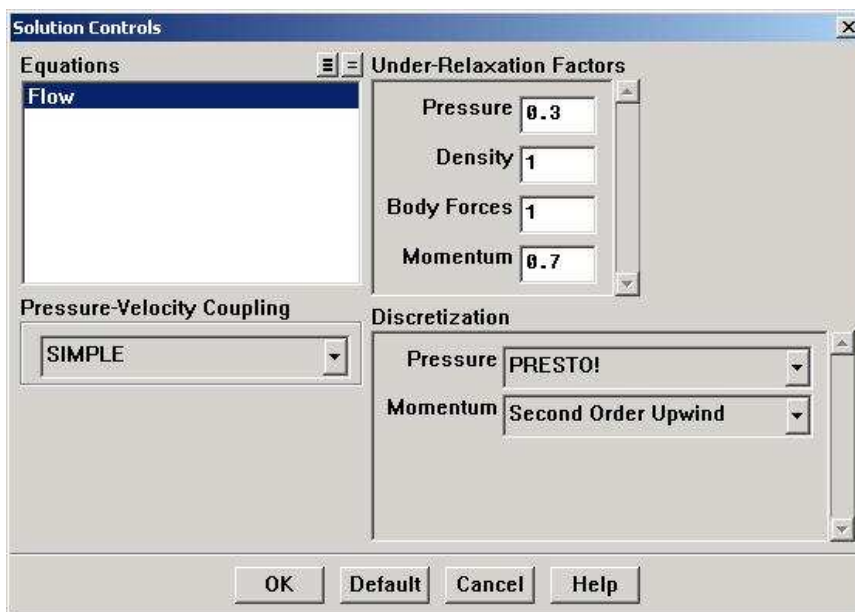


Figure 28-1 Solution Controls

Click OK.

AERODYNAMICS AND ITS APPLICATIONS

Before we initialize the case, for the purpose of the project, here we define the control volume to be used in gaining the data afterwards. The data will be implemented in the main equation to obtain lift and drag.

Surface > Line/Rake

Display > Grid

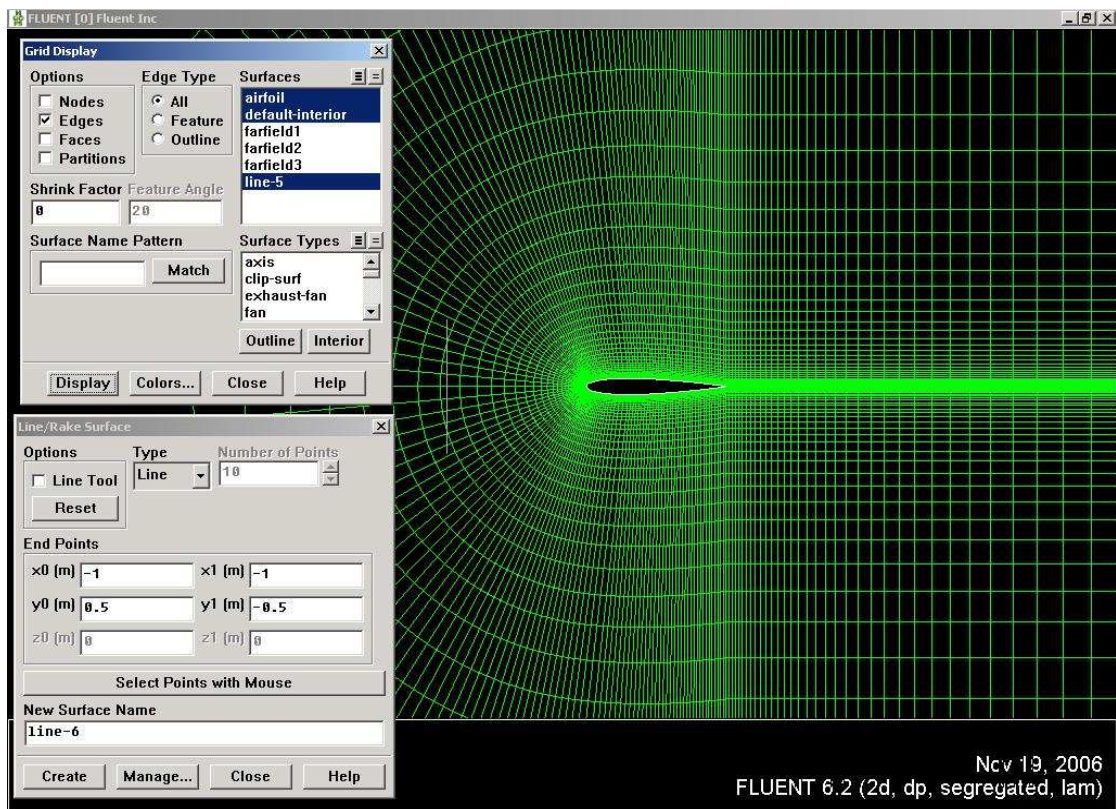


Figure 28-2 Defining the line

AERODYNAMICS AND ITS APPLICATIONS

Substitute the value for each line under the **End Points** and click **Create**. As each line is defined, display the line that has been created by displaying the grid

Table 28-1 Coordinate of the vertex for the lines

	x0	y0	x1	y1
Line-5	-1	0.5	-1	-0.5
Line-6	2	0.5	2	-0.5
Line-7	-1	0.5	2	0.5
Line-8	-1	-0.5	2	-0.5

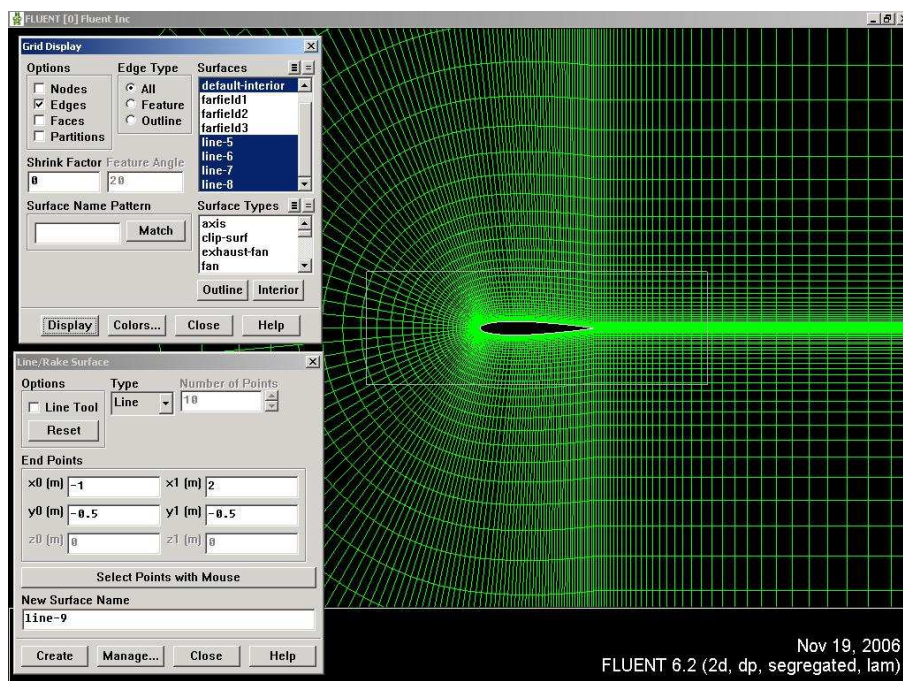


Figure 28-3 Lines defined

AERODYNAMICS AND ITS APPLICATIONS

Solve > Initialize > Initialize...

This is where we set the initial guess values (the base case) for the iterative solution. We will set these values to be the ones at the inlet. Select farfield1 under *Compute From*.

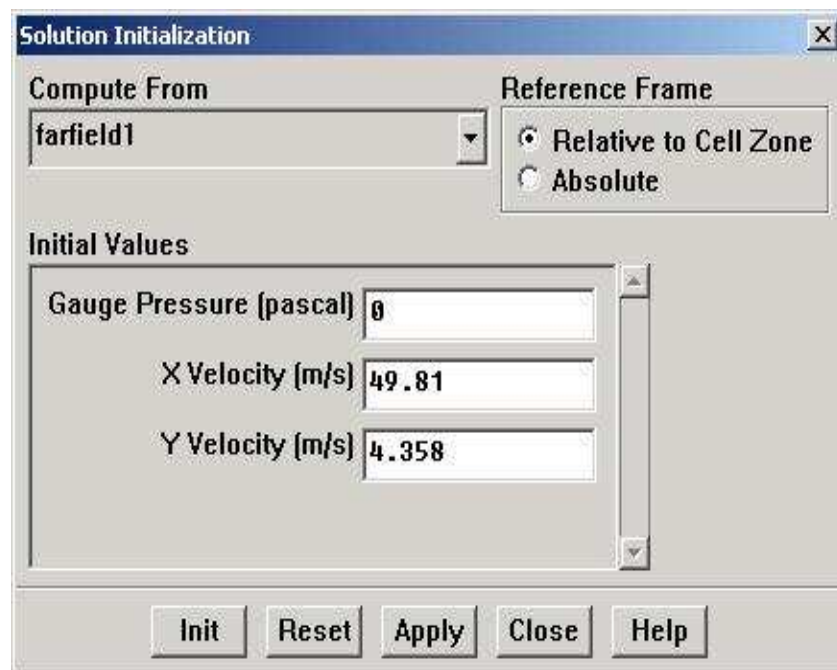


Figure 28-4 Initialization

Click *Init*, then

Solve > Monitors > Residual...

Now we will set the residual values (the criteria for a good enough solution). Once again, we'll set this value to $1e-06$.

AERODYNAMICS AND ITS APPLICATIONS

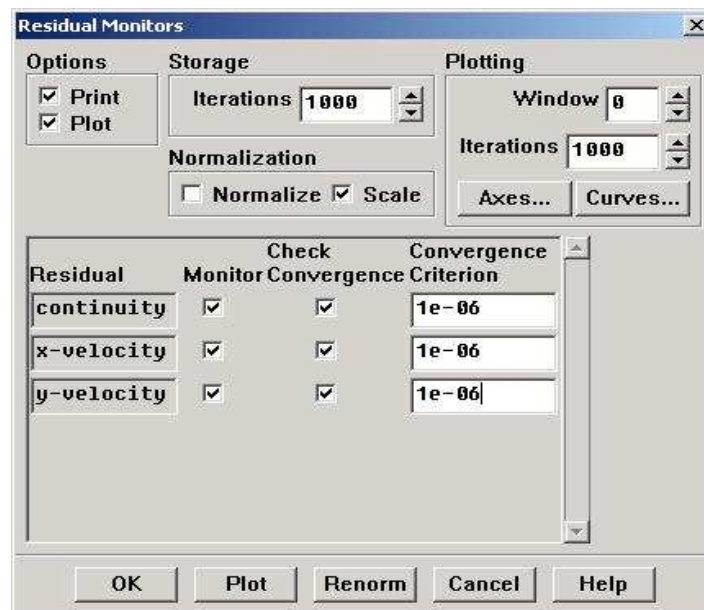


Figure 28-5 Residual Monitors

Click OK.

Further Reading

1. Anderson, John D., Jr. (2001). *Fundamentals of Aerodynamics*. New York, McGraw-Hill.
2. Bhaskaran, R. (2003). *Fluent Tutorials*. New York, Cornell University.
3. Currie, I.G. (1993). *Fundamental Mechanics of Fluids*. New York, McGraw-Hill Inc.

CHAPTER 29

COMPUTATING FORCES AND CONVERGENCE IN FLUENT

Solve > Monitors > Force...

Under Coefficient, choose Lift. Under Options, select Print and Plot. Then, Choose airfoil under Wall Zones.

Lastly, set the Force Vector components for the lift. The lift is the force perpendicular to the direction of the freestream. So to get the lift coefficient, set X to $-\sin(5^\circ) = -0.0872$ and Y to $\cos(5^\circ) = 0.9962$.

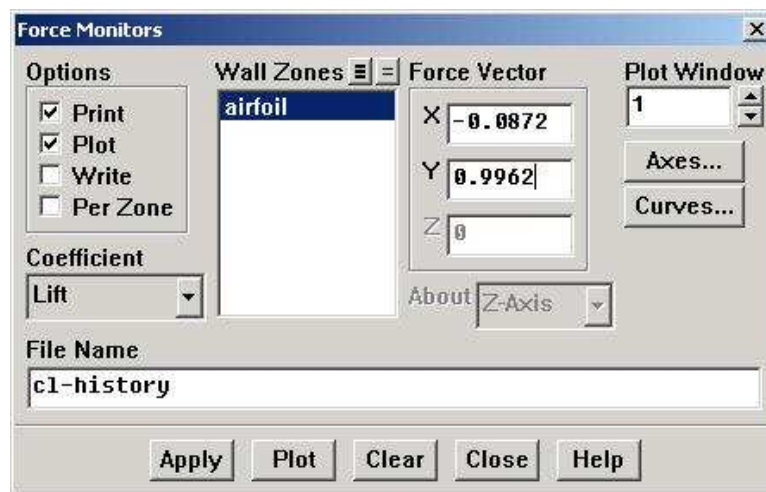


Figure 29-1 Lift Monitors

Click Apply for these changes to take effect.

AERODYNAMICS AND ITS APPLICATIONS

Similarly, set the Force Monitor options for the Drag force. The drag is defined as the force component in the direction of the freestream. So under Force Vector, set X to $\cos(5^\circ)=0.9962$ and Y to $\sin(5^\circ)=0.0872$. Turn on only Print for it.

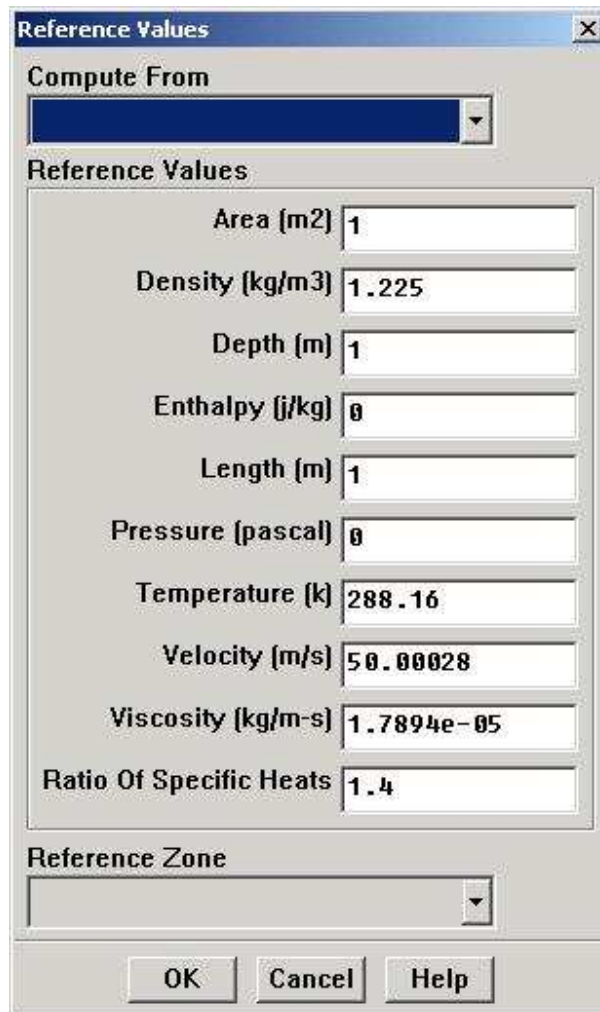


Figure 29-2 Drag Monitors

Report > Reference Values

Now, set the reference values to set the base cases for our iteration. Select farfield1 under Compute From.

AERODYNAMICS AND ITS APPLICATIONS



The image shows a 'Reference Values' dialog box with a title bar containing a close button (X). The dialog is divided into several sections:

- Compute From:** A dropdown menu that is currently empty.
- Reference Values:** A list of input fields with the following values:
 - Area (m²): 1
 - Density (kg/m³): 1.225
 - Depth (m): 1
 - Enthalpy (j/kg): 0
 - Length (m): 1
 - Pressure (pascal): 0
 - Temperature (k): 288.16
 - Velocity (m/s): 50.00028
 - Viscosity (kg/m-s): 1.7894e-05
 - Ratio Of Specific Heats: 1.4
- Reference Zone:** A dropdown menu that is currently empty.
- Buttons:** 'OK', 'Cancel', and 'Help' buttons are located at the bottom of the dialog.

Figure 29-3 Reference values

Click OK.

Main Menu > File > Write > Case...

Save the case file before you start the iterations.

Solve > Iterate

AERODYNAMICS AND ITS APPLICATIONS

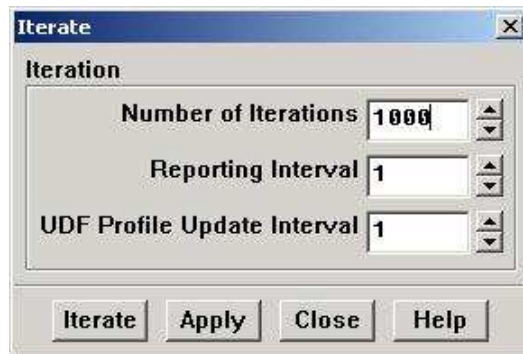


Figure 29-4 Iterate window

Just type in the appropriate number of iterations and it will stop automatically once the solution has converged.

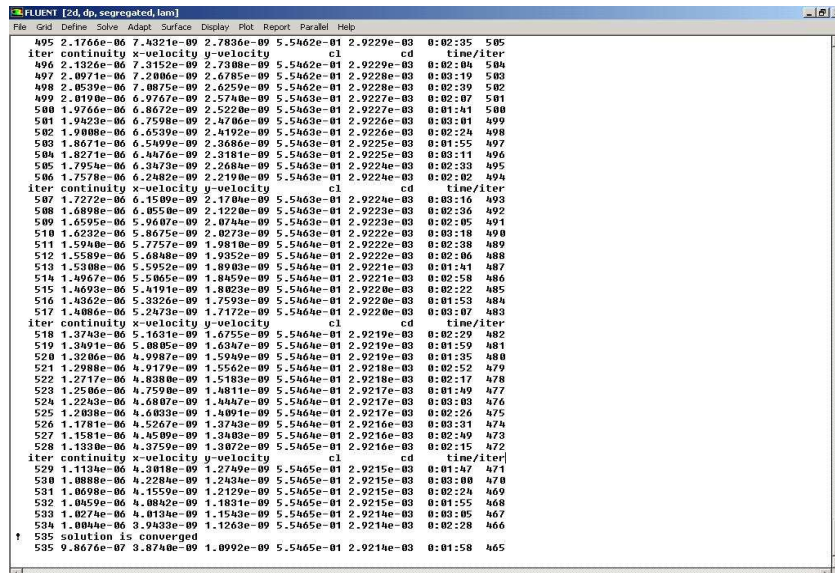


Figure 29-5 Converged iteration

AERODYNAMICS AND ITS APPLICATIONS

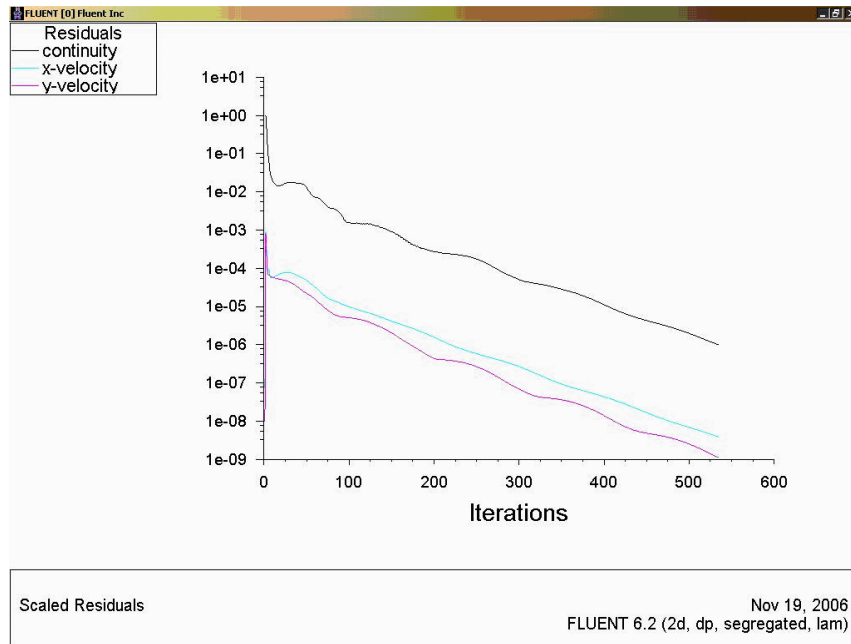


Figure 29-6 Iteration graph

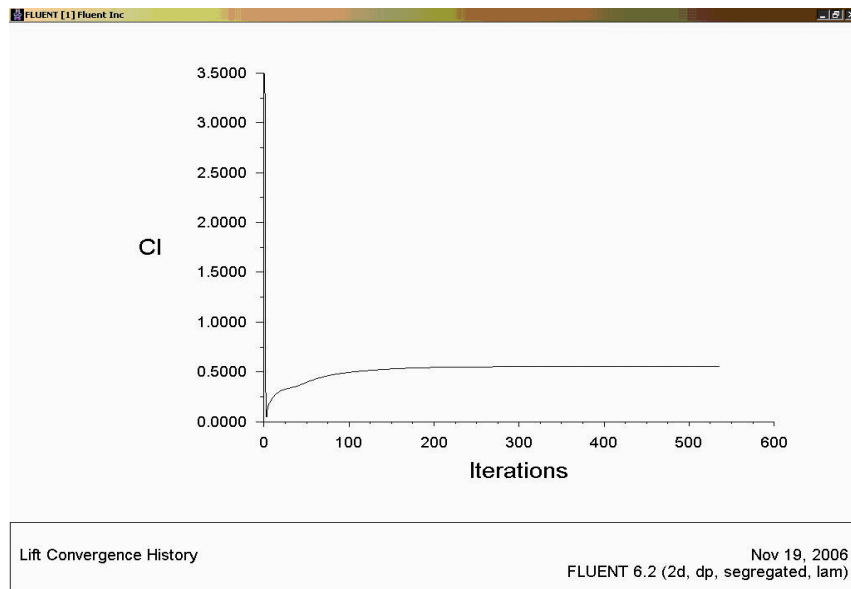


Figure 29-7 Iteration of Cl

AERODYNAMICS AND ITS APPLICATIONS

Main Menu > File > Write > Case & Data...

Save case and data after you have obtained a converged solution.

Further Reading

1. Anderson, John D., Jr. (2001). *Fundamentals of Aerodynamics*. New York, McGraw-Hill.
2. Bhaskaran, R. (2003). *Fluent Tutorials*. New York, Cornell University.
3. Currie, I.G. (1993). *Fundamental Mechanics of Fluids*. New York, McGraw-Hill Inc.

CHAPTER 30

ANALYSING RESULTS IN FLUENT

Analyze Results; Plot Pressure Coefficient; select Plot > XY Plot...

Change the Y Axis Function to Pressure..., followed by Pressure Coefficient. Then, select airfoil under Surfaces.

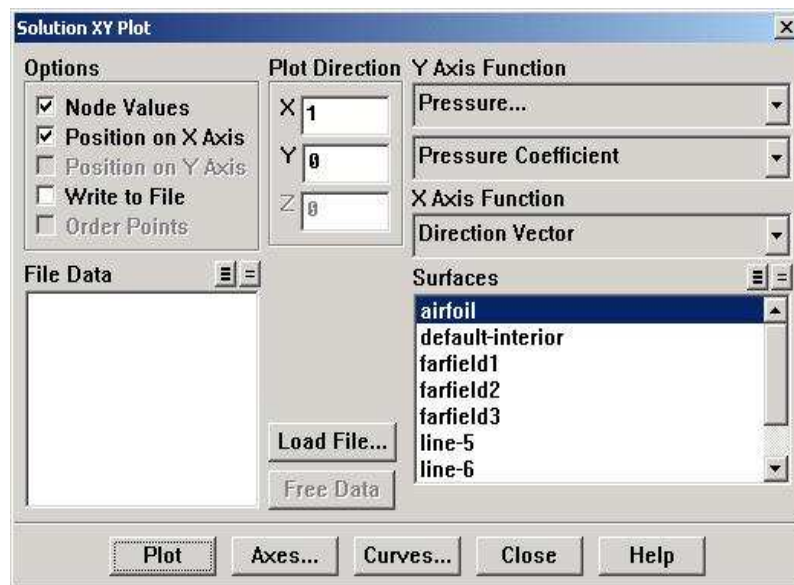


Figure 30-1 XY plot

Click **Plot**.

AERODYNAMICS AND ITS APPLICATIONS

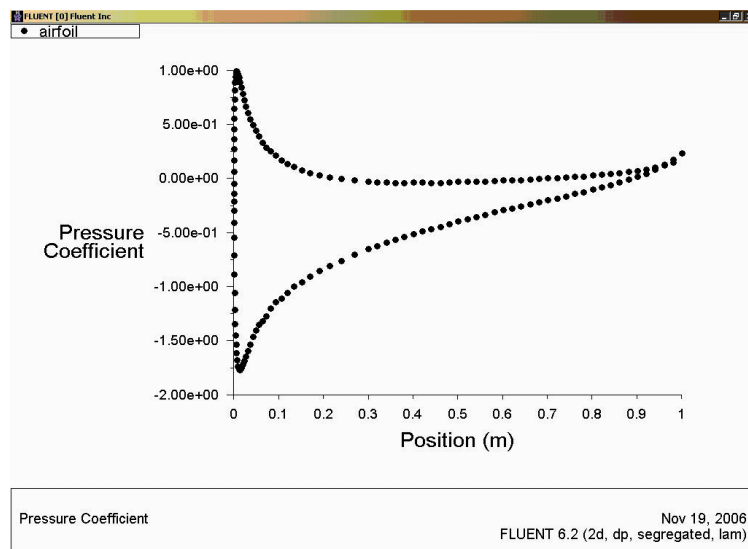


Figure 30-2Cp distribution for NACA0012 at 5 degrees

Plot Pressure Contours

Plot static pressure contours. In **Display > Contours...**

Select **Pressure...** and **Static Pressure** from under **Contours Of**. Click **Display**.

AERODYNAMICS AND ITS APPLICATIONS

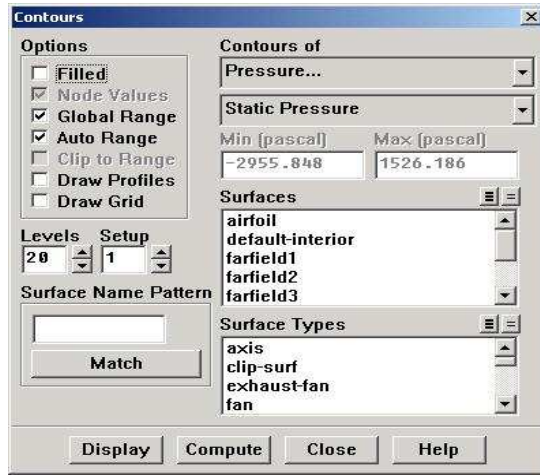


Figure 30-3 Contours display

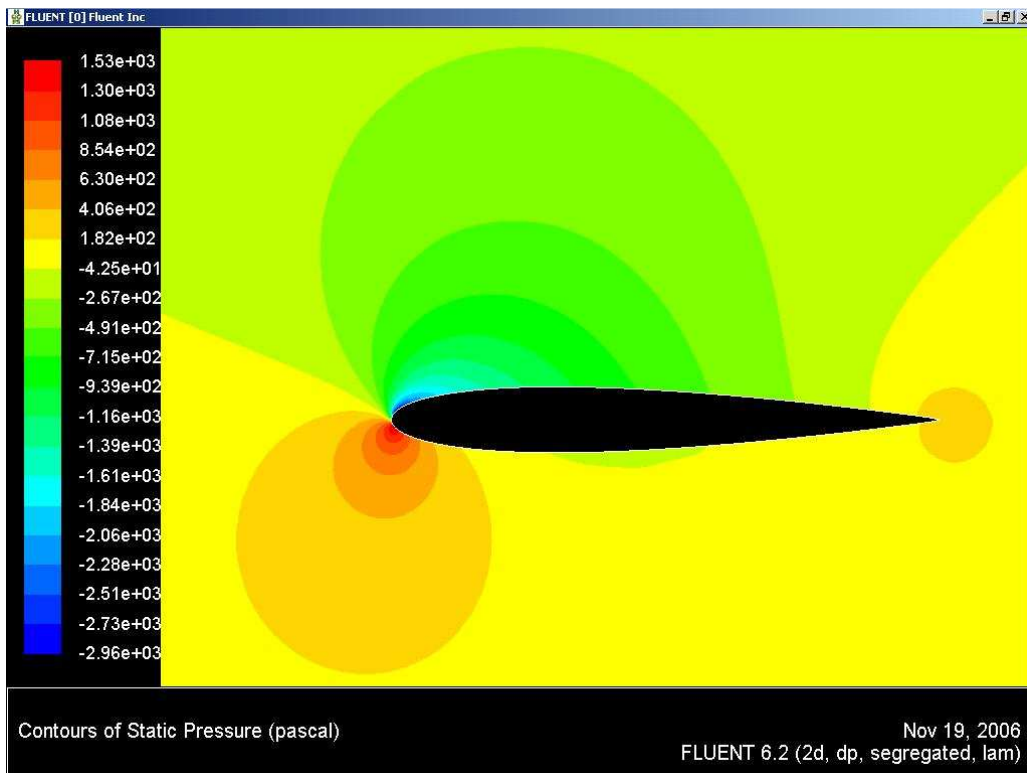


Figure 30-4 Static Pressure contour (NACA0012 at 5 deg)

AERODYNAMICS AND ITS APPLICATIONS

The figure above shows overall distribution of the static pressure on an airfoil. As we can see, the highest pressure occurs at the downside of the leading edge where the freestream hit directly the airfoil. Just above the leading edge, the lowest pressure occurs as it is here the highest velocity occurs as shown in the velocity diagram below.

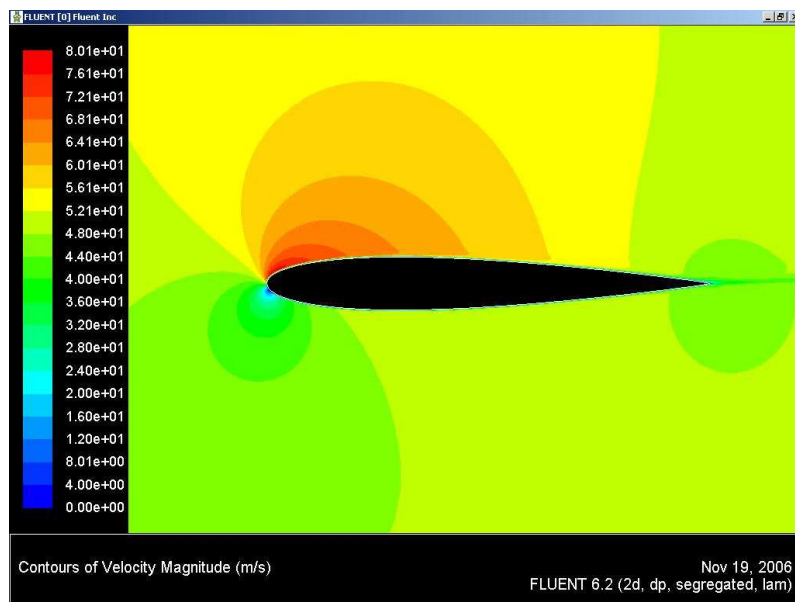


Figure 30-5 Contour of Velocity Magnitude (NACA0012 at 5 deg)

AERODYNAMICS AND ITS APPLICATIONS

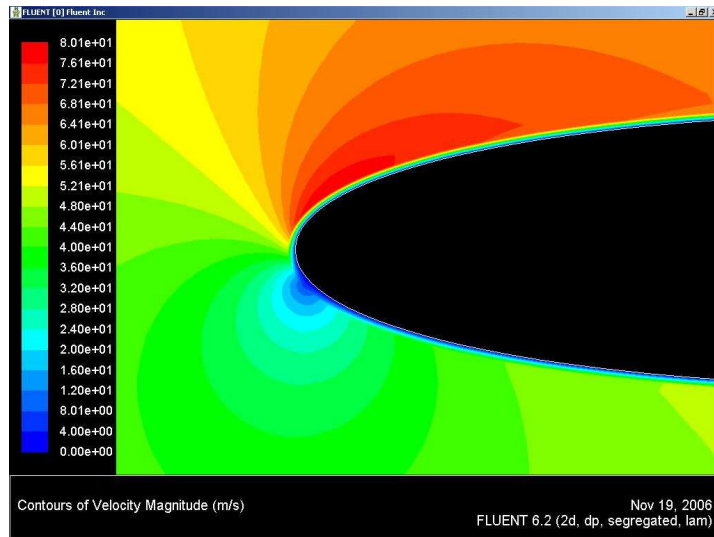


Figure 30-6 Zoomed contour of velocity (NACA0012 at 5 deg)

Also presented here are the contours of the boundary layer region near the leading edge.

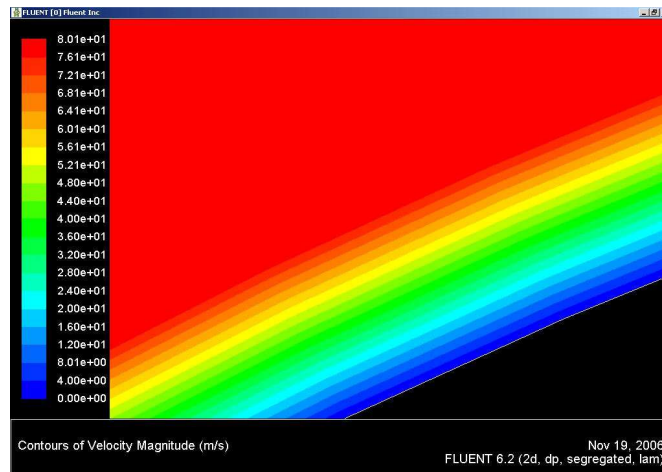


Figure 30-7 Boundary layer region

AERODYNAMICS AND ITS APPLICATIONS

Furthermore, here are the contours of x and y velocity with the control volume selected.

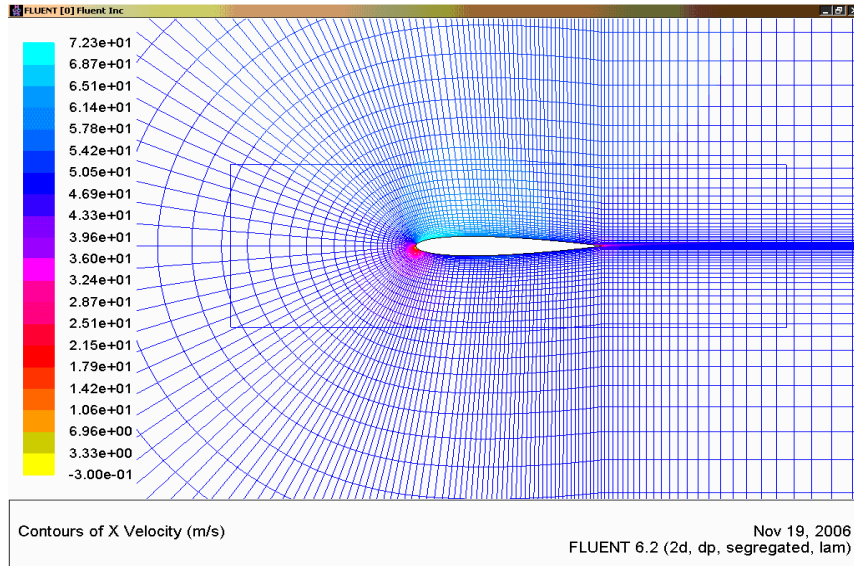


Figure 30-8 Contours of X Velocity

AERODYNAMICS AND ITS APPLICATIONS

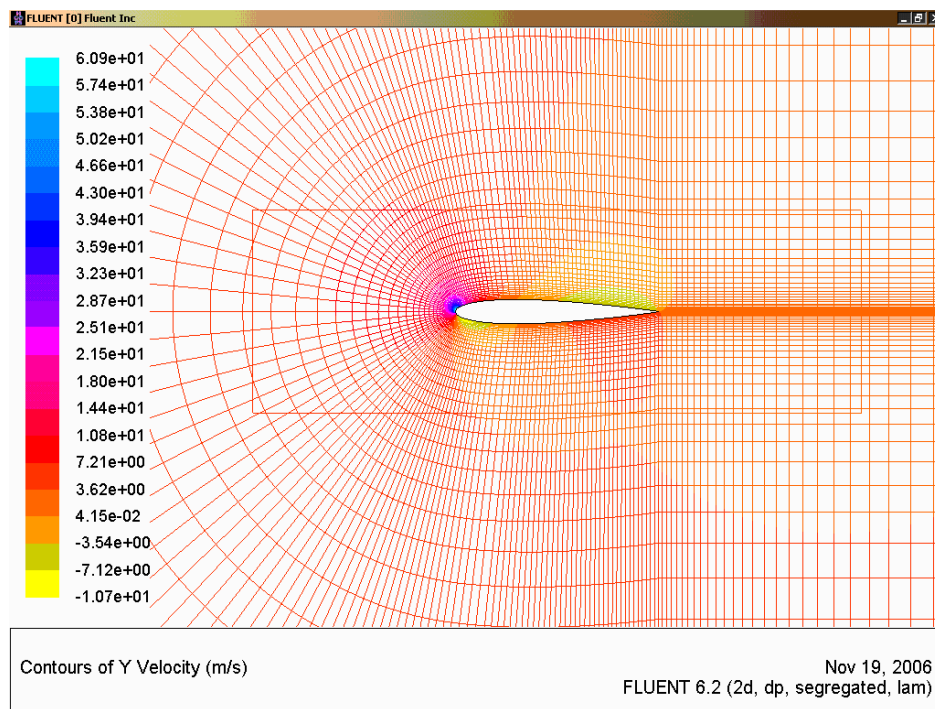


Figure 30-9 Contours of Y Velocity

Further Reading

1. Anderson, John D., Jr. (2001). *Fundamentals of Aerodynamics*. New York, McGraw-Hill.
2. Bhaskaran, R. (2003). *Fluent Tutorials*. New York, Cornell University.
3. Currie, I.G. (1993). *Fundamental Mechanics of Fluids*. New York, McGraw-Hill Inc.

CHAPTER 31

FLUENT RESULTS FOR NACA 0012

The result for the first airfoil NACA0012 at 50 m/s of free stream and 0° angle of attack are shown below.

NACA0012: 0 degrees

The Figure 31.1 shows that the static pressure is at the highest at the leading edge.

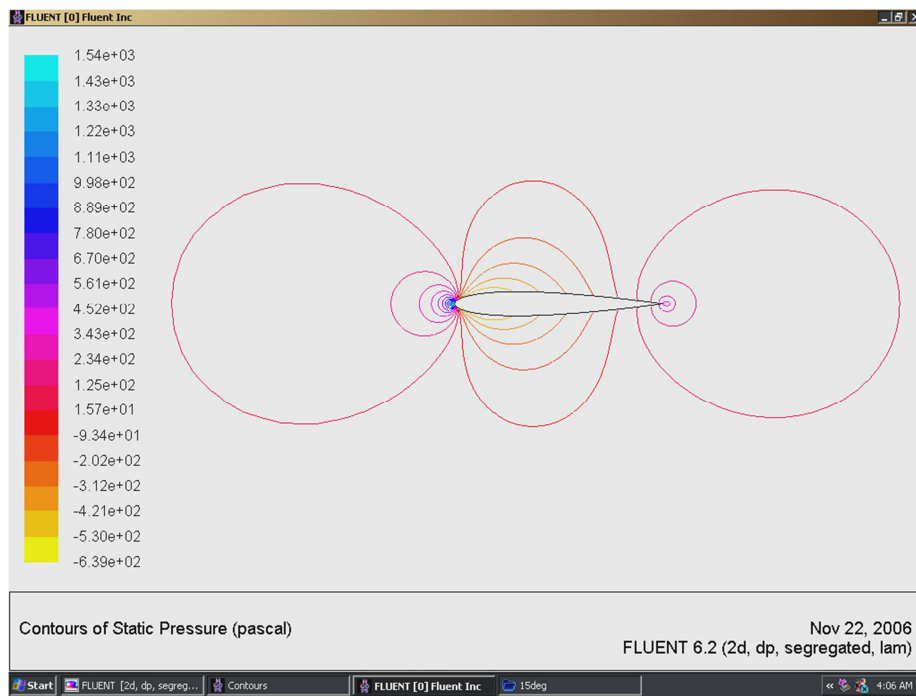


Figure 31-1 Contours of Static Pressure (NACA0012 at 0 deg, $Re = 3.0e6$)

AERODYNAMICS AND ITS APPLICATIONS

Also from the velocity vector diagrams below shows the lowest velocity is at the leading edge.

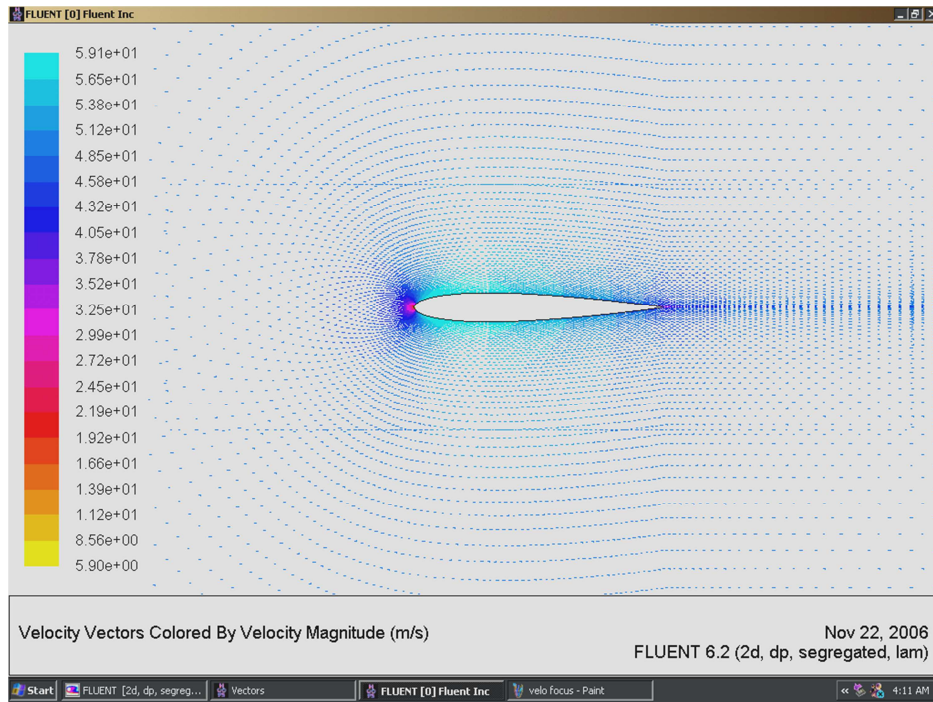


Figure 31-2 Velocity Vectors (NACA0012 at 0 deg, Re = 3.0e6)

AERODYNAMICS AND ITS APPLICATIONS

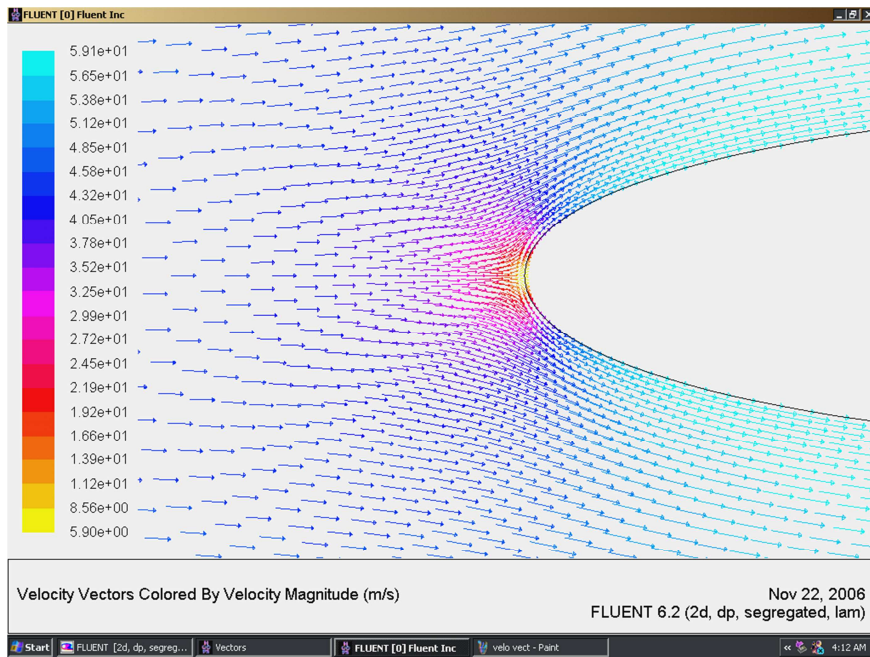


Figure 31-3 Velocity Vectors zoomed (NACA0012 at 0 deg, $Re = 3.0e6$)

From the figure of C_p distribution below we can see that the area inside the C_p data between the upper surface and the lower surface is almost zero indicating that the lift is nearly zero here.

AERODYNAMICS AND ITS APPLICATIONS

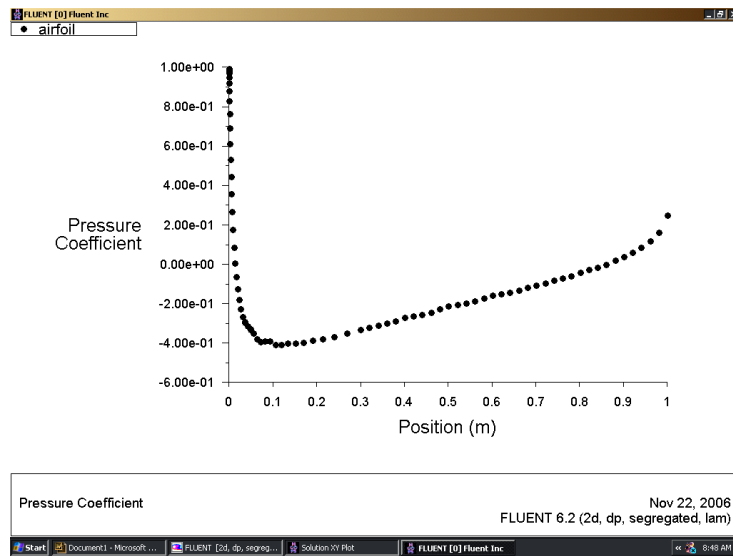


Figure 31-4Cp distribution for NACA0012 at 0 deg, $Re = 3.0e6$

NACA0012: 10 degrees

The figure below (Fig.31.5) shows the static pressure contour at 10 degrees angle of attack. The location of the lowest pressure has moved to a little above the leading edge.

AERODYNAMICS AND ITS APPLICATIONS

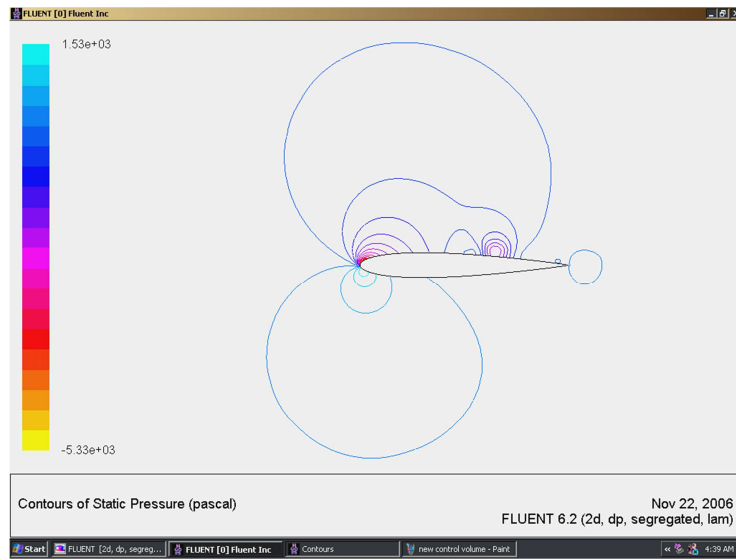


Figure 31-5 Contours of Static Pressure (NACA0012 at 10 deg, $Re = 3.0e6$)

The figure of velocity vector (Fig.31.6) shows some separation occurs at the upper surface of the airfoil. Also shown in the figure is the control volume used for the calculation of the Lift and Drag where we obtain all the data needed.

AERODYNAMICS AND ITS APPLICATIONS

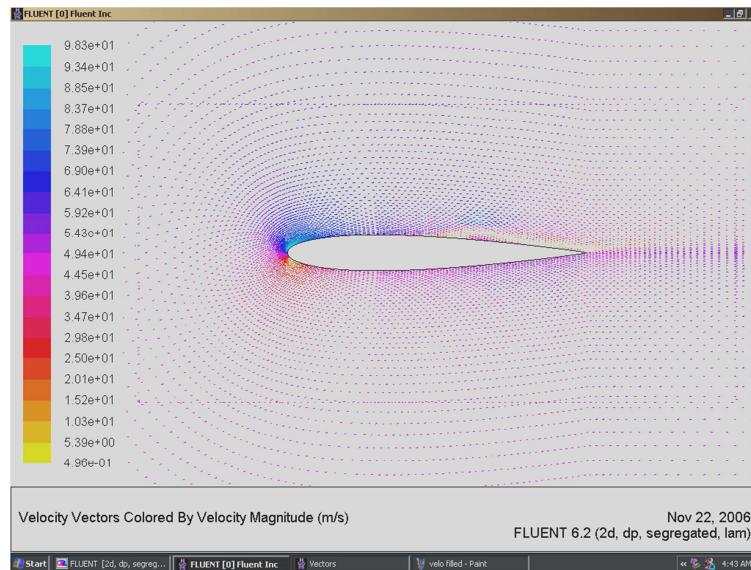


Figure 31-6 Velocity vectors for NACA0012 at 10 deg, $Re = 3.0e6$

This phenomenon of separation can be clearly seen from the Static Pressure graph below (Fig.31.7). A sudden abrupt change of pressure at around 0.5 m of the airfoil clearly shows where the separation start to occur. This will then affect the value of C_l calculated. But the effect is not as pronouce as when the airfoil reaches near stalling angle as we will see at the next angle of attack of 15 degrees.

AERODYNAMICS AND ITS APPLICATIONS

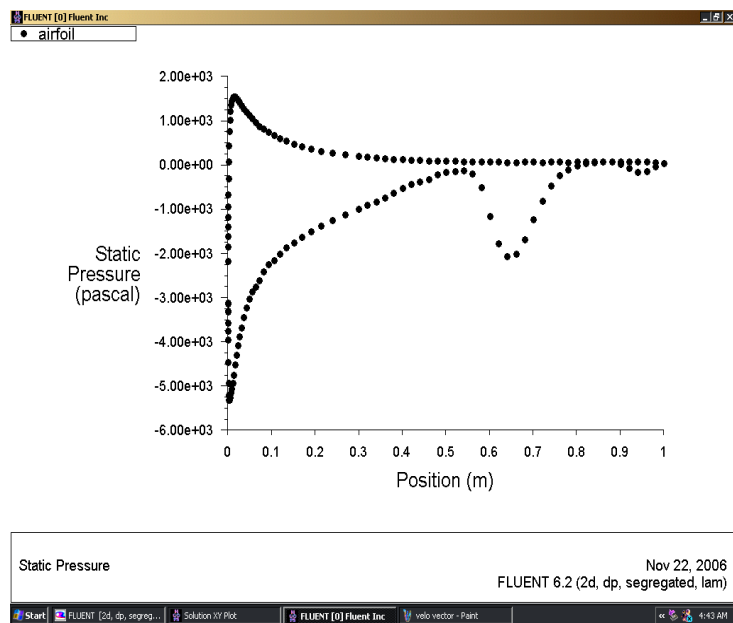


Figure 31-7 Graph of Static Pressure (NACA0012 at 10 deg, $Re = 3.0e6$)

NACA0012: 15 degrees

Here we shall examine how the flow behaves in the following velocity vector diagram (Fig.31.8).

AERODYNAMICS AND ITS APPLICATIONS

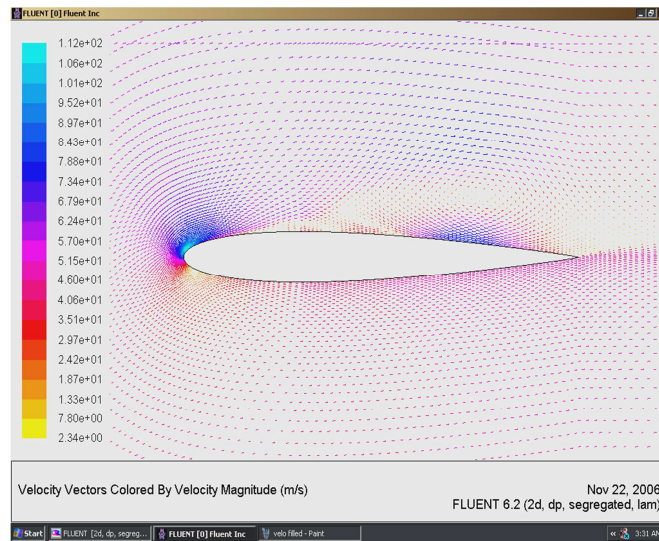


Figure 31-8 Velocity Vectors (NACA0012 at 15 deg, Re = 3.0e6)

Slightly after the leading edge there occurs a separation. This is also appears at the trailing edge. This creates a circulation above the upper surface of the airfoil. The effect is on how the FLUENT calculates the C_l and C_d . This effect is shown in the iteration figure below (Fig.31.9).

AERODYNAMICS AND ITS APPLICATIONS

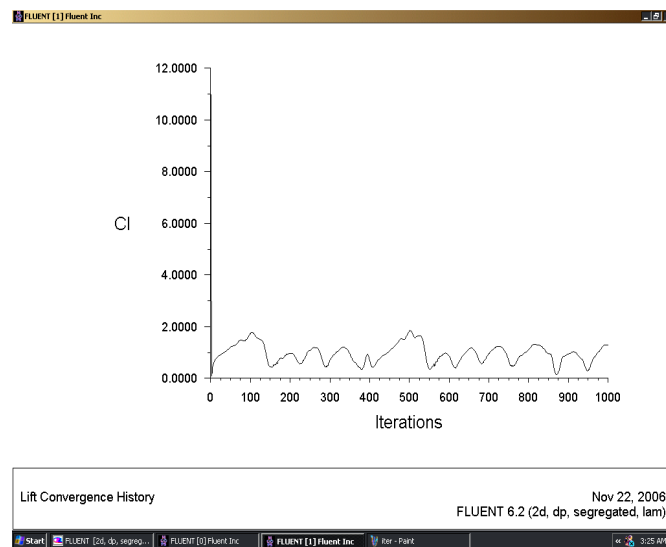


Figure 31-9 Lift Convergence History (NACA0012 at 15 deg, $Re = 3.0e6$)

Here the iterations of the continuity, x velocity and y velocity have never converged. It shows an oscillating behavior. That is why it is hard to get an accurate result for the flow analysis here.

AERODYNAMICS AND ITS APPLICATIONS

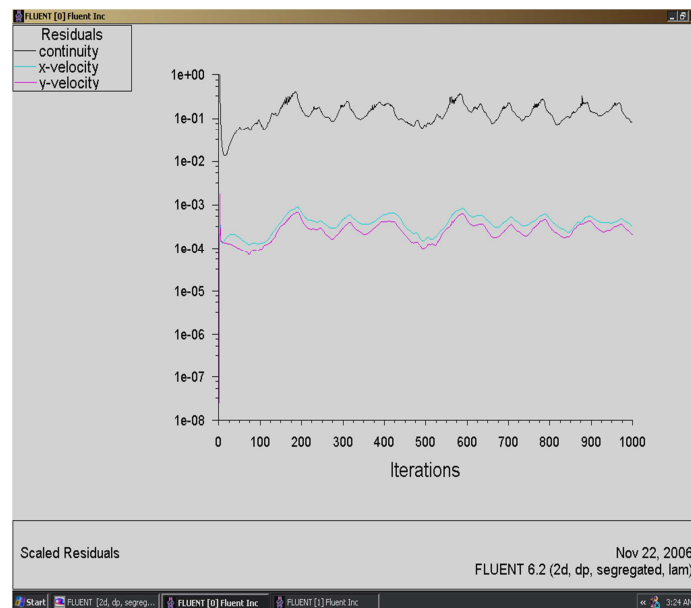


Figure 31-10 Scaled Residuals (NACA0012 at 15 deg, $Re = 3.0e6$)

Further Reading

1. Anderson, John D., Jr. (2001). *Fundamentals of Aerodynamics*. New York, McGraw-Hill.
2. Bhaskaran, R. (2003). *Fluent Tutorials*. New York, Cornell University.
3. Currie, I.G. (1993). *Fundamental Mechanics of Fluids*. New York, McGraw-Hill Inc.

CHAPTER 32

FLUENT RESULTS FOR NACA 4412

NACA4412: 0 degrees

It is a different case when we deal with a nonsymmetric airfoil compared to NACA0012 which is a symmetric airfoil. For NACA0012, at zero angle of attack, the lift reaches zero. Meanwhile, for a cambered airfoil like NACA4412, there exists a lift force even at zero angle of attack. This is shown by the area under the graph shown by the Cp distribution figure below (Fig. 32-1).

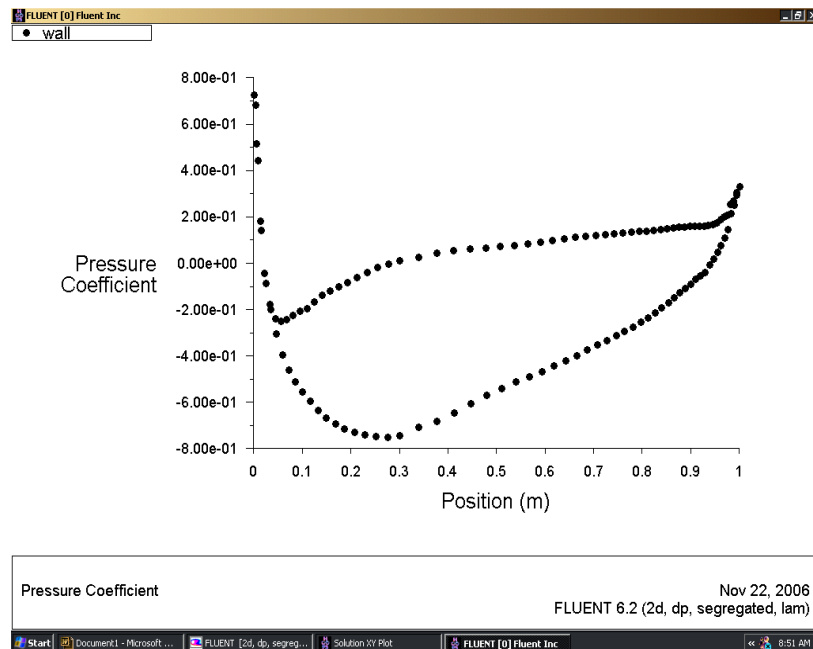


Figure 32-1 Cp distribution over NACA4412 at 0 deg, $Re = 3.0e6$

AERODYNAMICS AND ITS APPLICATIONS

The larger the area between the upper surface and the lower surface of the C_p values, the higher is the Lift.

NACA4412: 5 degrees

The area is more apparent as shown in the figure below (Fig.32-2). The figure shows the C_p distribution of NACA4412 at 5 degrees angle of attack. This shows that the higher the angle of attack gets, the higher the lift force.

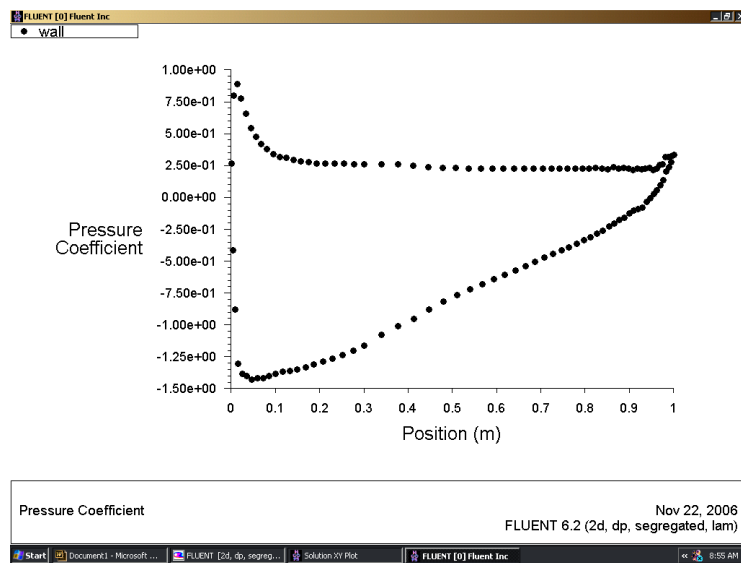


Figure 32-2 C_p distribution over NACA4412 at 5 deg, $Re = 3.0e6$

NACA4412: 10 degrees

AERODYNAMICS AND ITS APPLICATIONS

From all of the result obtained by FLUENT for the C_l and C_d , the result for this case is the most accurate comparing to the experimental data.

One of the reasons is the attachment of the flow around the airfoil. The figure below (Fig.32-3) illustrates that. The velocity contour shows how well the flow is attached to the surface of the airfoil, thus producing a good condition for FLUENT to apply numerical calculation to obtain the lift and drag forces.

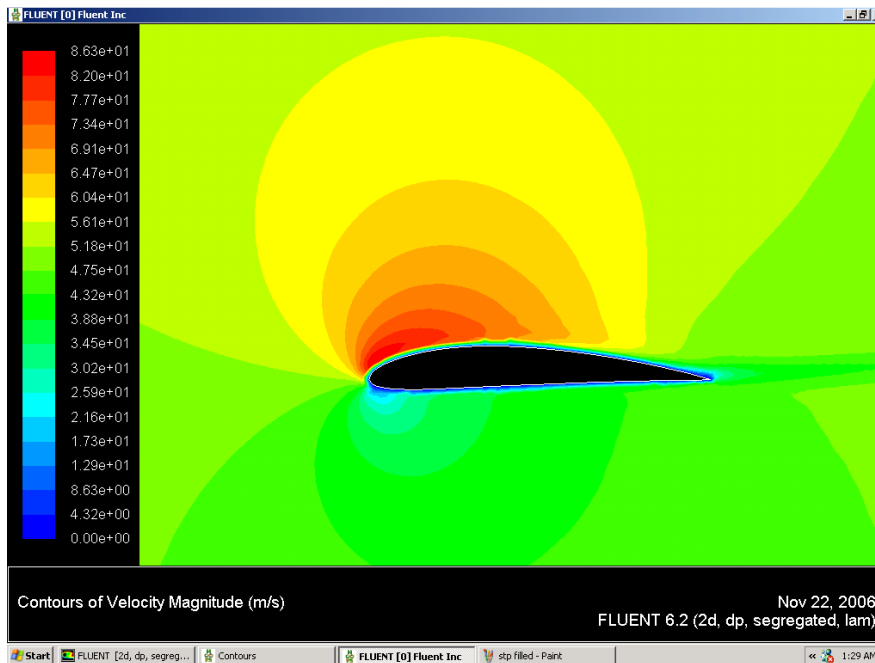


Figure 32-3 Contours of Velocity over NACA4412 at 10 deg, $Re = 3.0e6$

AERODYNAMICS AND ITS APPLICATIONS

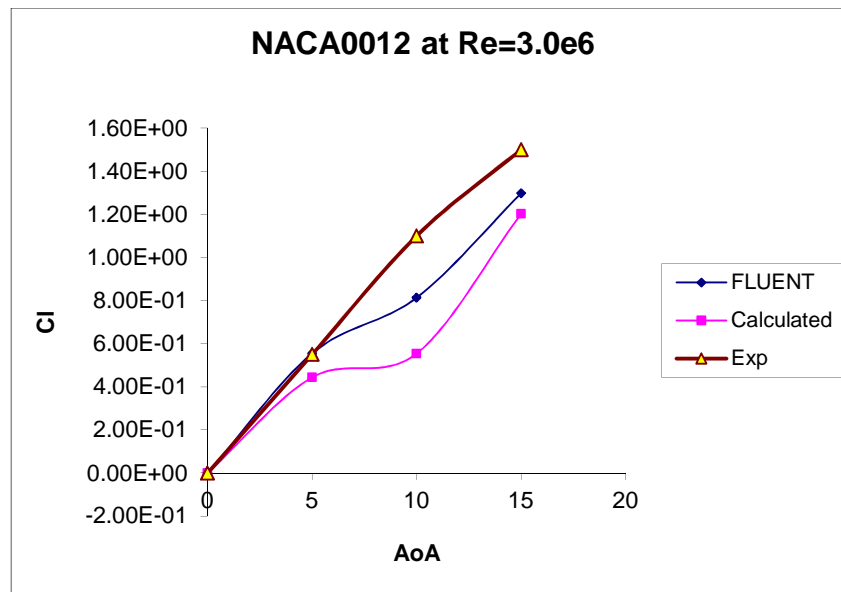


Figure 32-4 Graph of C_l versus Angle of Attack for NACA0012 at $Re=3.0e6$

From Fig. 32-4, the FLUENT result is very good at 0 and 5 angles of attack. However, at 10 and 15 degrees, the values are less than the experimental values but with no large discrepancy. The same thing appears to be for the calculated values. At 0 and 5 angles of attack, the values are quite close. Nonetheless, at 10 and 15 degrees the values are not closed especially at 10 degrees where the difference is about half of the experimental value.

AERODYNAMICS AND ITS APPLICATIONS

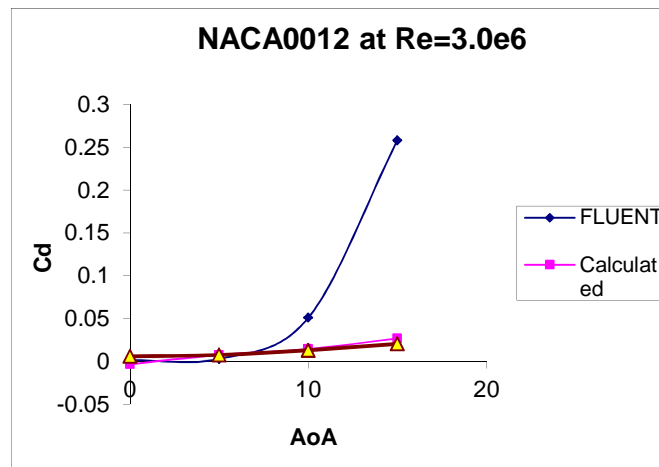


Figure 32-5 Graph of Cd versus Angle of Attack for NACA0012 at Re=3.0e6

From Fig. 32-5, what we can see is the calculated values of Cd have a very good agreement with the experimental values. However, FLUENT results are not very good at 10 and especially 15 degrees angle of attack.

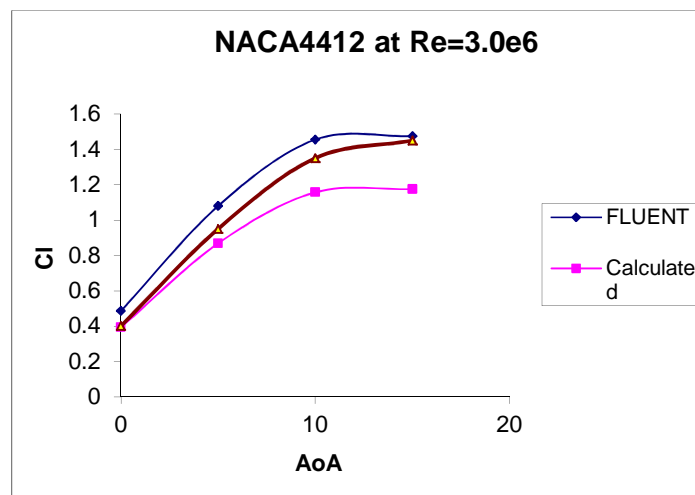


Figure 32-6 Graph of Cl versus Angle of Attack for NACA4412 at Re=3.0e6

AERODYNAMICS AND ITS APPLICATIONS

From Fig. 32-6, we can see good agreement of both the FLUENT and calculated results when compared to the experimental values especially at zero angle of attack for the calculated value and at 15 degrees for FLUENT value. However, the calculated values of C_l tend to deviate with increasing angles of attack.

Further Reading

1. Anderson, John D., Jr. (2001). *Fundamentals of Aerodynamics*. New York, McGraw-Hill.
2. Bhaskaran, R. (2003). *Fluent Tutorials*. New York, Cornell University.
3. Currie, I.G. (1993). *Fundamental Mechanics of Fluids*. New York, McGraw-Hill Inc.

CHAPTER 33

DESIGNING A MODEL FOR WIND TUNNEL TESTING

In this chapter an attempt will be made to describe the designing and fabrication of a small scale model of rigid airship that can be tested in the IIUM low speed wind tunnel. This model is actually a half model airship, which can be assumed to be axisymmetric. The initial design of the airship is shown in the figure below:

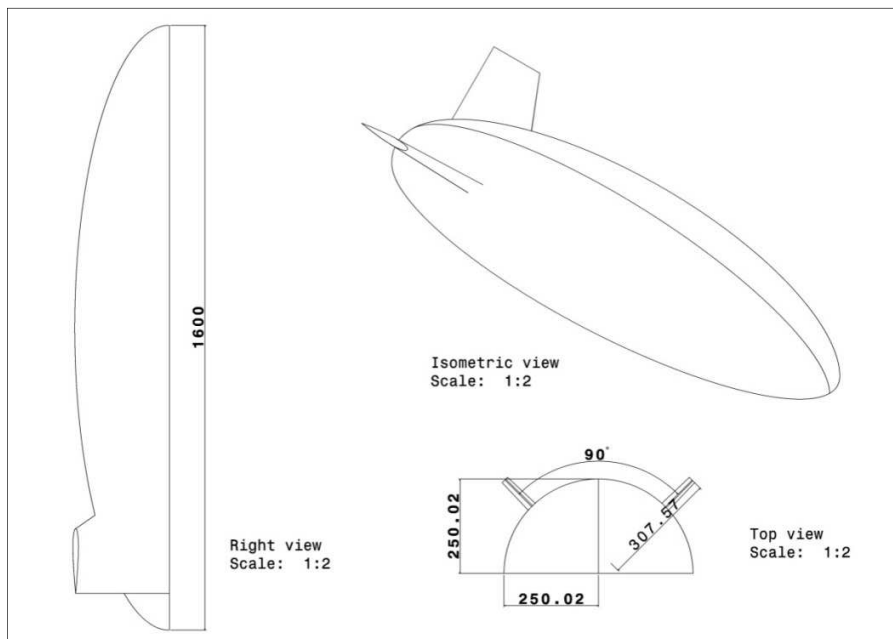


Figure 33-1 Initial design of rigid airship

AERODYNAMICS AND ITS APPLICATIONS

Dimensions:

Table 33-1 Dimensions of airship

Length	1.6m
Width	0.5m
Height	0.25m

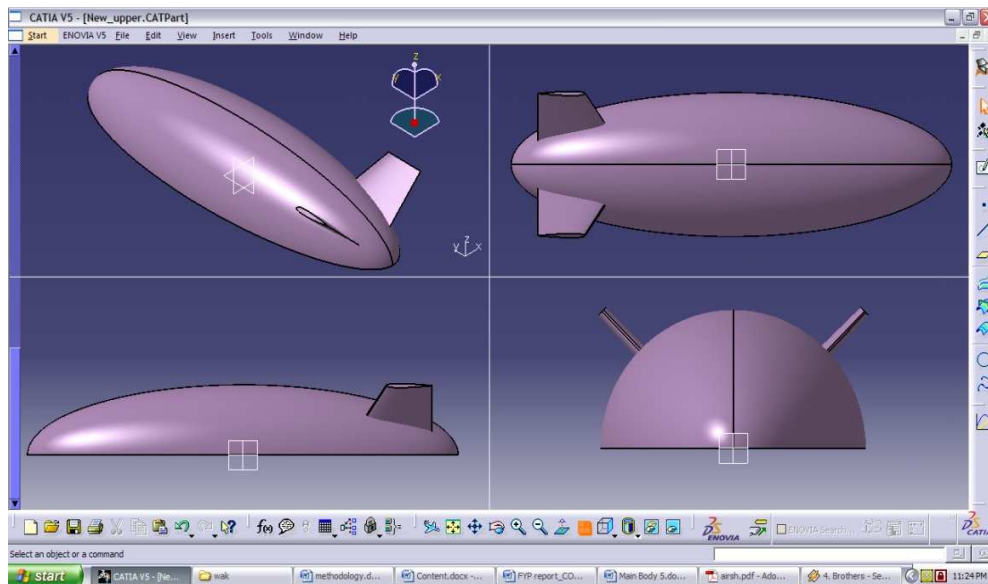


Figure 33-2 Three dimensional view of designed airship using CATIA.

The structural design is mainly to maintain the shape and structure of the model during the measurement of its pressure distribution and forces in wind tunnel. It has to be strong enough to resist the wind flow approximately 20 m/s. Figures shown below depict the main structural features of the model.

AERODYNAMICS AND ITS APPLICATIONS

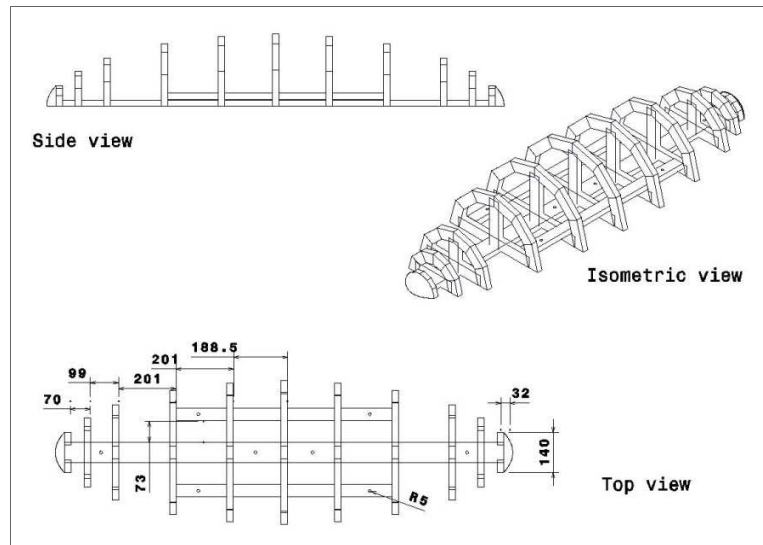


Figure 33-3 Drawings of frame structure (dimensions are in mm).

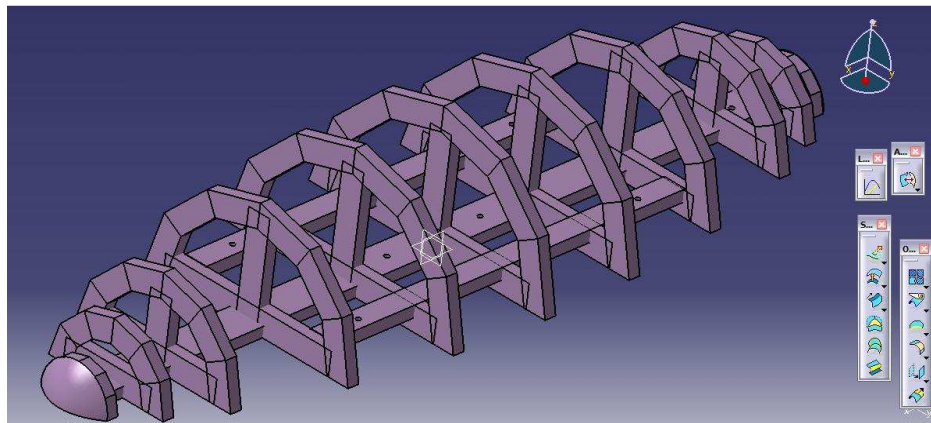


Figure 33-4 CATIA illustration of the base and frame structure.

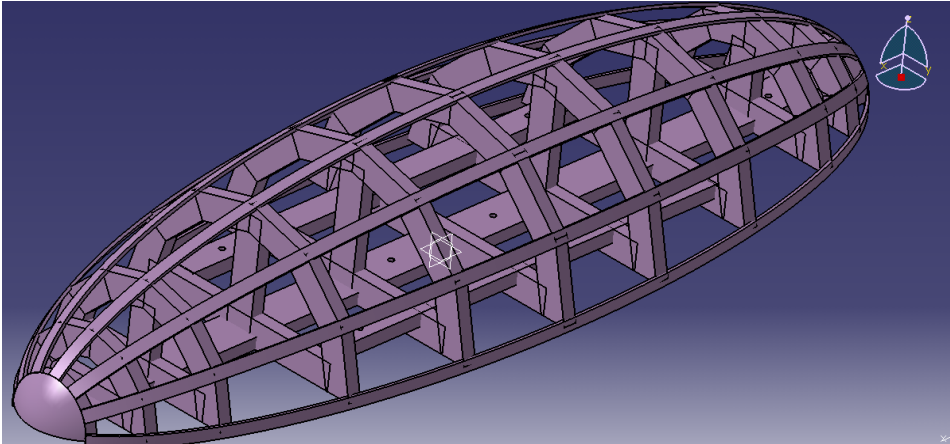


Figure 33-5 CATIA illustration of the frame structure and the stringers.

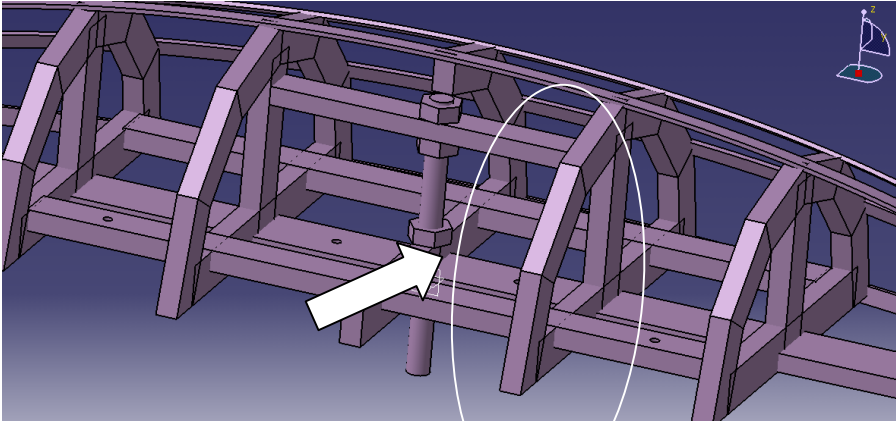


Figure 33-6The mounting structure indicated by the arrow

AERODYNAMICS AND ITS APPLICATIONS

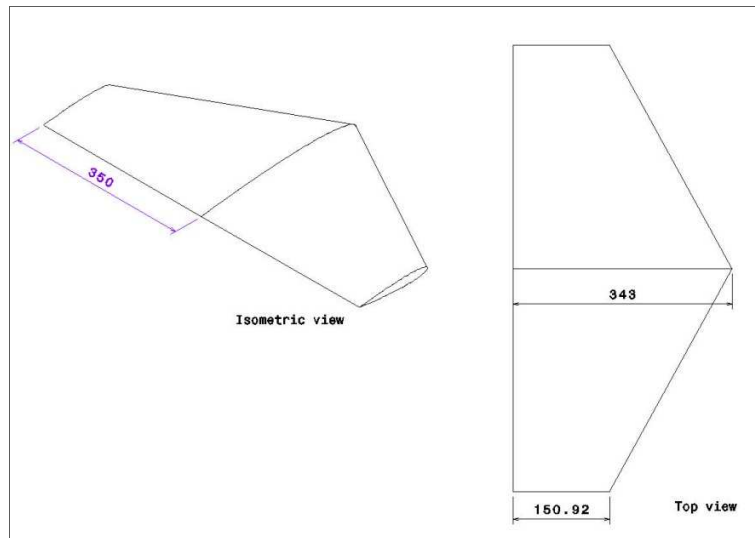


Figure 33-7The tail structure drawing.

The complete structural design of the model.

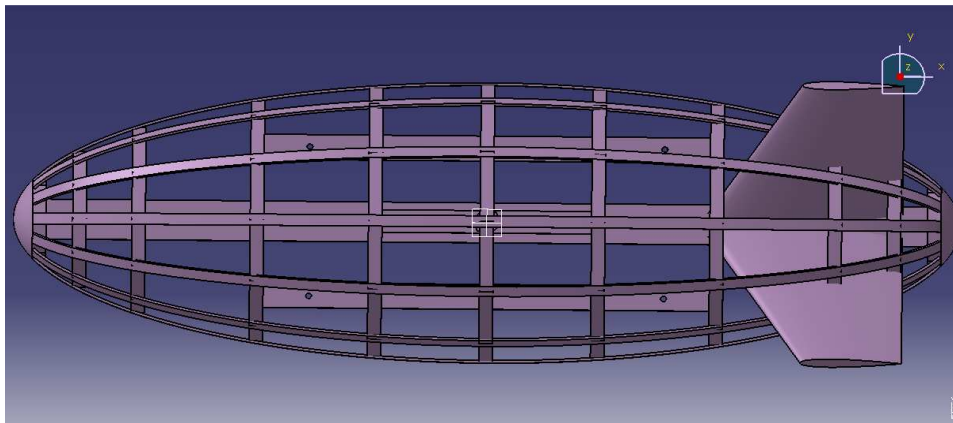


Figure 33-8 Top view of the model.

AERODYNAMICS AND ITS APPLICATIONS

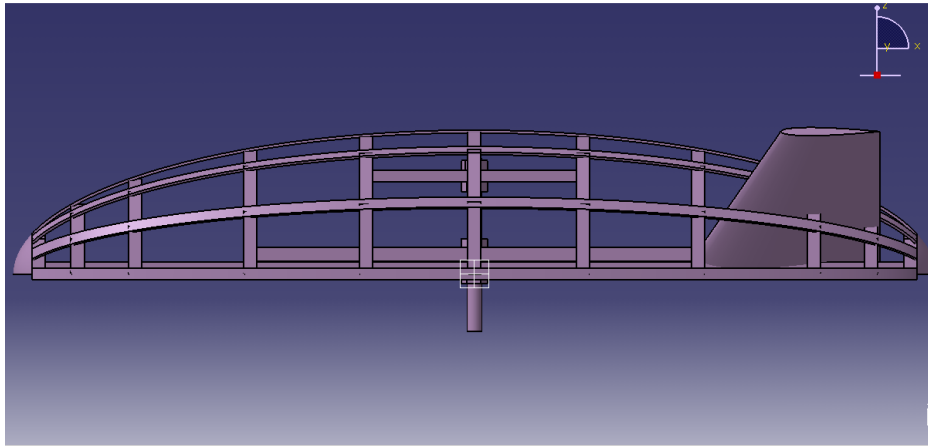


Figure 33-9 Side view of the model.

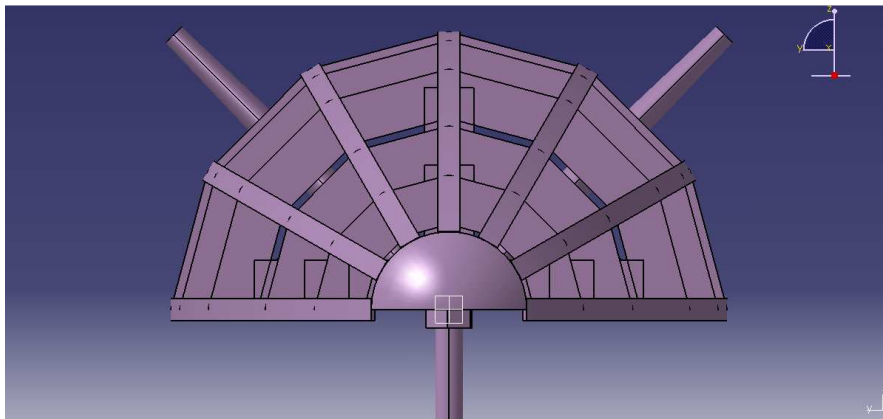


Figure 33-10 Front view of the model.

AERODYNAMICS AND ITS APPLICATIONS

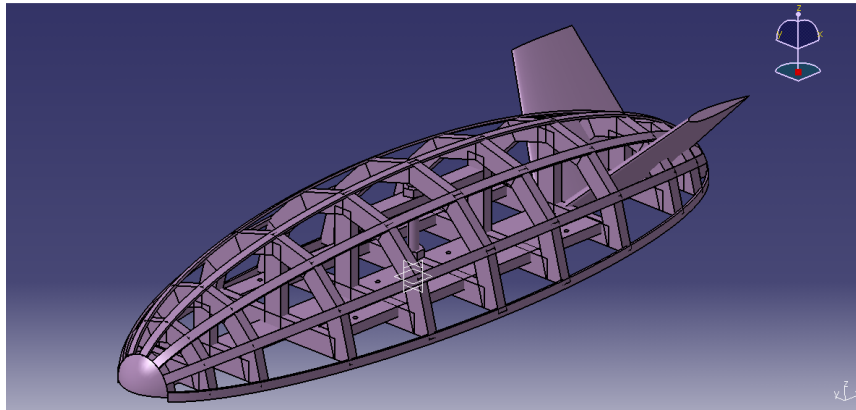


Figure 33-11 Isometric view of the model.

Further Reading

Khoury, G. A. & Gillette, D. (1999). *Airship Technology*, United Kingdom, Cambridge University Press.

Beckwith, T. G., Maragoni, R. D. & Lienhard, J. H. *Mechanical Measurements*. Sixth Edition. Prentice Hall

Barlow, J. B., Rae, Jr., W. H., and Pope, A. 1999. *Low Speed Wind Tunnel Testing*. USA, John Wiley and Sons.

Anderson, Jr., J.D. (2005), *Fundamentals of Aerodynamics*, Fourth Edition, McGraw Hill

CHAPTER 34

SELECTING MATERIAL AND CONSTRUCTING MODEL FOR WIND TUNNEL TESTING

This chapter provides a step by step procedure to make simple models using simple techniques and locally available materials. This procedure is suitable for simple tests for classroom and UG final year project applications. Professional wind tunnel testing model methods are discussed in [3]. The model is first drawn to scale according to the previous published data. The model built is made as close as possible to the geometries of the available data, but a compromise between what material is available in the market and price has to be made. Also, the materials used have to consider whether it can withstand the testing in the wind tunnel.

In this particular project, the material used for the mainframe of the model is wood since the wood offers good strength to weight ratio and easy to fabricate and repair. It is actually much like composite materials in that it has different properties in different directions. Each piece of wood is unique so it requires craftsman-like skills to manufacture aircraft with wood.

For the stringers, the material used is bamboo stick. After the bamboo sticks were reduced to the required thickness, it becomes easier to bend into the desired shape. Reducing the thickness of these bamboo stick actually will reduce its strength but it still strong enough to resist the airflow. Since the shape of the model in this project is semi-elliptic shape, these bamboo sticks were perfectly bended into the shape of the model plus it is easy to be found and cheap.

AERODYNAMICS AND ITS APPLICATIONS

In view of the fact that the model will be installed in the wind tunnel, it has to be strong enough to sustain the wind flow especially the support system. The support system is designed made of steel bolt which has a diameter about 20mm and fasteners to make sure it will not rotate. The steel material has high strength even though it is heavier than aluminum. But the weight is not of concern, because this model will lie on the floor of the wind tunnel test section.

The skin for the model is another important component to be considered. Since this project is mainly to measure the aerodynamic forces and pressure distribution in wind tunnel testing, the skin of the model should be as smooth as possible so that there is no disturbance to the air flow over the model. Thus, the best material to be used as the skin is thin aluminum plate. It is because it will not only give the smooth surface, but it can be easily shaped.

CONSTRUCTION PROCESSES

Tools and Equipments

The following is a list of tools and equipment that have been used while constructing the half model airship:

- Saws, Engineering's square, Electric hand drill, Cutting machine, Steel ruler, Scales, mixing pump, or balance scales to mix resin, Cardboards, Silicon sealant, Masking tape.

Fabrication processes

1. Frame structure construction

The frame of the model was made of wood and bamboo stick. The first task is to reduce the thickness of seven bamboo sticks into the dimension of approximately 1.8m long, 0.02m

AERODYNAMICS AND ITS APPLICATIONS

wide and 5mm thick. This will give an elastic characteristic to the bamboo stick so that it will easily bended into desired shape.



Figure 34-1 Bamboo stick (for stringers).



Figure 34-2 Finishing of the bamboo stick

Then the process was continued by cutting the woods in six different length which have 12 pieces for each length. The lengths are 0.130m, 0.125m, 0.112m, 0.086m, 0.063m and 0.036m.

AERODYNAMICS AND ITS APPLICATIONS

The edges of each piece have to be trimmed into 15 degrees from the width direction. This will make the frame is likely a rounded shape.



Figure 34-3 Wood cutting process



Figure 34-4 Final shape of wood pieces

After completing the cutting process, these woods were combined to make round shape by using a glue which is called 'Bostik'. This type of glue will give strong bonding between the wood pieces and have curing time about 30 minutes. To make the frame stronger, some multiple nails were embedded at the intersection of the wooden pieces.

AERODYNAMICS AND ITS APPLICATIONS



Figure 34-5 Wood gluing process.



Figure 34-6 Final shape of the wood (for frame structure)

After all the glue at the intersections of the wooden pieces were cured, these were attached to the base which has dimensions of 1.6m long, 0.08m wide and 0.015m thick by using nails. This base acting as the backbone of the model. To make the frame structure stronger, there are additional woods attached to the left and right of the frame so that the frame will not moved.

AERODYNAMICS AND ITS APPLICATIONS



Figure 34-7 Frame structure assembly



Figure 34-8 Final shape of the frame structure

Once the frame is completed, this is the time to attach the stringers made of bamboo sticks to the frame structure. Attaching these stringers was done by using the same glue as before with the addition of copper wire. This copper wire was used to fasten the attachments so that the bamboo stick will not return to its initial shape and is fixed to the desired shape. The copper wire will be removed after the glue was perfectly cured.

AERODYNAMICS AND ITS APPLICATIONS



Figure 34-9 Attaching bamboo stick to the frame structure



Figure 34-10 Final shape of the attachment

2. Tapping points

The tapping points on the model were made by using very tiny hollow stainless steel needle in order to get better result in the pressure measurements testing. Ideally these tapping holes should be less than 0.2 mm. These needles were attached to silicon tubes by using a silicon sealant as the connector to the tubes inside the wind tunnel.

AERODYNAMICS AND ITS APPLICATIONS



Figure 34-11 The stainless steel needles



Figure 34-12 Silicon tubes

AERODYNAMICS AND ITS APPLICATIONS

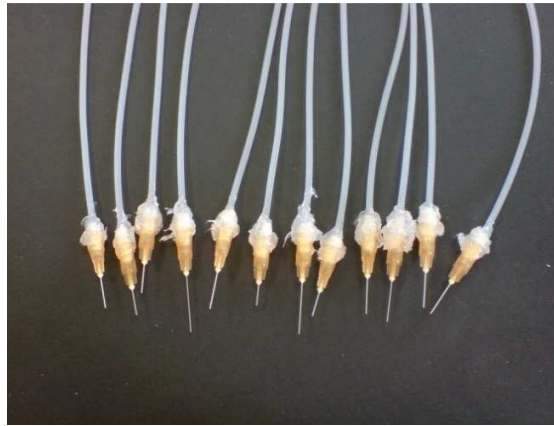


Figure 34-13 Tubes connection to the needle



Figure 34-14 Tapping point attachment process

After that, there are 22 holes were drilled on the top stringer for the tapping point attachment. This was done by using an electric driller with 1mm diameter of drill bit. By completing the drilling process, the needles which have been connected to the tubes were attached to the stringer through the holes and fixed it using silicon sealant. The final diameter of the finished tapping point should be $\sim 0.1\text{mm}$.

AERODYNAMICS AND ITS APPLICATIONS



Figure 34-15 Fixing the tapping points



Figure 34-16 Final shape of the tapping points

Suggestions for further reading

1. Khoury, G. A. & Gillette, D. (1999). *Airship Technology*, United Kingdom, Cambridge University Press.
2. Beckwith, T. G., Maragoni, R. D. & Lienhard, J. H. *Mechanical Measurements*. Sixth Edition. Prentice Hall.
3. Barlow, J. B., Rae, Jr., W. H., and Pope, A. 1999. *Low Speed Wind Tunnel Testing*. New York: John Wiley and Sons.

AERODYNAMICS AND ITS APPLICATIONS

CHAPTER 35

FINAL MODEL ASSEMBLY TECHNIQUES

Tail and bow cap construction

The tail for this model was designed to have a symmetric airfoil which is NACA0012. The tail and the bow cap were made using foam. Before cutting the foam, templates have to be made in order to get smooth cutting surfaces of the desired shape. The resulting core can be no better than the templates that are used to produce the core. The shape and finish of the core is directly related to the shape and finish of the template. In this project, cardboard is used as it will not deform due to the heat from the hot wire during cutting. For the tail, the foam was cut into a tapered shape which have dimension of 0.343m of the root chord length, 0.15m of the tip chord length and 0.35m span. For bow cap, the foam was cut into 0.14m diameter and 0.04m thick of a cylindrical shape.

AERODYNAMICS AND ITS APPLICATIONS

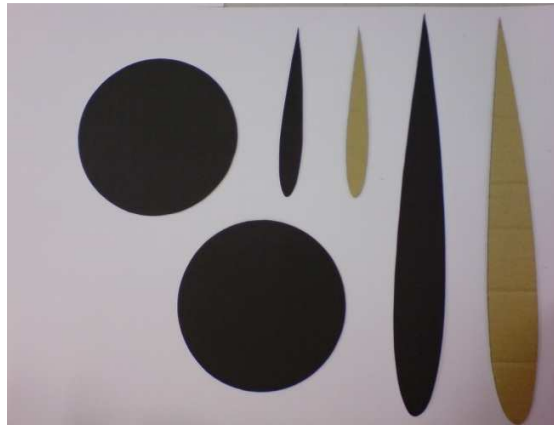


Figure 35-1 Tail and bow cap templates

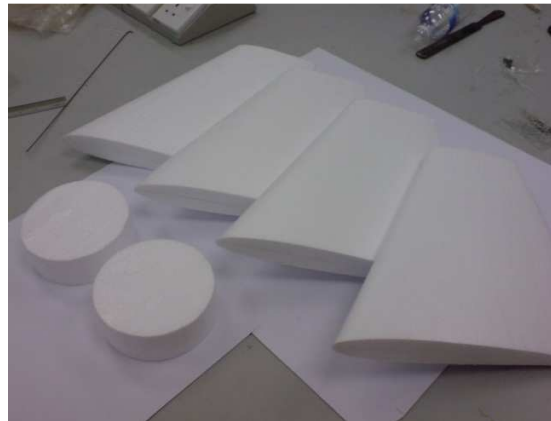


Figure 35-2 Tail and bow cap shape (made of foam)

After complete the cutting process, these tail and bow cap were gone through a sanding process to make the surface finish as smooth as possible. Then, at the frame structure, a tail support attachment was made using a thin aluminum plate. To make the tail attachment stronger, the intersection between the tail and aluminum plate was glued by using epoxy resin. Epoxies were used as main resin matrix. This resin must be mix with a specific amount of hardener.

AERODYNAMICS AND ITS APPLICATIONS

Epoxies are the basic resin used in most amateur-built aircraft. Epoxies are hardened through a process called “crosslinking”. Epoxies are essentially long chains of molecules that interweave when hardened to form a strong matrix of crosslinked chain. This provides an inner structural strength to the resin. Epoxies are packaged in two parts which are a resin and a hardener. During lay-up the mixing ratio of are 4:1 (4 resin to 1 hardener) .The cure time for resin matrix is 24 hours under a room temperature.



Figure 35-3 Tail support attachment

AERODYNAMICS AND ITS APPLICATIONS



Figure 35-4 Tail attachment

Then, the bow cap was divided into two parts, one for the front and the other one for rear. Before attaching the bow cap to the frame structure, five through holes were drilled on each bow cap for the needle attachment (tapping points). After that the needles were attached and fixed using silicon sealant. Both of the bow caps were attached to the frame structure and fix it using fast cured glue.



Figure 35-5 Rear bow cap attachment



Figure 35-6 Front bow cap attachment

3. Skin construction

The skin of the model was made using carboards instead of thin aluminium plate. The cardboard also has smooth surface which is smooth enough to let the airflow moving on it and it has lower price than aluminium thin plate. The cardboard was cut into the shape of each section of the frame. Then it pasted on the frame structure using masking tape. To make it stronger and smoother, epoxy resin was apply on the cardboard. Several layer of epoxy resin was applied in order to get better surface finish.

AERODYNAMICS AND ITS APPLICATIONS



Figure 35-7 Skin attachment process

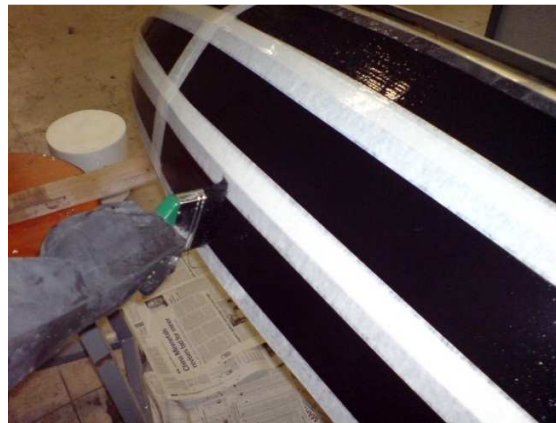


Figure 35-8 Application of epoxy resin



Figure 35-9 Final shape of the model

4. Base structure construction and mounting attachment

For the base structure, the material used is plywood. The complete frame and skin structure was put on the plywood, then the shape of the base was drawn onto the plywood. After that, the plywood was cut into the desired shape by referring to the lines made on the plywood itself. Then it is cut into two pieces so that it will be easy to attach to the base of the model. Before attaching this base structure to the model, a 20mm diameter bolt was attached to the base center of the model which will function as the mounting structure. The bolt was fastened using 4 nuts to make sure it is strong enough and is not loosened when the model is installed in the wind tunnel.

After that, the base structure was attached to the structure using 24 screws to make it easy for attachment and detachment.



Figure 35-10 Model base cutting process

AERODYNAMICS AND ITS APPLICATIONS



Figure 35-11 Final shape of model base



Figure 35-12 Mounting bolt connection



Figure 35-13 Base model attachment



Figure 35-14 Complete shape of the base model

5. Finishing of the complete model

After complete all the above processes, the remaining work is the finishing of the model. The model was turned into black in colour using spray paint. This colour was chosen because the model will be used for flow visualization. White smoke will be used to observe the airflow. Using black colour will give a clearer view of the airflow above the model.

AERODYNAMICS AND ITS APPLICATIONS



Figure 35-15 Spray paints



Figure 35-16 Painting with black colour



Figure 35-17 Complete shape of the model

Suggestions for further reading

1. Khoury, G. A. & Gillette, D. (1999). *Airship Technology*, United Kingdom, Cambridge University Press.
2. Beckwith, T. G., Maragoni, R. D. & Lienhard, J. H. *Mechanical Measurements*. Sixth Edition. Prentice Hall.
3. Barlow, J. B., Rae, Jr., W. H., and Pope, A. 1999. *Low Speed Wind Tunnel Testing*. New York: John Wiley and Sons.

CHAPTER 36

SETTING UP MODEL FOR WIND TUNNEL TESTING

Wind tunnel tests are performed in order to get particular experimental data related to the performance of the vehicle such as lift, drag and moments. Forces and moments from control surfaces provide information to ensure satisfactory handling. Hinge moments of these control surfaces are needed by the control system engineers. Detailed force distributions are used by the structural design group to optimize the structure.

General distributions of forces on a model are obtained by pressure plotting the surface. Hypodermic tubing is inserted from inside the model to finish flush with the surface. The other end of the tubing is connected to a pressure sensor, which records the static pressure at the surface of the model.

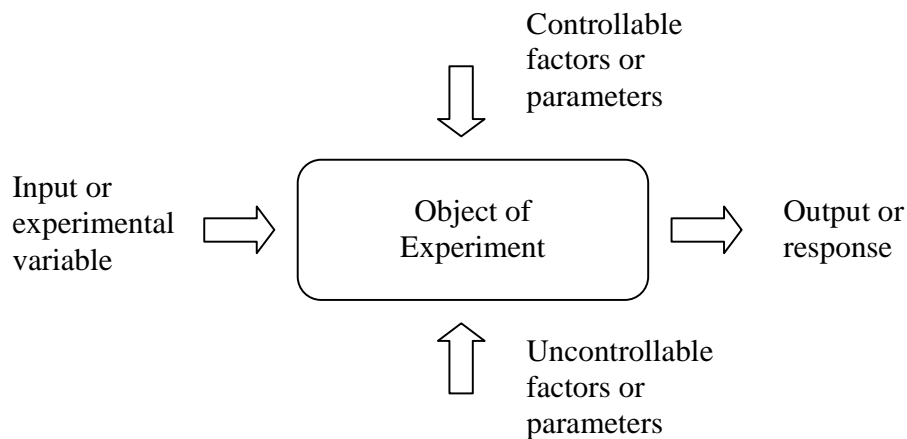


Figure 36-1 Conceptual model of an experimental setup

AERODYNAMICS AND ITS APPLICATIONS

A block diagram representation of a wind tunnel experiment is shown above. The elements of the input vector are variables such as angle of model pitch, roll, or yaw and the pressure drop across the tunnel nozzle. The elements of which can be controlled will be variables such as model size, tunnel size, model materials, model construction process, time of conduct of the experiment and choice of mounting arrangement. Some variables may appear in either the input vector or the controllable factors depending on immediate purposes. The elements of output vector will be responses such as force and moment components as indicated by the balance, pressure readings from the pressure-measuring system, flow visualization and noise. Elements from the uncontrollable factors include such variables as turbulence level of the incoming stream, temperature, model deformation under loads and surface deterioration with time.

The IIUM Low Speed Wind Tunnel

The test section of IIUM WT has dimensions of 2.25m x 1.5m x 6m. It is a removable test section, where the whole structure can be moved on rails by means of 4 steel wheels, to provide an easy access to the test section whenever it is necessary. The side-walls are made from modular acrylic glass, which allows dismounting for installation of model or setting a customized traversing probe.



Figure 36-2 View of empty test section

Model installation

The airship model was installed in the wind tunnel by attaching the base structure of the model to the mounting slot located in the floor of the test section. This was done by rotating the model since the mount structure of the model is actually a bolt with the size about 20mm diameter.

After the model has been fastened, the distance of the base of the model and the floor of the test section was measured which is about 50mm. This to make sure that the model is not too high above the floor to avoid the incorrect measurement for half model testing and not too close with the floor of the test section to avoid the boundary layer region generated on the floor of the test section.

AERODYNAMICS AND ITS APPLICATIONS



Figure 36-3 Installing the model in the test section

Connecting the tubes

After complete installation of the model, the tubes for tapping points were connected to the tubes provided in the wind tunnel. There are 32 tapping points along the top line of the airship model. These tapping points have to be carefully connected in order to get good measurement. But before connected to the wind tunnel tubes, these tapping points and the tubing should be tested to make sure that there is no leakage in the connection. This is done by using a special equipment which is called pressure calibrator.



Figure 36-4 Tube connection

Pretesting

Before running the experiment to measure the pressure distribution and forces of the model, a pretest session has to be performed with the maximum velocity and angle of attack planned to ensure that the model installed will not be blown off or result in detached components. In this session, the connected tubes were also observed whether it will disconnected or not due to the air speed and turning angle.



Figure 36-5 Pre test session

Running the experiment

1. Pressure and force measurement

The experiment was run by the engineers of the wind tunnel. The input data were keyed into the computer including the model size and measurement required. The velocity of the wind was adjusted to 20m/s and is kept constant throughout the experiment. Once it reaches the constant value, the data of pressure distribution was recorded for different angle of attack (0° , 5° , 10° , 15° , 20° , 25° and 30°). The model inside the test section was observed to make sure there are no disturbances and the components not flown away.

After completing the pressure measurement experiment, the tubes connections were disconnected to continue with the force measurement experiment. This will give the accurate value of forces measured since there is no disturbance around the model.



Figure 36-6 Pressure measurement testing at 25° angle of attack

2. Flow visualization

The second experiment is about flow visualization over the model. After completing the first experiment, several black cardboard sheets were pasted onto the wall and floor of the test section in order to get clear and better visualization of flow above the model since it uses white smoke. The smoke generator was installed from the bottom of the test section. After its installation, the wind tunnel was run at 10m/s and the flow was recorded. After about a minute, the wind tunnel was shut down in order to observe the flow at very low speeds.



Figure 36-7 Flow visualization experimental set up

Suggestions for further reading

1. Khoury, G. A. & Gillette, D. (1999). *Airship Technology*, United Kingdom, Cambridge University Press.
2. Beckwith, T. G., Maragoni, R. D. & Lienhard, J. H. *Mechanical Measurements*. Sixth Edition. Prentice Hall.
3. Barlow, J. B., Rae, Jr., W. H., and Pope, A. 1999. *Low Speed Wind Tunnel Testing*. New York: John Wiley and Sons.

CHAPTER 37

WIND TUNNEL TEST RESULTS

From the wind tunnel experiment, the data obtained regarding the pressure and force measurement are shown in the table below. The location of the tapping points were illustrated in the following figures. But it shows only the front half of the model. The tapping points location for rear half of the model are the same as the front half. These tapping point located along the top center of the model. Since it is an axisymmetric model, it is assumed that the pressures are same around the model for zero degree angle of attack. Sample of results are shown next.

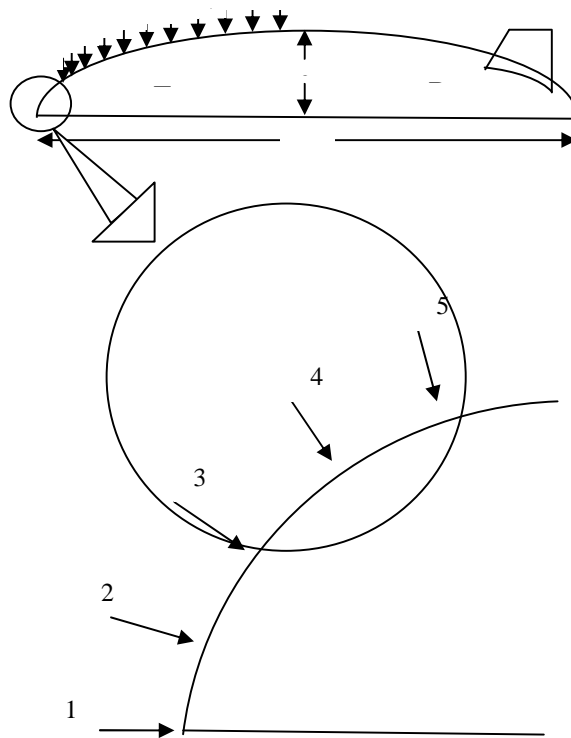


Figure 37-1 Location of tapping points for pressure measurement

AERODYNAMICS AND ITS APPLICATIONS

1. Result for pressure measurement

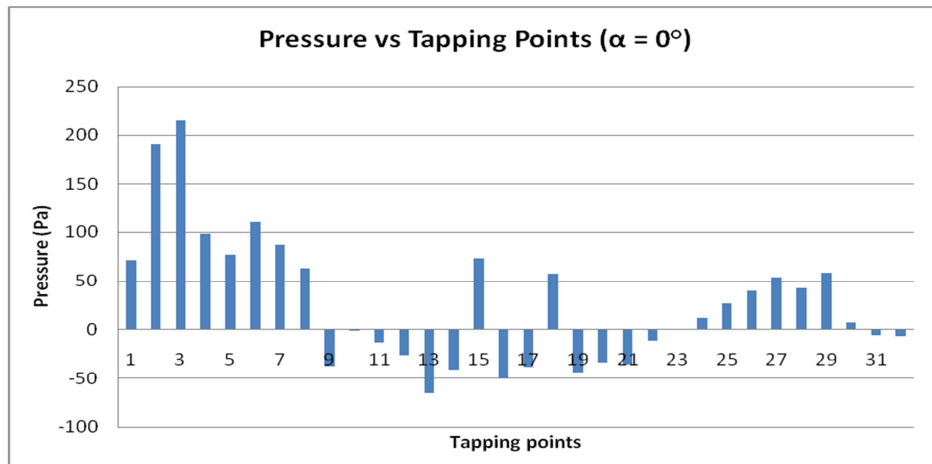


Figure 37-2 Graph of pressure vs tapping points for $\alpha = 0^\circ$.

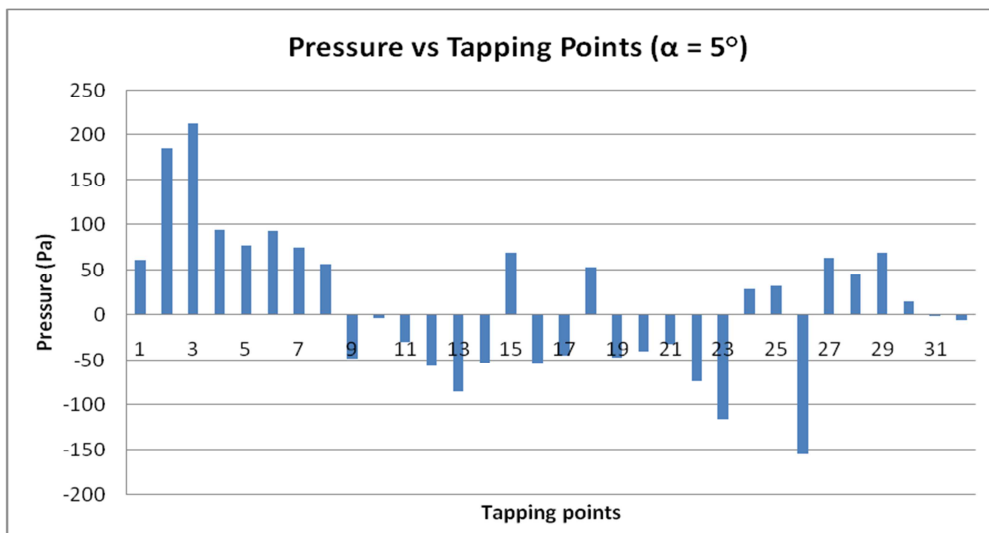


Figure 37-3 Graph of pressure vs tapping points for $\alpha = 5^\circ$.

AERODYNAMICS AND ITS APPLICATIONS

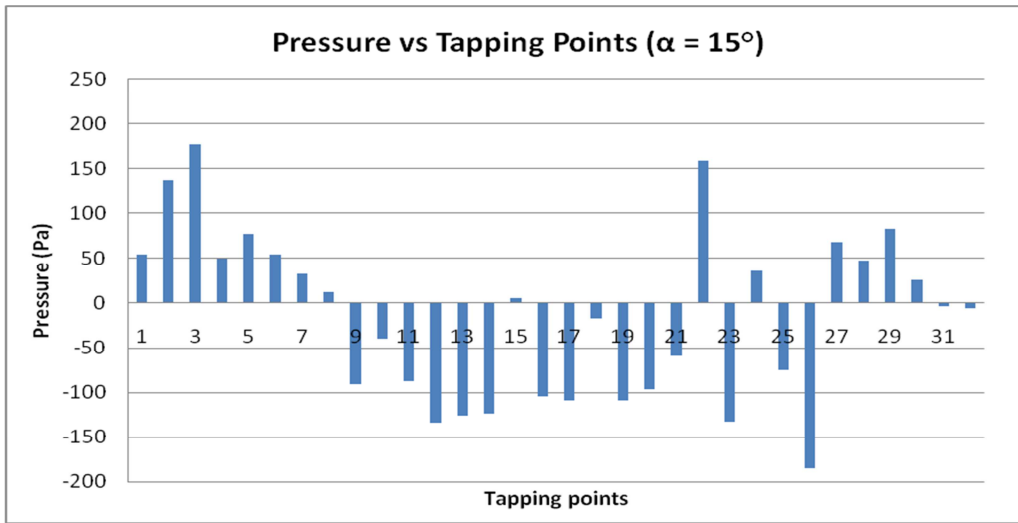


Figure 37-4 Graph of pressure vs tapping points for $\alpha = 15^\circ$.

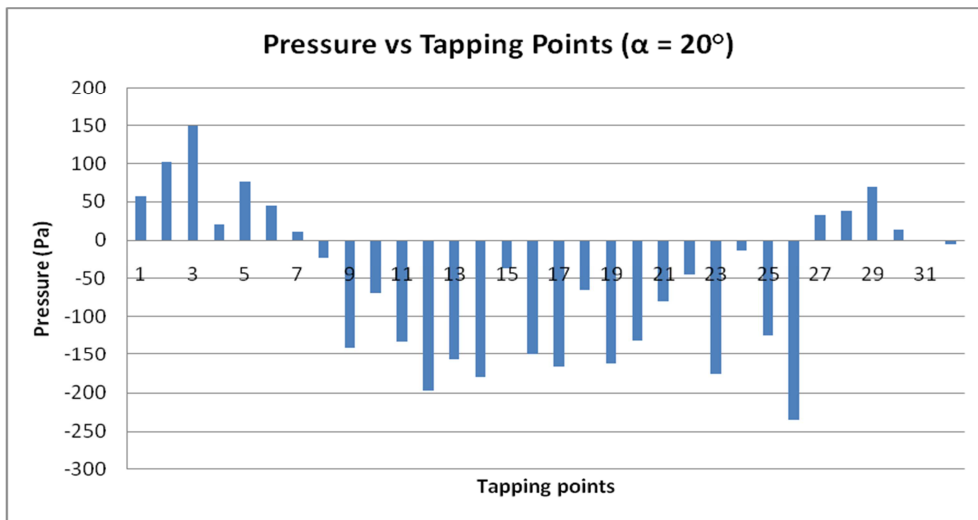


Figure 37-5 Graph of pressure vs tapping points for $\alpha = 20^\circ$.

AERODYNAMICS AND ITS APPLICATIONS

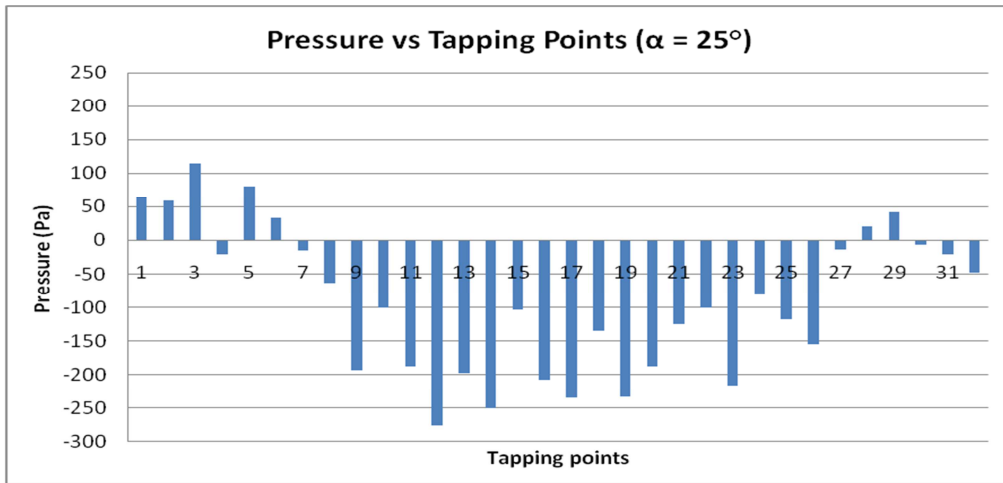


Figure 37-6 Graph of pressure vs tapping points for $\alpha = 25^\circ$.

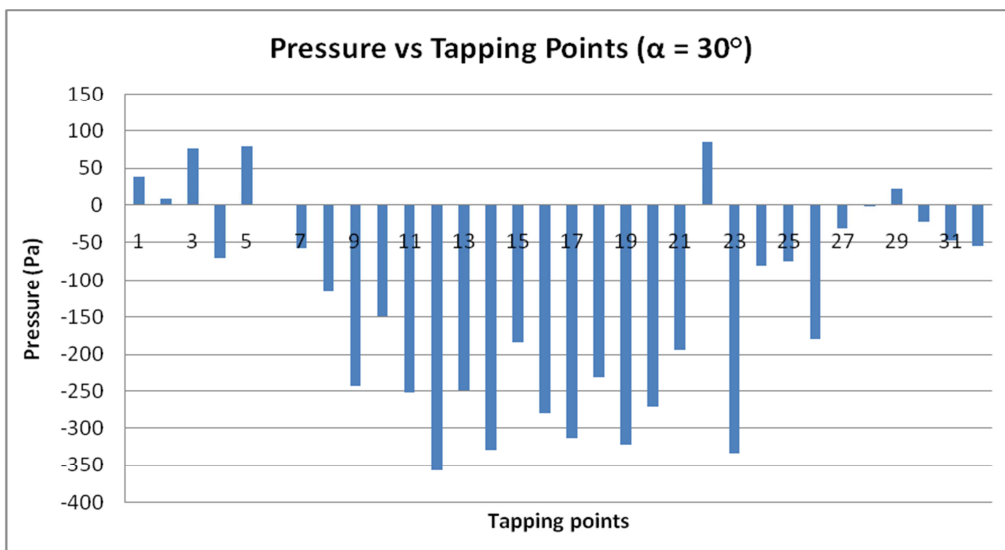


Figure 37-7 Graph of pressure vs tapping points for $\alpha = 30^\circ$.

AERODYNAMICS AND ITS APPLICATIONS

2. Results for forces measurement

The forces acting on the airship model were converted to coefficients. A sample of the results is shown in the table below.

Table 37-1 Lift, drag and moment coefficients with respect to its angle of attack

Coefficients	Alpha (degrees)						
	0	5	10	15	20	25	30
CL(lift)	0.039467	0.261451	0.492606	0.720814	0.851203	1.041771	1.304158
CD(drag)	0.208	0.184204	0.144177	0.103964	0.203832	0.218672	0.19329
Cm(pitch)	-0.00427	0.021788	0.031423	0.026857	0.064411	0.045428	-0.00802

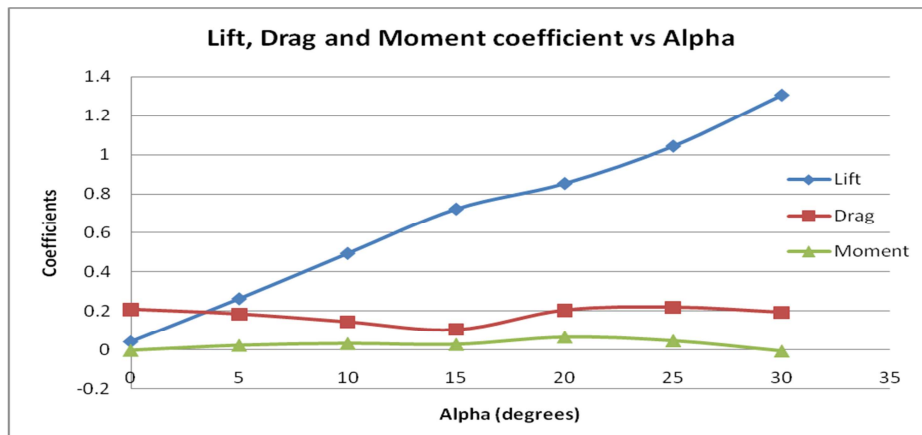


Figure 37-8 Graph of lift, drag and moment coefficient

3. Result for flow visualization

Samples of flow visualization results are shown in the figures below. In the absence of a proper smoke machine, the PIV particle generator ‘smoke’ was used to get the best possible results. Much better visualization is expected from a proper smoke machine.

The flow visualization results show that most of the flow remains attached to the airship.



(a)

(b)

- Figure 37-9 Series of flow visualization pictures. (a) Flow visualization at speed of 10m/s.**
(b) Flow visualization after the wind tunnel is shut down to let the velocity of airflow reduce from 10m/s until it stops.

Suggestions for further reading

1. Abbot, I.H., Von Doenhoff, A.E. (1959). *Theory of Wing Sections*. New York, McGraw-Hill Inc.
2. Anderson, John D., Jr. (2001). *Fundamentals of Aerodynamics*. New York, McGraw-Hill Inc.
3. Bhaskaran, R. (2003). *Fluent Tutorials*. New York, Cornell University.
4. Currie, I.G. (1993). *Fundamental Mechanics of Fluids*. New York, McGraw-Hill Inc.
5. Hoffman, K.A., Chiang, S.T., Siddiqui, S., Papadikis, M. (2002). *Fundamental Equations of Fluid Mechanics*. Kansas, Engineering Education System.
6. Munson, B.R., Young, D.F., Okiishi, T.H. (2002). *Fundamentals of Fluid Mechanics*. New York, John Wiley & Sons Inc.

AERODYNAMICS AND ITS APPLICATIONS

7. Versteeg, H.K., Malalasekera, W. (1995). *An Introduction to Computational Fluid Dynamics; The Finite Volume Method*. Harlow, Longman Group Ltd.
8. Zhu, G., Bearman, P.W., Graham, J.M.R. (2002). *Prediction of Lift and Drag Using Velocity and Vorticity Fields*. London, Aeronautical Journal.
9. Khoury, G. A. & Gillette, D. (1999). *Airship Technology*, United Kingdom, Cambridge University Press.
10. Beckwith, T. G., Maragoni, R. D. & Lienhard, J. H. *Mechanical Measurements*. Sixth Edition. Prentice Hall
11. Barlow, J. B., Rae, Jr., W. H., and Pope, A. 1999. *Low Speed Wind Tunnel Testing*. USA, John Wiley and Sons.
12. Anderson, Jr., J.D. (2005), *Fundamentals of Aerodynamics*, Fourth Edition, McGraw Hill
13. Konstantinov, L. *The Basics of Gas and Heat Airship Theory*.
14. Website: www.aeronautics.com/airship
15. Mueller, J. B. and Paluszek, M. A. *Development of an Aerodynamic Model and Control Law Design for a High Altitude Airship*, Princeton Satellite Systems, Princeton.
16. Munk, M.M. *The Aerodynamic Forces On Airship Hulls*, National Advisory Committee For Aeronautics.

AERODYNAMICS AND ITS APPLICATIONS

APPENDIX

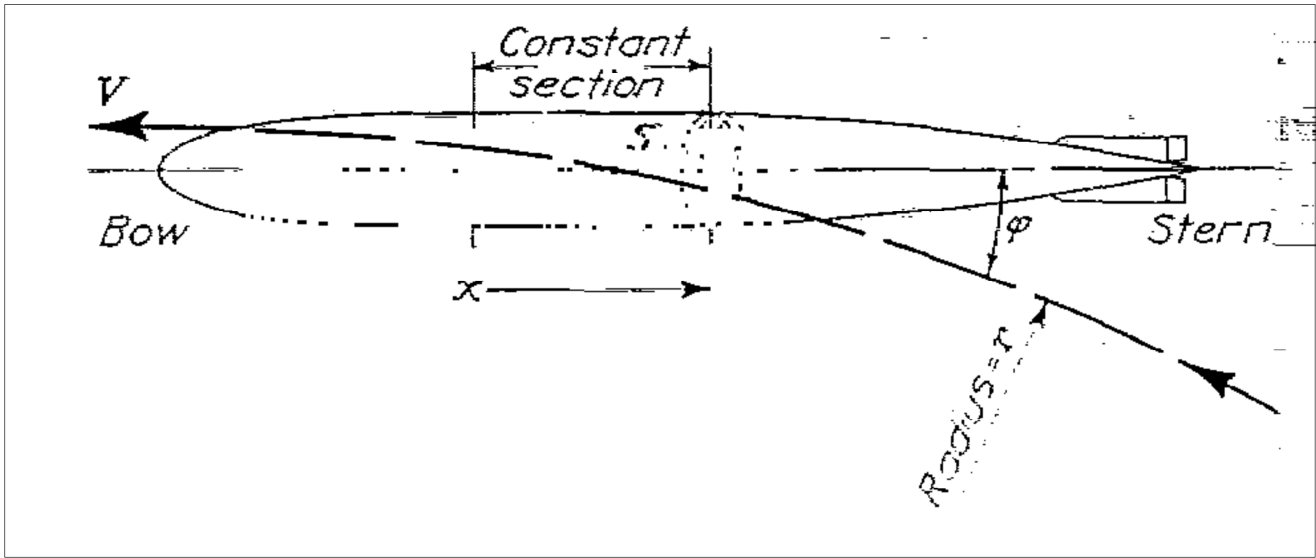


Figure A.1: Airship model

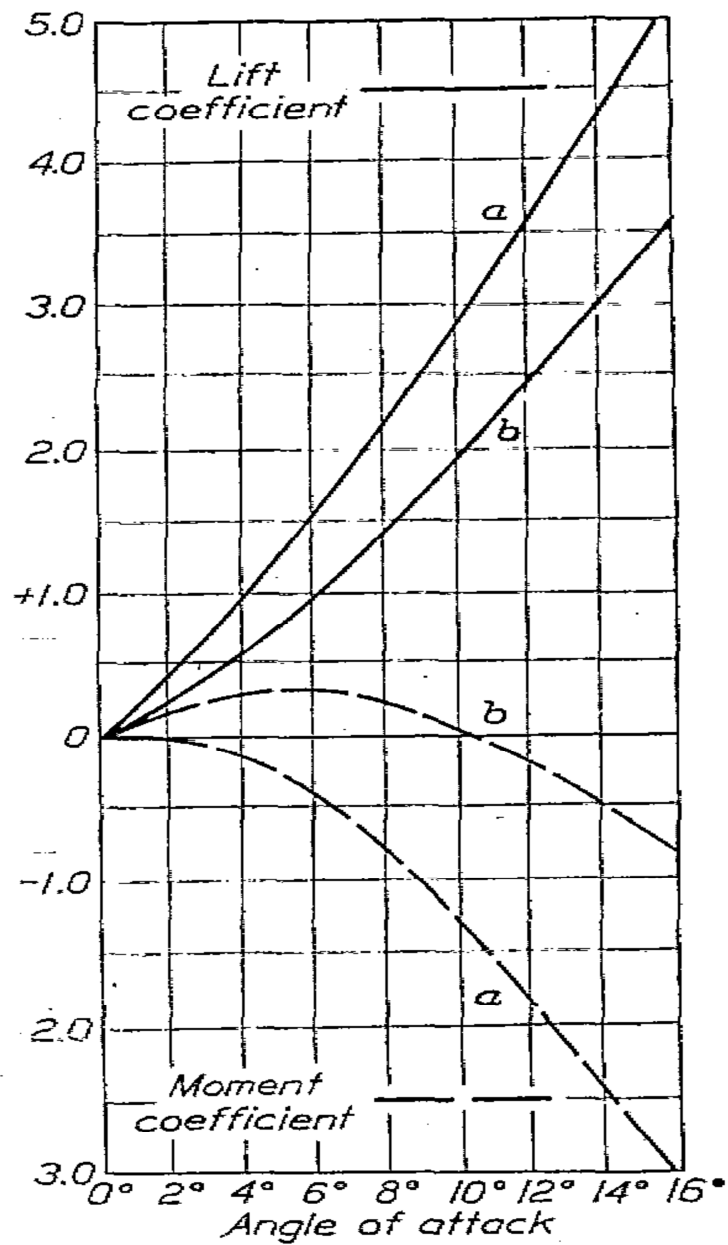


Figure A.2: The lift and moment coefficient